WDL-TR-E320
MARCH 1963

EFFECT of the SU upon ANTENNA TEMPERATURE

by
Albert R. Giddis

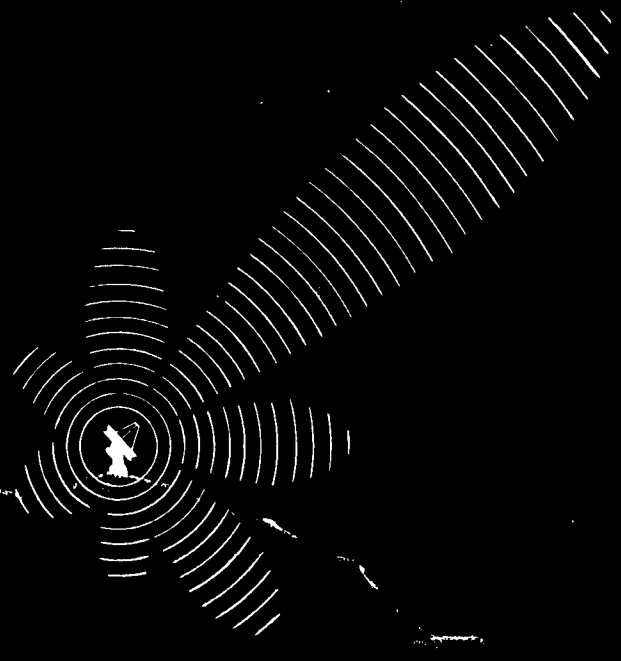

HILCO
Ford Motor Company
WDL DIVISION PALO ALTO, CALIFORNIA

ADDENDA ET ERRATA

Page	Item
2-1	In line 7 of Section 2.2, the frequency "3000" should read "9400".
2-2	Add "(after Swarup)" to title of Fig. 2-1.
2-3	Do. Fig. 2-2.
2-10	The label "OUTBURSTS (TYPE II)" identifies the dashed curve (after Coutrez) that begins in the upper left-hand corner of Fig. 2-6 as well as the burst data indicated by x's in the upper right-hand corner. The solid curve in the lower right-hand portion of the figure should be labelled "SVC (AFTER KAKINUMA and SWARUP)".
3-5	In the first paragraph under Section 3.2.1, line 4 should read "for the 60-foot, 85-foot and 210-foot reflectors...". In line 5, delete "60-foot".
3-7	At the beginning of line 4, add "For the 'min' conditions,".
3-17	In Section 3.2.2.2 lines 3 to 6 should read as follows: "and will be identical in general for the same diameter-frequency product. For example, the 30-foot/1200 Mc antenna temperature curve in Figure 3-5 and the 60-foot/600 Mc curve in Figure 3-6 exhibit maxima and minima at the same angles."
3-33	At the end of line 7, add "at vertical polarization."
4-3	In Fig. 4-1 the second G_T in the numerator of the equation for C/N should read "G_R".
A-29	In the second rectangular block from the bottom of the first column, the "Z" should be replaced by "I" in two places.

WDL Technical Report E320

EFFECT OF THE SUN
upon
ANTENNA TEMPERATURE

by

Albert R. Giddis

Antenna Systems Laboratory

March 1963

PHILCO CORPORATION
A Subsidiary of Ford Motor Company
Philco WDL Division
Palo Alto, California

FOREWORD

This report on the Effect of the Sun on Antenna Temperature was made possible by support from several sources. The report itself was prepared and published with funds from the Advanced Solar Probe Study directed by William Kellar of the Advanced Systems Engineering Department. The computations of solar antenna temperature using the Philco-2000 computer were financed under the Independent Development Programs administered by Dr. Donald Linden. These numerical results were made possible originally by using computer programs that were developed last year in a study of antenna noise performed by the author for the Air Force Space Systems Division under Contracts AF04(647)-829 and AF04(695)-113.

The author wishes to acknowledge the contributions made by Jack Richardson and Carol Dunbar of the Mathematical Analysis Department in developing the computer programs, by Doris Levenson of the Communication Sciences Department in performing calculations and in preparing some of the figures, and by Chet Creider of the Engineering Proposals and Presentations Department in editing the report and in managing its production.

The cover was designed by James Bennett.

CONTENTS

ILLUSTRATIONS

TABLES

SECTION 1
INTRODUCTION

1.1 OBJECTIVE

The objective of this investigation is to compute from analytical models of the quiet sun and from measurements of its flux density the effect of solar radiation upon antenna noise temperature.

1.2 SCOPE

Section 2 describes the spatial and spectral properties of solar radio noise. In particular, brightness temperature distributions over the sun at several frequencies are introduced.

Section 3 accomplishes the following: (a) discusses the method by which antenna temperature is evaluated, (b) systematizes and interprets Philco-2000 computer computations of antenna temperature due to radiation of the quiet sun into the pattern of pencil-beam antennas, (c) compares antenna temperature contributed by the sun with that contributed by other extraterrestrial sources, and (d) evaluates the effect of the earth's atmosphere and ground on the total noise temperature of an antenna.

Section 4 applies the results from the previous section to calculate the carrier-to-noise ratio of a telemetry link between a ground station and a space probe one astronomical unit away, and the carrier-to-noise ratio of a voice link between a ground station and a satellite in a 6000-mile orbit.

Section 5 lists the references consulted during the study.

Section 6 is an appendix in which are presented characteristics of solar radio emission, a derivation of antenna temperature, samples of the input and output data associated with the Philco-2000 computations, analytical notes on solar antenna temperature, and documentation for the computer program.

1.3 BACKGROUND

A broad investigation of antenna temperature due to extraterrestrial sources and ground thermal radiation has been reported recently by the author (Ref. 1) and includes computations of solar antenna temperature. Some of the work reported in the present report has been combined with these earlier efforts in a comprehensive paper on the influence of natural noise upon antenna system performance (Ref. 2).

SECTION 2
SOLAR RADIO NOISE

2.1 INTRODUCTION

In this section the spatial and spectral properties of solar radio noise are described. Measured values of flux density from the quiet and active sun are presented along with brightness temperature profiles derived from models of the solar atmosphere.

2.2 BRIGHTNESS TEMPERATURE

Several measured distributions of brightness temperature over the sun have been published (Refs. 1 - 15). These are generally referred to as radio maps, an example of which is shown in Figure 2-1 for the quiet sun at S-band (Ref. 9). In addition, experiments yielding one-dimensional profiles of brightness temperature have been reported (Refs. 15 - 19). These maps and profiles represent the condition of the radio sun over the past 15 years at frequencies ranging from 80 Mc to 3000 Mc. Measured distributions vary according to the time of observation during the sun's 27-day rotation about its axis at the equator and during the 11-year sunspot cycle, and include the effect of active regions. A map of the average quiet sun at S-band during 1960 is shown in Figure 2-2 (Ref. 10). The variation of the quiet-sun component with time during the solar cycle is uncertain.

In a general study, therefore, it is preferable to use brightness temperature profiles derived from models of the quiet sun to compute nominal values of antenna temperature. Smerd at the Commonwealth Scientific and Industrial Research Organization in Australia has derived sets of brightness temperature profiles at frequencies between 60 Mc and 30,000 Mc by using the Allen-Baumbach model of coronal

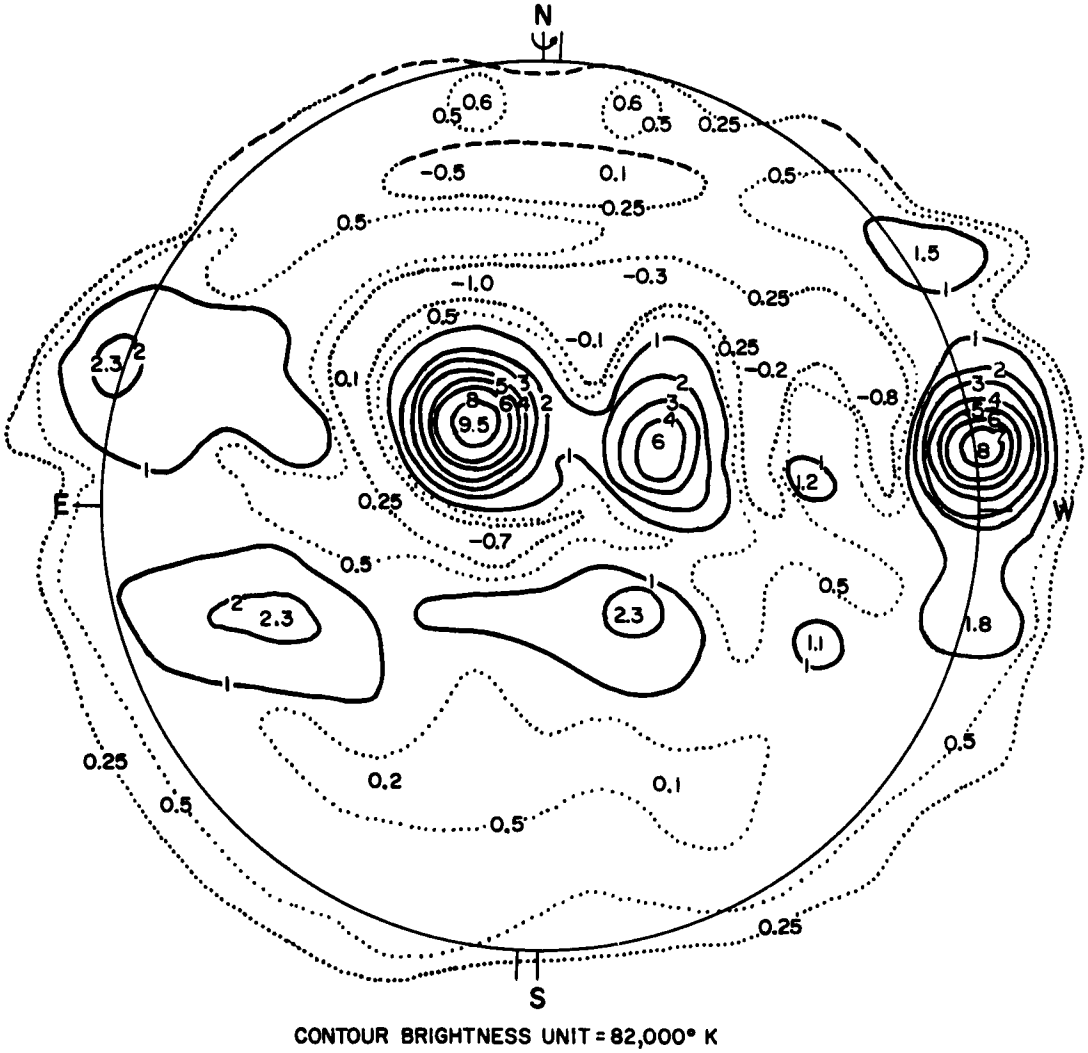

Figure 2-1 Radio Map of the Sun at S-Band

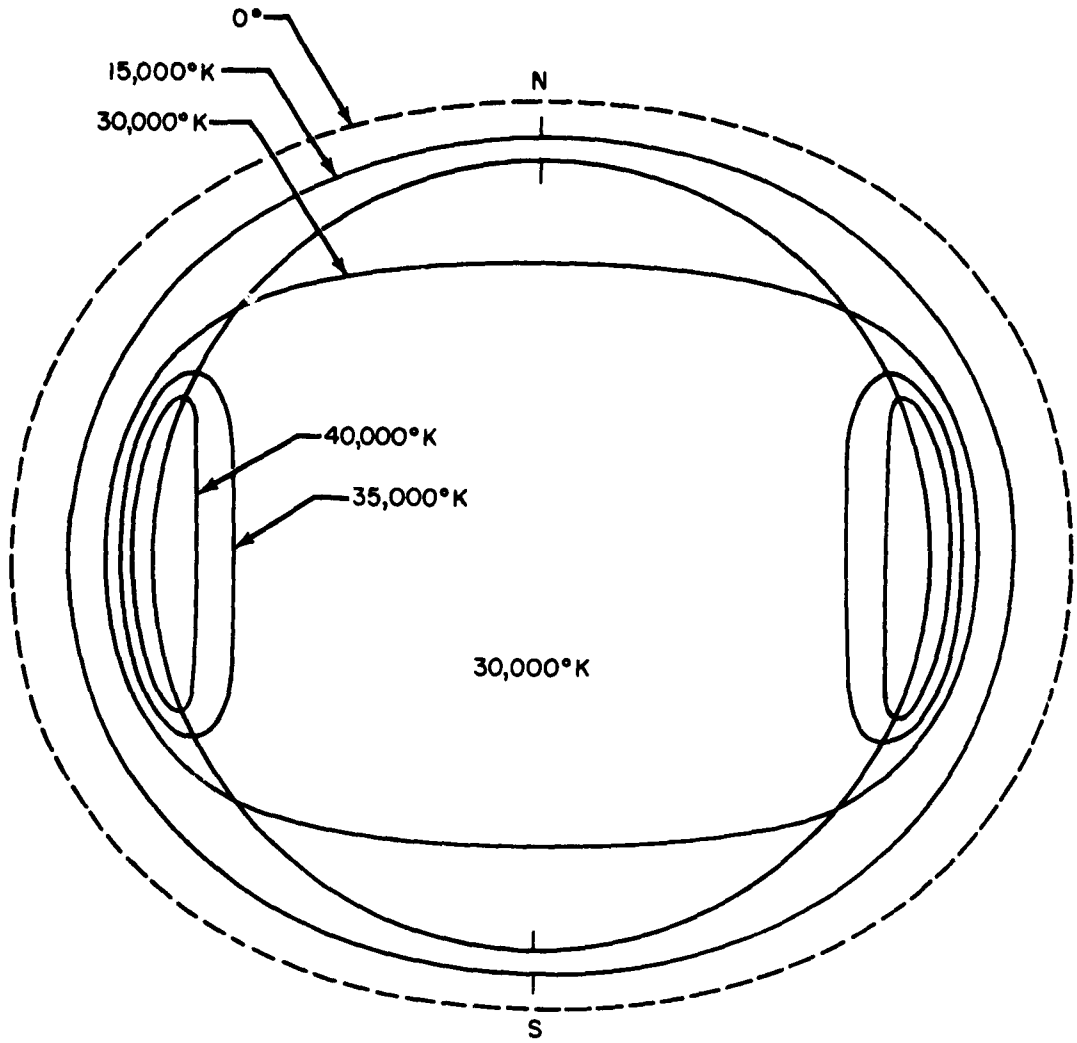

Figure 2-2 Map of Average Quiet Sun at S-Band

electron density, an adjusted Cillié-Menzel model of chromospheric electron density, and uniform coronal and chromospheric electron temperatures of 10^6°K and 3×10^4°K respectively (Ref. 20). A representative set of profiles is shown in Figure 2-3, where the brightness temperatures are plotted as a function of distance in solar radii from the center of the optical disc. The distributions are assumed to be spherically symmetrical.

Swayze at Philco WDL has developed a complementary set of brightness temperature profiles for a symmetrical sun at frequencies between 5 Mc and 2300 Mc by using the van de Hulst model of coronal electron density, empirical models of chromospheric electron density, and distributions of coronal and chromospheric electron temperatures based on several existing models (Ref. 21). Figure 2-4 illustrates profiles at 2300 Mc derived from two limiting models of density and temperature.

The range of brightness temperatures between the "max" and "min" profiles characterizes possible values which the sun can assume. At this time no firm correlation can be made between these values and sunspot number.

2.3 APPARENT TEMPERATURE

When discussing solar noise, a recurring parameter is the "apparent temperature." The apparent temperature is determined by converting the measured flux density to an equivalent uniform brightness temperature over the optical disc. The relation used is based on the Rayleigh-Jeans approximation to Planck's radiation law for equivalent black-body radiation:

$$T_a = \frac{F\lambda^2}{2k\Omega_s} \qquad (2\text{-}1)$$

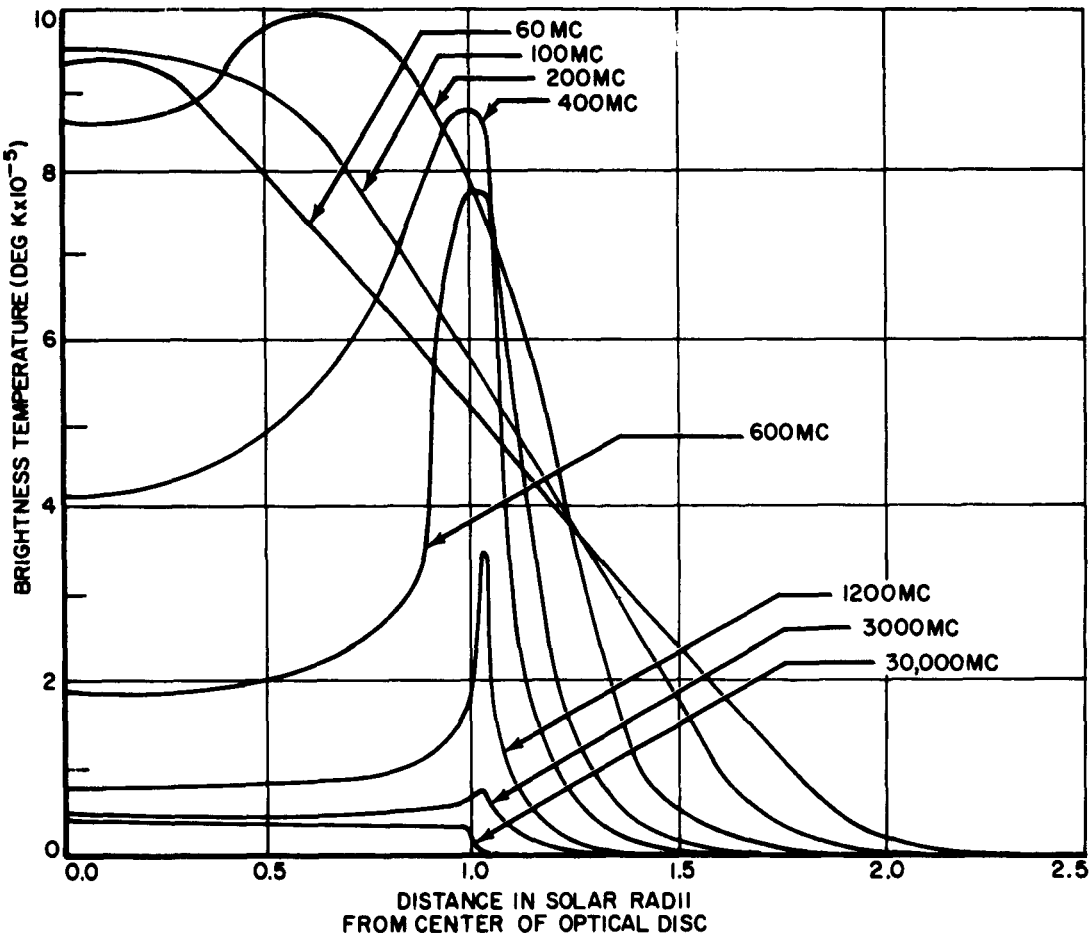

Figure 2-3 Brightness Temperature Profiles (after Smerd)

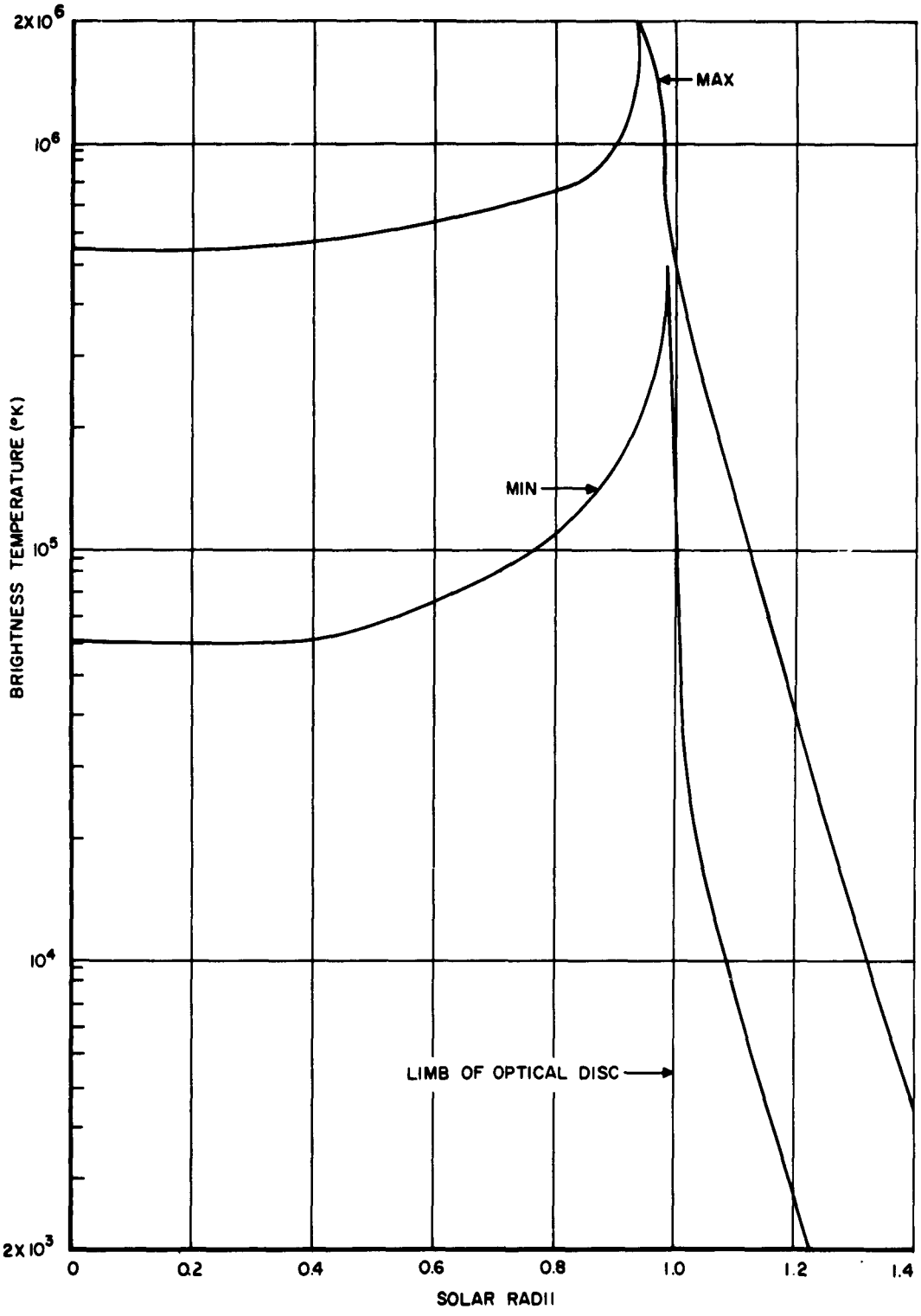

Figure 2-4 Brightness Temperature Profiles at 2300 Mc (after Swayze)

where

T_a = apparent temperature of the sun (deg. K)

F = measured flux density (watts/meter^2/cps)

λ = wavelength of radiation (meters)

k = Boltzmann's constant (joules/deg. K)

Ω_s = solid angle subtended by the sun (steradian).

This concept is valid for determining antenna temperature when the antenna beamwidth is large compared to the angle subtended by the radio sun. In this case, the antenna temperature T_A is simply

$$T_A = T_a \Omega_s \frac{G_o}{4\pi} \qquad (2\text{-}2)$$

where G_o is the on-axis gain of the antenna. The antenna temperatures computed in this study, however, are based not on this simplified concept of a uniform disc temperature but rather on the brightness temperature distributions described above in Section 2.2.

The apparent temperatures plotted in Figure 2-5 are those observed since 1943 at various frequencies between 25 Mc and 70,000 Mc (Refs. 22 - 37). The solid curve represents the spectrum during the last sunspot maximum; the dashed curve represents a condition midway between the peak and minimum of a sunspot cycle. No curve has been drawn for a sunspot minimum condition because of the scarcity of data. More measurements will be recorded during the International Quiet-Sun Year.

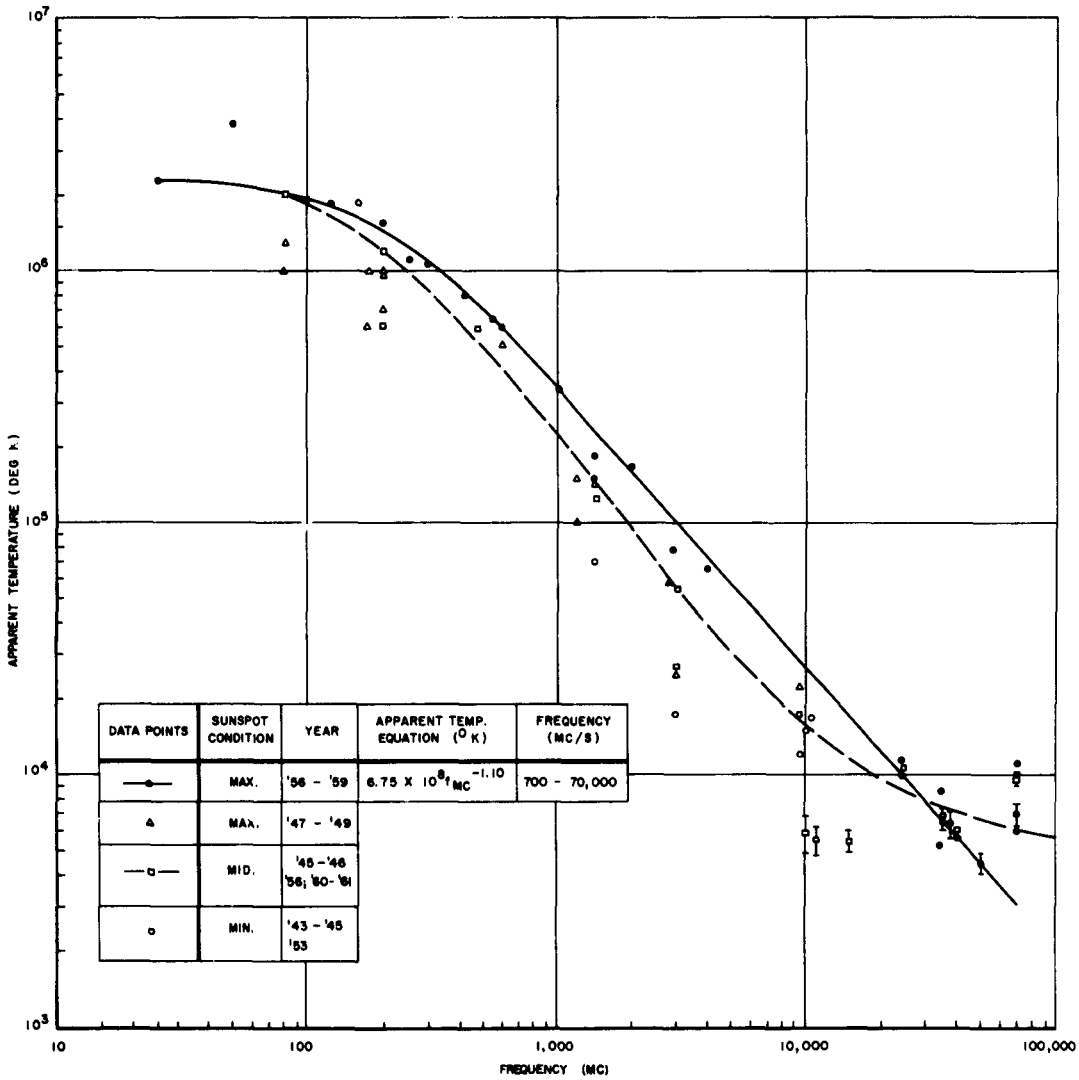

Figure 2-5 Apparent Temperature Spectrum of the Quiet Sun

2.4 ACTIVE SUN

Solar bursts will raise the flux density from one to four orders of magnitude, depending on frequency and time during the solar cycle. Examples of this behavior are shown in Figure 2-6, where measured flux densities of the quiet and active sun are plotted versus frequency (Refs. 28, 38 - 46). At S-band, a typical burst would be about 2×10^{-19} watts/meter^2/cps, one order of magnitude higher than the quiet sun at its maximum flux. Some S-band bursts have been recorded as high as 10^{-18} watts/meter^2/cps.

Thermal noise from the quiet sun is nonpolarized, but burst radiation may be polarized. Noise bursts are circularly polarized, although at times they generate traces of linear polarization. Outbursts are generally nonpolarized at meter wavelengths but may be circularly polarized at centimeter wavelengths. The slowly varying component associated with sunspots is pseudo-thermal and partially circularly polarized throughout its spectrum. Continuum radiation is partially circular.

Table 6-1 in Section 6.1 of the Appendix summarizes some of the principal features of solar noise during quiet and active periods. The tabulation includes the following items: (1) frequency range over which observations have been performed, (2) duration of the radiation and any cyclical behavior, (3) diameter of the apparent source of radiation, its order-of-magnitude flux density and corresponding apparent temperature, (4) predominant polarization component, and (5) phenomena associated with the observed radio noise. The table is divided into three parts that correspond to meter-wave radiation (Refs. 24, 40, 47 - 53), decimeter-wave radiation (Refs. 45 - 46, 48, 51 - 52), and centimeter-wave radiation (Refs. 39, 41, 46, 54 - 56).

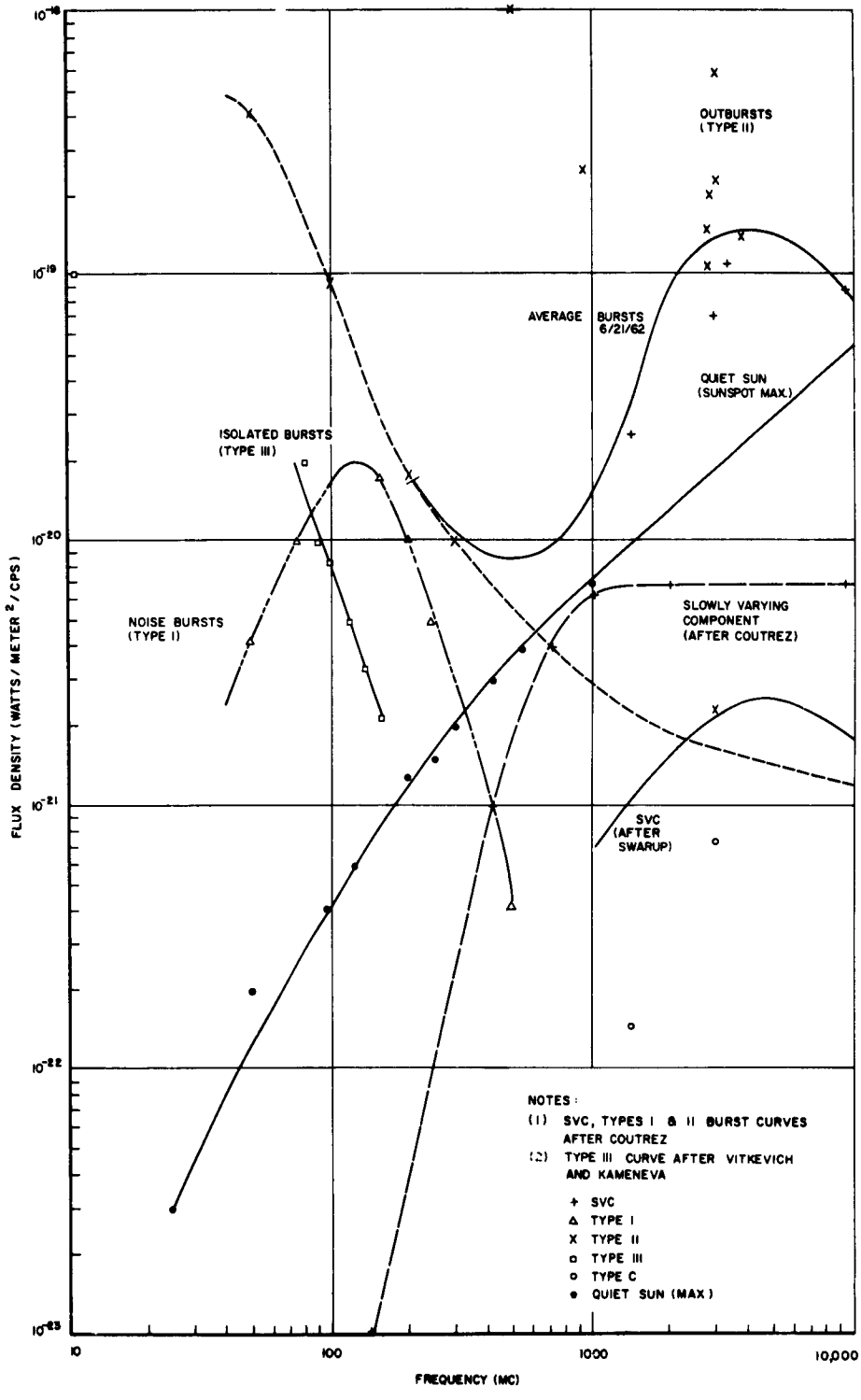

Figure 2-6 Flux Density Spectrum of the Quiet and Active Sun

2.5 ORIGIN OF RADIO EMISSION

The source of thermal emission from the quiet sun consists of clouds of hot hydrogen dissociated into protons and electrons by ultra-violet radiation.

At short wavelengths, the cooler electron temperature of the photosphere can be seen near the center of the sun, and "limb brightening" is observed. Near the edges, a greater depth of the hot corona is found in the observer's line of sight, giving an increased brightness in a ring just outside the visible limb of the sun. At 200 Mc or so, it occurs across the solar equator but not near the poles; at higher frequencies it makes a bright ring around the sun.

At long wavelengths, the galactic background begins to exceed the brightness temperature of the quiet sun, so that the sun progresses from a bright disc at decimeter wavelengths to a grey disc in the radio sky at meter wavelengths.

Non-thermal radiation from the active sun is associated with sunspots which generate electric fields that accelerate charged particles. Energy from high-temperature regions inside the sun may be transmitted from below the photosphere into the corona as magneto-hydrodynamical waves.

Noise bursts (Type I) are generated in or near an intense magnetic field above the sunspots. At frequencies above 60 Mc, sunspot radiation merges into radiation from calcium plages or faculae, which seem to control the rise and fall of steady radiation from the sun during the solar cycle.

Slow-Drift (Type II) and Fast-Drift (Type III) bursts are generated by a flare-caused wave (perhaps cosmic rays) that travels from the photospheric surface in the vicinity of a sunspot outward through successively thinner layers of the corona. Type III bursts are sometimes accompanied by material called "puffs," which are ejected from the flare at a speed equal to the radio outbursts.

SECTION 3
ANTENNA TEMPERATURE

3.1 INTRODUCTION

The computation of antenna temperature for a given brightness temperature distribution $T_b(\theta, \phi)$ and a given antenna power pattern $G(\theta, \phi)$, where (θ, ϕ) are angular coordinates in a spherical coordinate system, is based upon the following relation:

$$T_A = \frac{\int_0^{2\pi} \int_0^{\pi} \frac{G(\theta, \phi)}{G_o} T_b(\theta, \phi) \sin\theta \, d\theta \, d\phi}{\int_0^{2\pi} \int_0^{\pi} \frac{G(\theta, \phi)}{G_o} \sin\theta \, d\theta \, d\phi} \qquad (3\text{-}1)$$

where G_o is the antenna gain on-axis. The derivation of this equation is based upon the Rayleigh-Jeans law and can be found in Section 6.2 of the Appendix.

The function $T_b(\theta, \phi)$ varies with the source of radiation, time, location of the ground station, weather, solar activity, and the frequency of propagation. In this study, the primary source of radiation is the sun as described by the brightness temperature profiles in the previous section. The computer operates on tabulations of brightness temperature vs. angular distance from the center of the optical disc. A sample of such a tabulated brightness-temperature profile at 2300 Mc is given in Table 6-2 in Section 6.3 of the Appendix.

A significant portion of the normalized, pencil-beam, antenna power pattern $G(\theta, \phi)/G_o$ used for computations of antenna temperature is plotted in Figure 3-1. The pattern in this figure is based upon measurements at 2300 Mc of a 60-foot telemetry-and-data antenna developed by

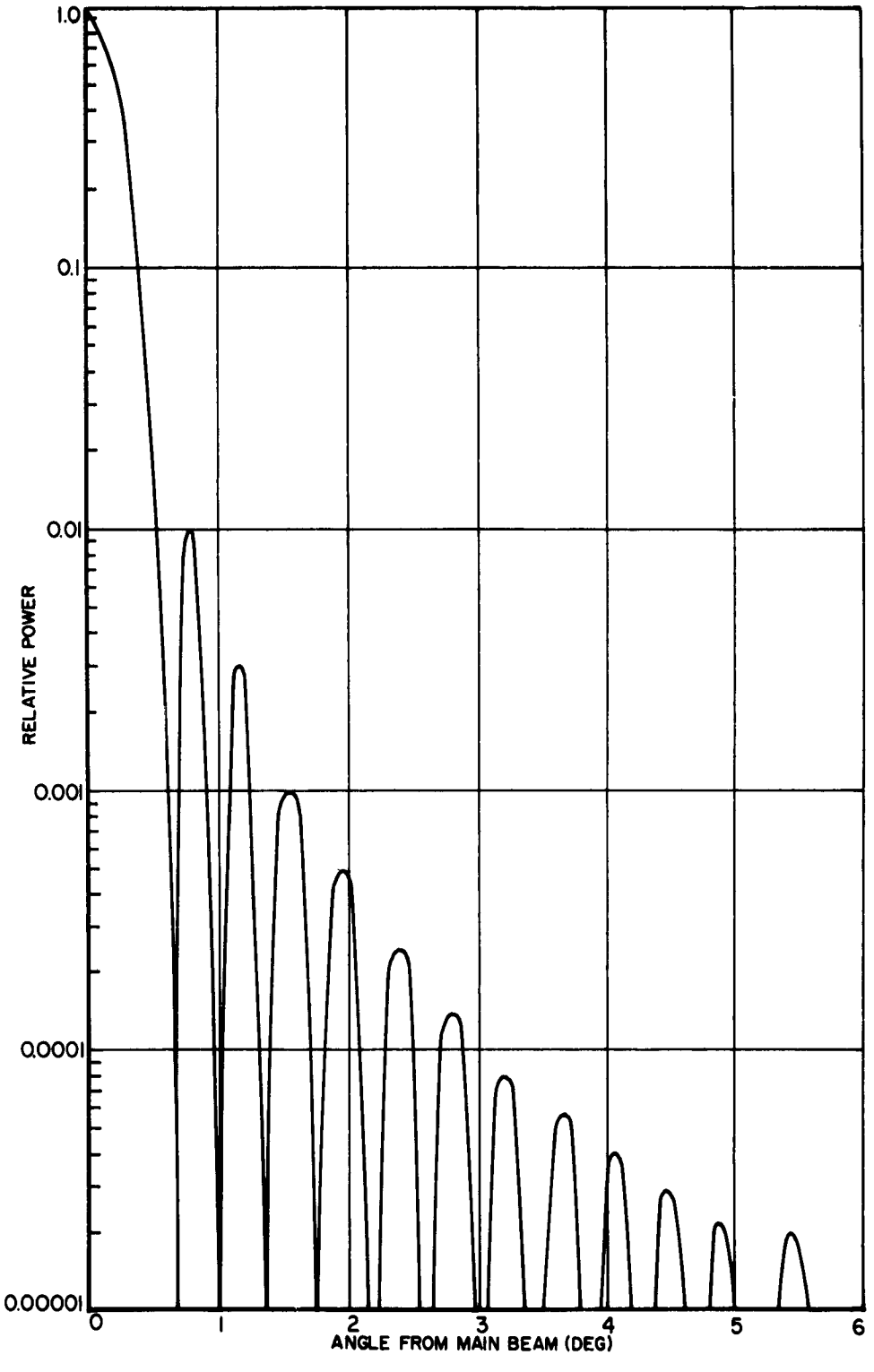

Figure 3-1 Normalized Antenna Power Pattern

Philco WDL. A sample of the power pattern used as input to the computer is shown tabulated in Table 6-3, Section 6.3, of the Appendix. The pattern shape or relative power levels are held invariant with frequency and diameter; that is, pattern detail remains the same except for a scaling factor which stretches or compresses the pattern in angle according to a corresponding decrease or increase of the diameter and/or frequency. For a frequency f_{Mc} in Mc and a diameter D_{ft} in feet, the angular scaling factor is the following:

$$K = \frac{2300}{f_{Mc}} \cdot \frac{60}{D_{ft}} \qquad (3\text{-}2)$$

In addition to the brightness temperature and the antenna pattern, the computer is fed two sets of coordinates which locate the main beam relative to the source. A sample of tabulated distances is given in Table 6-4, Section 6.3 of the Appendix. Attention is directed to the input data form illustrated in Table 6-5 which provides the coding format necessary to expedite the computations of antenna temperature. A sample of the output from the computer is shown in Table 6-6.

In Section 6.4 of the Appendix, several analytical notes relative to coordinate systems and integrations basic to computing antenna temperature due to the sun are presented (Ref. 1).

In Section 6.5 of the Appendix, documentation for the solar-radiation computer program (SUNRAD) is provided (Ref. 2) and should be consulted by the reader in order to appraise himself of the capabilities and limitations of the computer program before using it.

The values of antenna temperature which are available from this study are predicated on negligible absorption in the troposphere and ionosphere. This condition can be realized normally during fair weather and low geomagnetic activity at frequencies between 100 Mc and 10,000 Mc and at elevation angles above 10°. Otherwise, the absolute

absorption and its gradient across the antenna pattern must be taken into account. The absorption of extraterrestial flux will decrease the antenna temperature contributed by the radio noise source, and the lossy atmosphere will generate thermal absorption noise into the antenna. The absorption gradient weights the relative contribution of different parts of the pattern to the total antenna temperature.

The effect of the atmosphere on antenna temperature will be demonstrated in Section 3.4 after the results of solar antenna temperature computations are analyzed and interpreted in Sections 3.2 and 3.3 below.

3.2 SOLAR ANTENNA TEMPERATURE

With a Philco-2000 computer, antenna temperature contributed by non-polarized radiation from the quiet sun has been computed as a function of frequency between 60 Mc and 30,000 Mc and as a function of the angular distance of the sun from the axis of the main beam for circular apertures ranging from 4 feet to 1000 feet.

The choice of reflector sizes is based upon the current or planned uses of these reflectors for space communication and radio astronomy (Refs. 3, 4). Four-foot reflectors characterize directive antennas aboard space probes and may typify steerable reflectors aboard synchronous satellites. Ten-foot reflectors are envisioned for mobile satellite communication stations on land and at sea and on manned orbital space stations. Reflectors with diameters of 30 feet, 60 feet, and 85 feet are familiar as ground station antennas for satellite and space-probe links and as radio telescopes. In addition to existing 85-foot antennas, 210-foot reflectors will eventually become part of the DSIF network for deep-space communication. The 210-foot steerable reflector at the Australian National Radio Astronomy Observatory outside

Sydney and the 300-foot transit reflector at the (American) National Radio Astronomy Observatory in Green Bank, West Virginia, characterize large single-aperture radio telescopes useful up to S-band. The 1000-foot spherical reflector at the Arecibo Ionospheric Research Facility in Puerto Rico will soon be completed.

3.2.1 Results for 2300 Mc

Figure 3-2 shows the solar contribution to antenna temperature of 4-, 60-, 85-, 210- and 300-foot reflectors at 2300 Mc using Swayze's solar models. Both "max" and "min" conditions have been computed for the 85-foot and 210-foot reflectors, whereas only the "min" condition has been computed for the 4-foot, 60-foot and 300-foot reflectors. The "max" and "min" curves characterize possible values of antenna temperature, and no attempt should be made to relate these values to sunspot number.

The subsidiary maxima of the antenna temperature curves of the 60-foot and 85-foot reflectors correspond to a coincidence between the peaks of the antenna side lobes and the limb brightening of the sun's brightness temperature. As the antenna side lobes diminish, this peaking effect becomes negligible. For the same reason, it is absent in the temperature plots for the 210-foot and 300-foot reflectors, whose patterns decrease quickly with angle. In the latter cases, the angle subtended by the sun is much broader than the antenna beams and encompasses the near-in side lobes. Therefore, the antenna temperature curves are dominated by the brightness temperature profile; in fact, their detail is essentially that of the profile. On the other hand, since the beam of the 60-foot reflector is comparable in size to the sun (nearly 0.5 deg.), the antenna temperature curve still displays the influence of the antenna's minor-lobe structure. Similarly, the curve of the 4-foot reflector follows the response of its main beam. It is expected that at greater

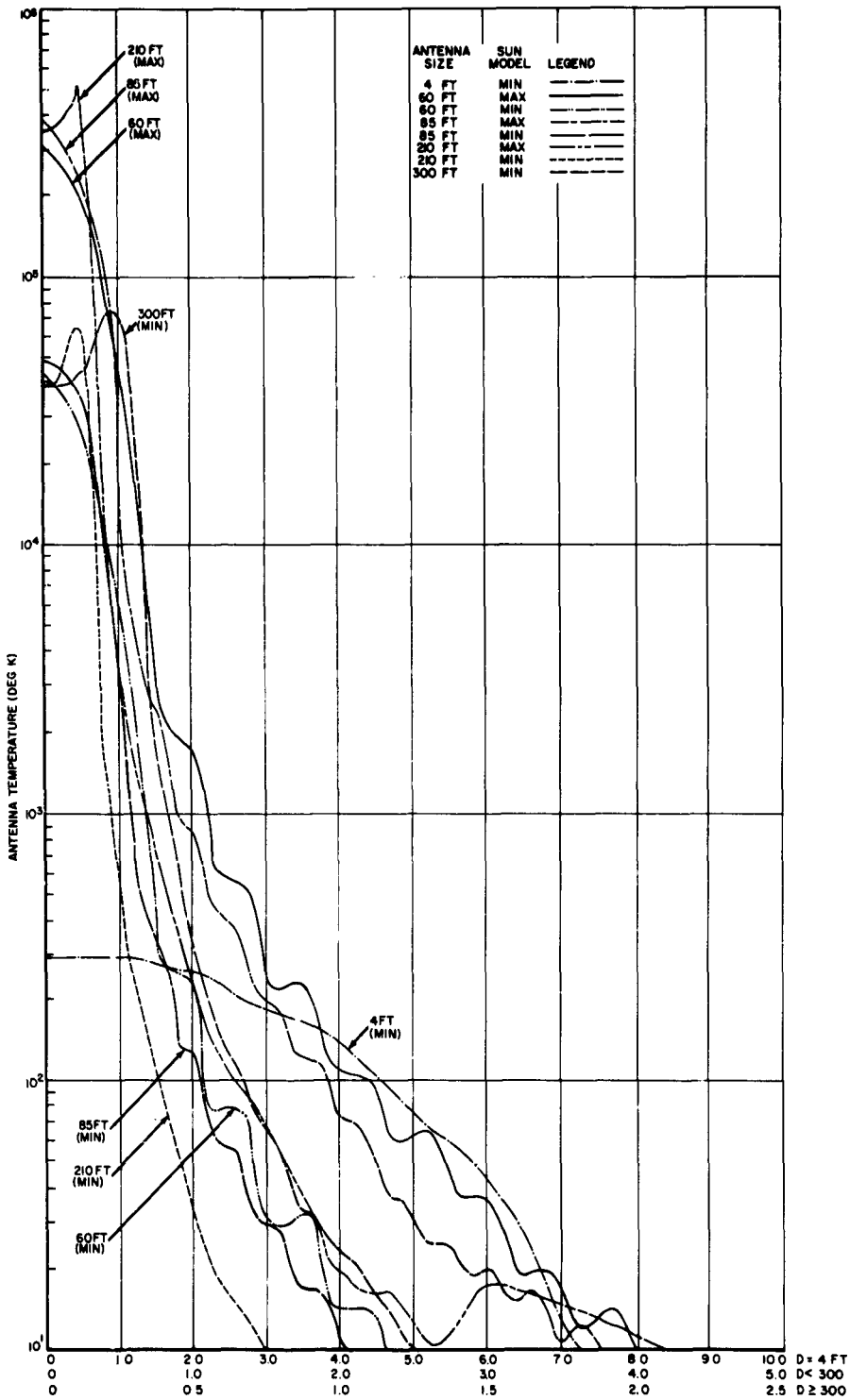

Figure 3-2 Antenna Temperature of Various Reflectors at 2300 Mc vs. Angle off Main Beam

angles the minor lobes of the antenna also determine the variation of antenna noise. Since the beamwidth is much greater than the size of the sun, the sun appears to be nearly a point source.

The on-axis temperatures of the 60- and 85-foot reflectors are somewhat greater than those of the 210- and 300-foot reflectors, because the increased brightness temperature near the limb intercepts a part of the main beam; whereas, for the larger apertures whose main beams fall well within the optical limb, the limb brightening intercepts a part of the pattern which is lower in relative power response. The main beams resolve a lower temperature region on the average. The same might be said in comparing the on-axis antenna temperatures of the 60-foot reflector and the narrower-beam 85-foot reflector. However, in this case, the increased gain of the larger aperture tends to compensate for its resolution of a lower average brightness temperature.

The peaks in the antenna temperature for the 210- and 300-foot reflectors occur at the same angle from the main beam. The curves have been plotted with different angular scales, as indicated on the abscissa.

3.2.1.1 Comparison with Telstar Hornparabola. In a preliminary report on the performance of Telstar I, Bell Telephone Laboratories shows a curve of receiving system noise temperature vs. angle off the center of the sun for the 67-foot hornparabola at 4170 Mc (Ref. 5). As shown in Figure 3-3, the plot is a smooth, monotonic decrease of noise temperature which merges into a system background noise of 33°K. The general feature of the curve agrees with one of the curves in Figure 3-2 for which the diameter-frequency product is nearly the same and the solar profiles are similar in shape: the 85-foot reflector at 2300 Mc. If measurements were to be made at more points and if the curve were then to be drawn through all points rather than smoothed as was done, the type of variations or wiggles shown in Figure 3-2 for the 85-foot reflector would also be apparent for the BTL horn in Figure 3-3.

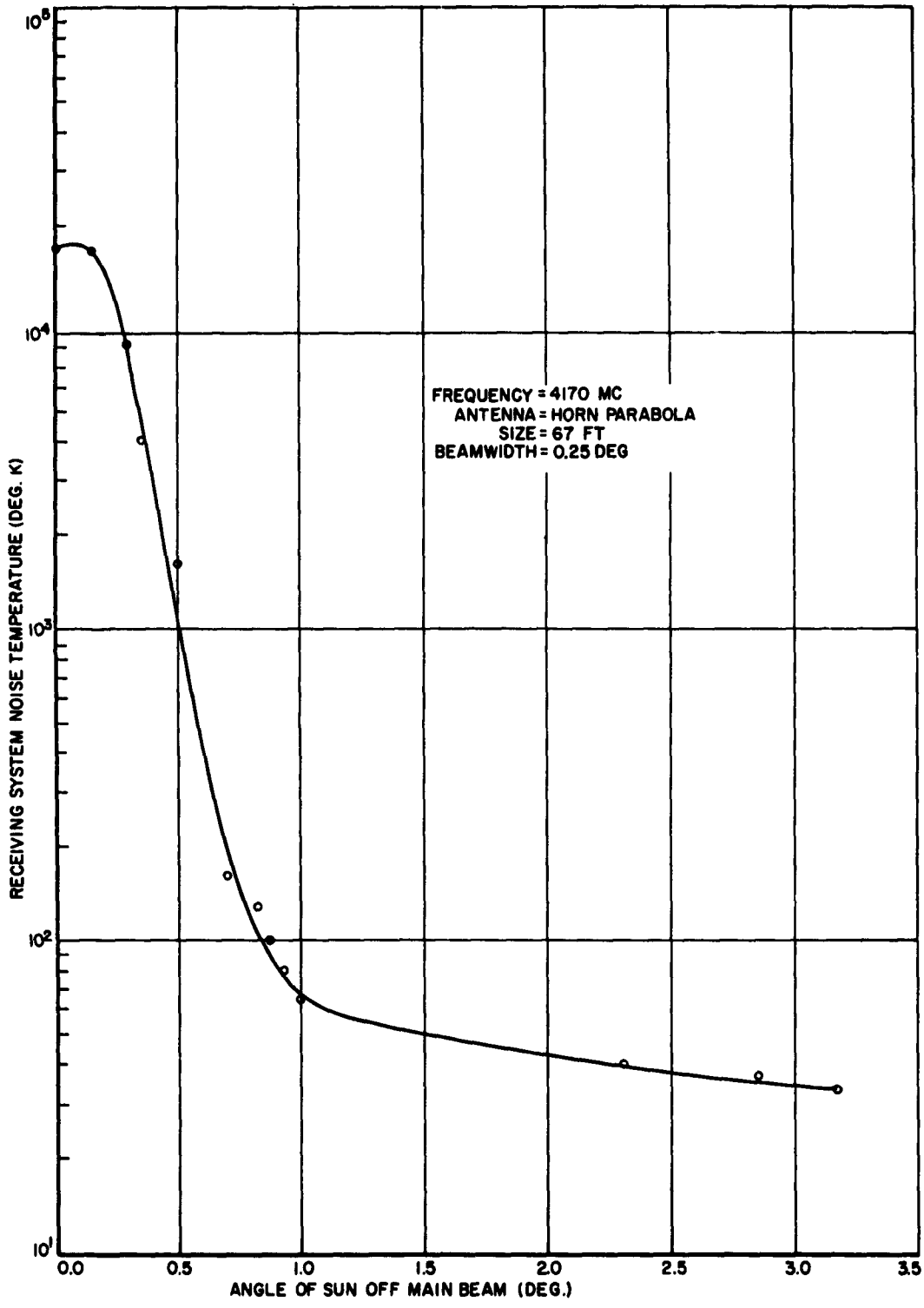

Fig. 3-3 BTL Receiving System Noise Temperature Near the Sun

3.2.2 Results with Smerd's Profiles

Using Smerd's solar model, the antenna temperature of 85- and 210-foot reflectors at 100 Mc has been computed and plotted in Figure 3-4. In addition, the solar antenna temperatures of 30-, 60-, 300- and 1000-foot reflectors have been computed at frequencies between 60 Mc and 30,000 Mc and plotted as a function of angular distance of the sun from the main beam in Figures 3-5, 3-6, 3-7, and 3-8. The curves reflect behavior similar to that observed in Figure 3-2. The mean galactic temperatures are drawn in for comparison.

These plots of antenna noise temperature (and, equivalently, antenna noise power) correspond to antenna power patterns that result when the sun, an extended source rather than a point source, is used in patterning the antenna. In general, the effect of an extended radiator upon an antenna pattern is to fill in the nulls, lower the side lobes, and broaden the main beam.

3.2.2.1 Beam Broadening. From the curves of Figures 3-2 to 3-8, relative beam broadening, or the ratio of the angular width at the half-temperature points to the half-power antenna beamwidth, is plotted as a function of diameter and of frequency in Figures 3-9 and 3-10 respectively. The BTL value appears to be 2.4 for the 67-foot horn at 4170 Mc with an average half-power beamwidth of 0.25 deg.

One will notice from Figure 3-10 that the same diameter-to-wavelength ratios, or alternately the diameter-frequency products, yield the same beam broadening, except at 100 Mc and 2300 Mc. The difference in beam broadening at 2300 Mc can be attributed to the difference in solar model at this frequency. However, the similarity in the shape of the curve remains because the profiles at UHF and microwave frequencies are similar in their limb brightening features. At 100 Mc, however, the

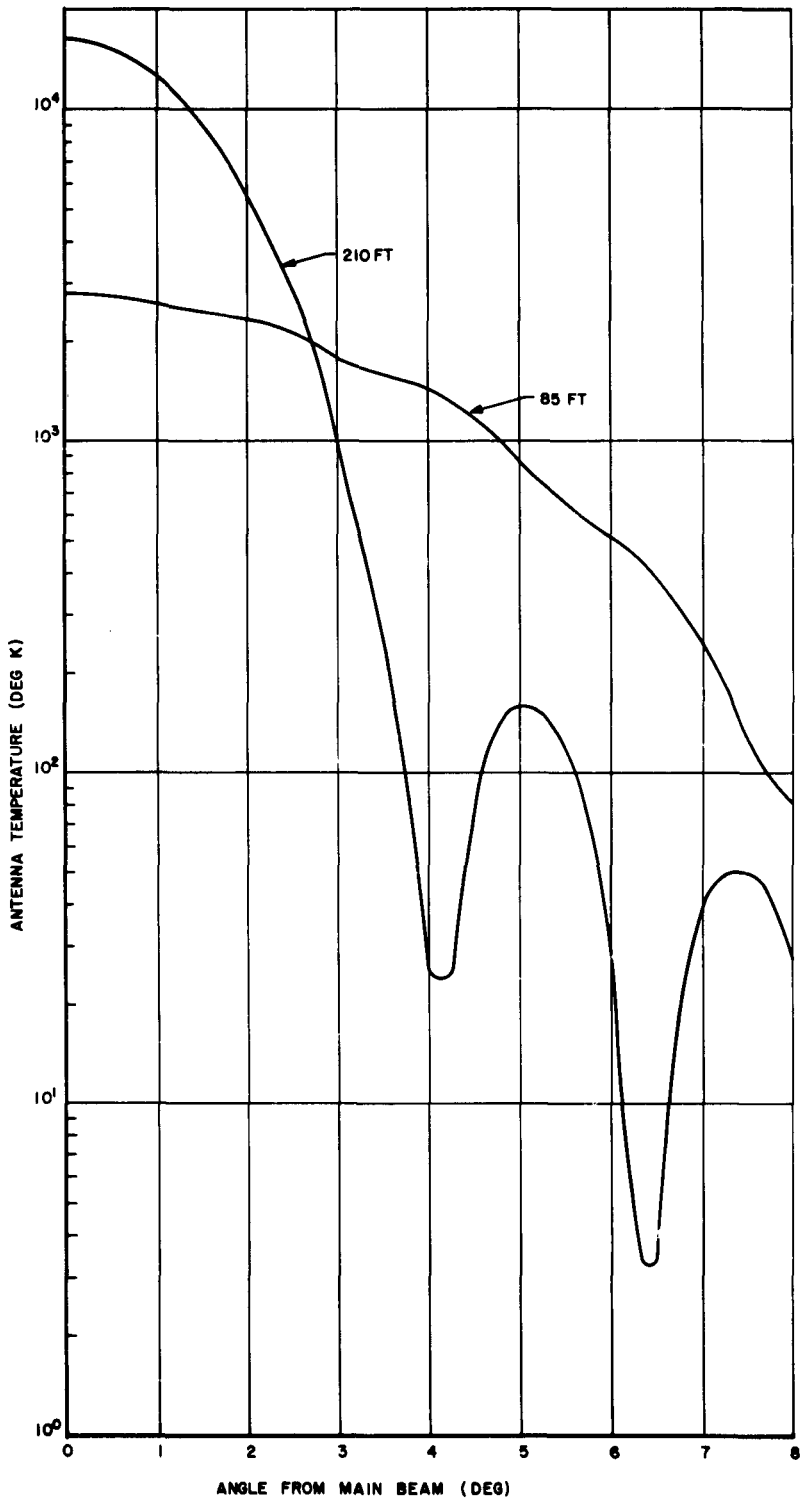

Figure 3-4 Antenna Temperature of 85- and 210-Foot Reflectors at 100 Mc vs. Angle off Main Beam

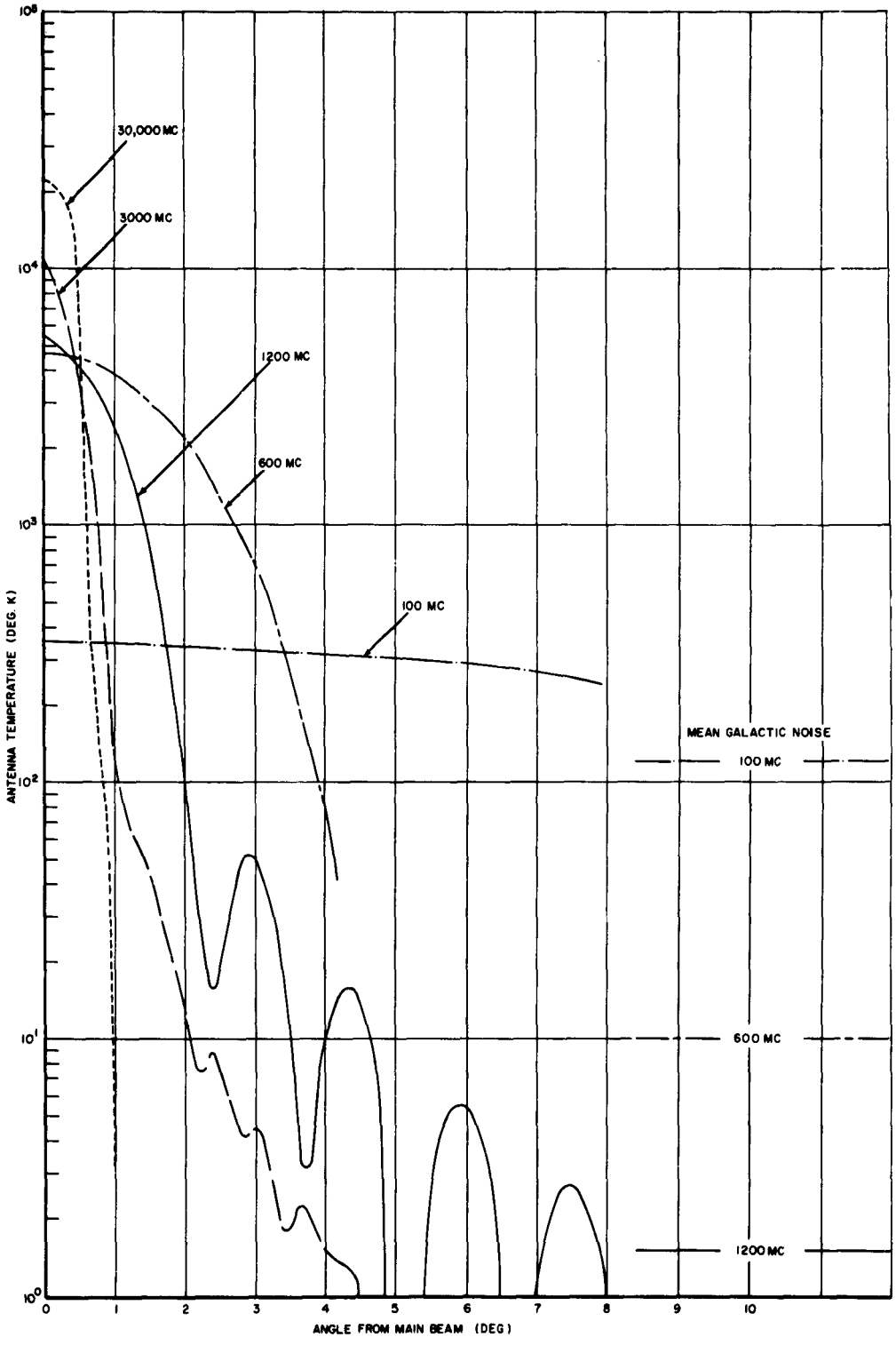

Figure 3-5 Antenna Temperature of 30-Foot Reflector vs. Angle off Main Beam

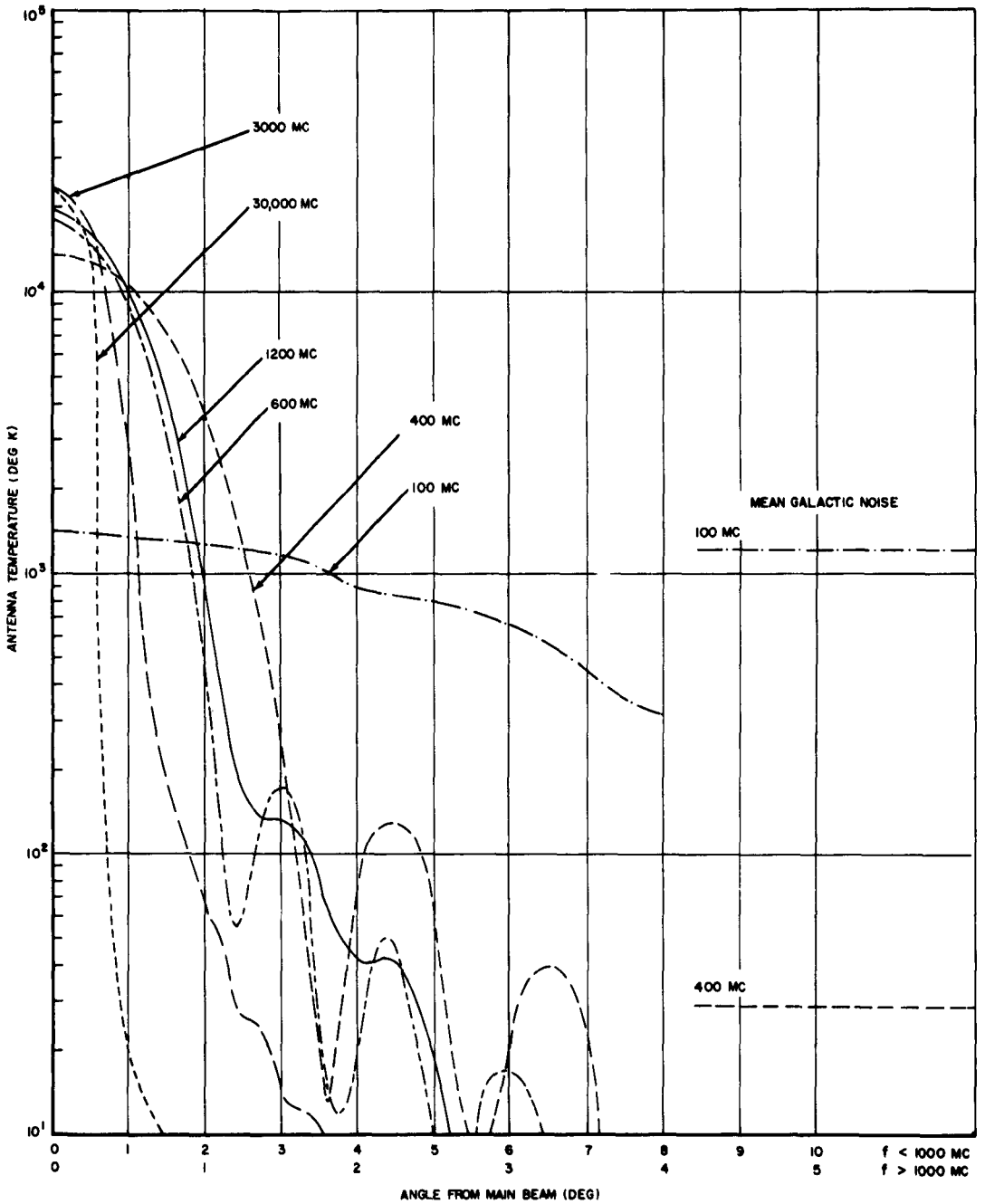

Figure 3-6 Antenna Temperature of 60-Foot Reflector vs. Angle off Main Beam

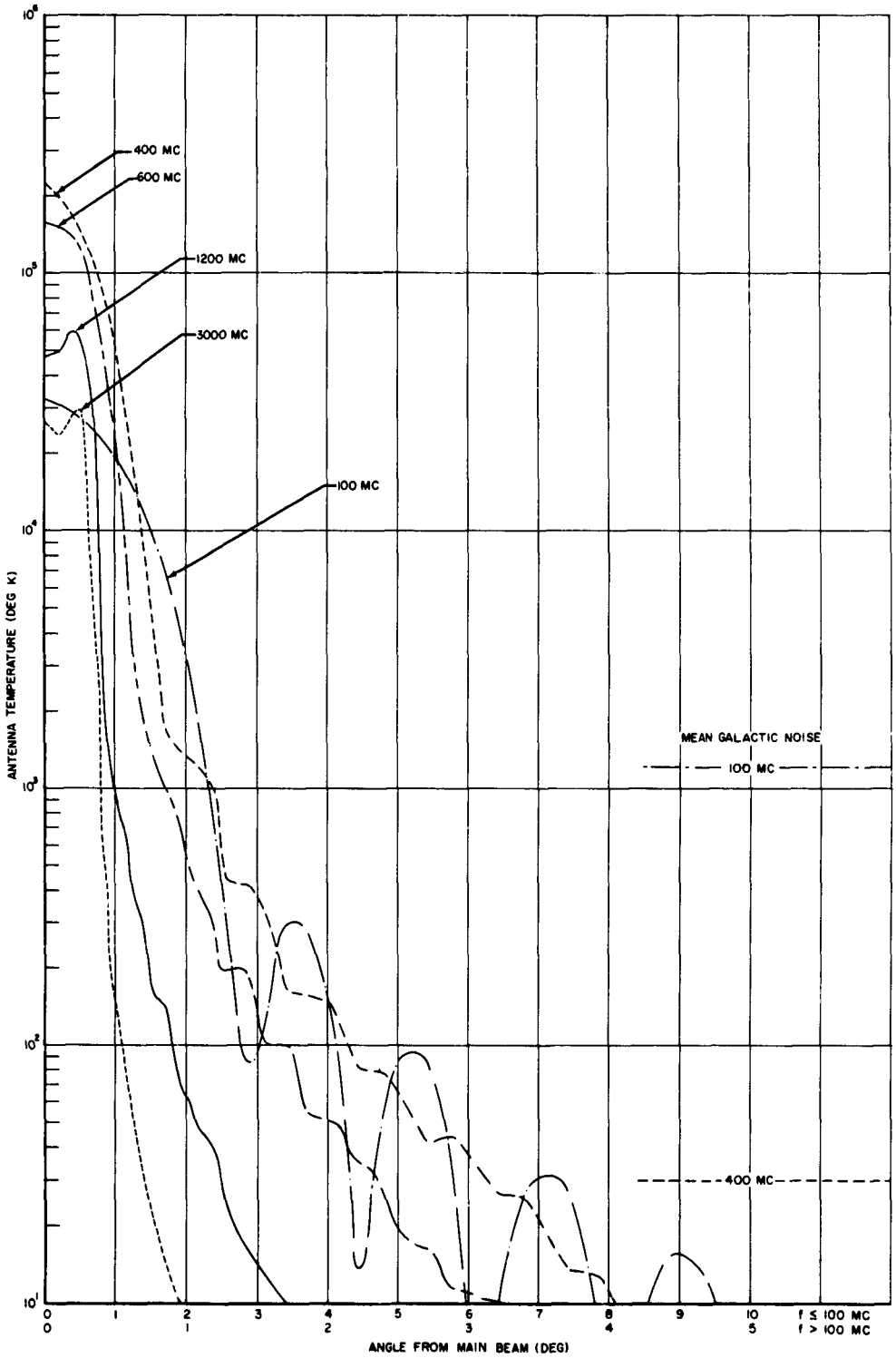

Figure 3-7 Antenna Temperature of 300-Foot Reflector vs. Angle off Main Beam

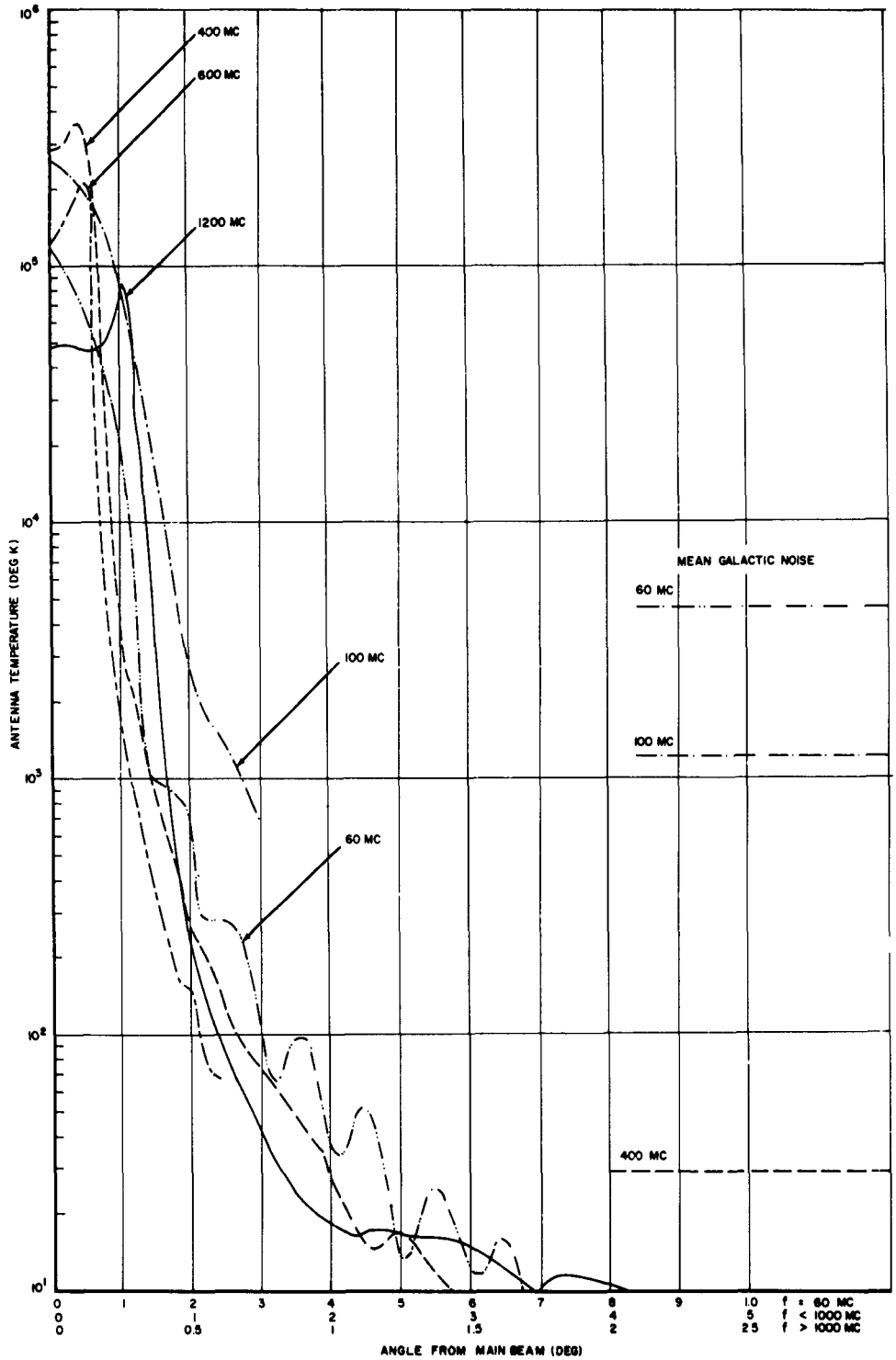

Figure 3-8 Antenna Temperature of 1000-Foot Reflector vs. Angle off Main Beam

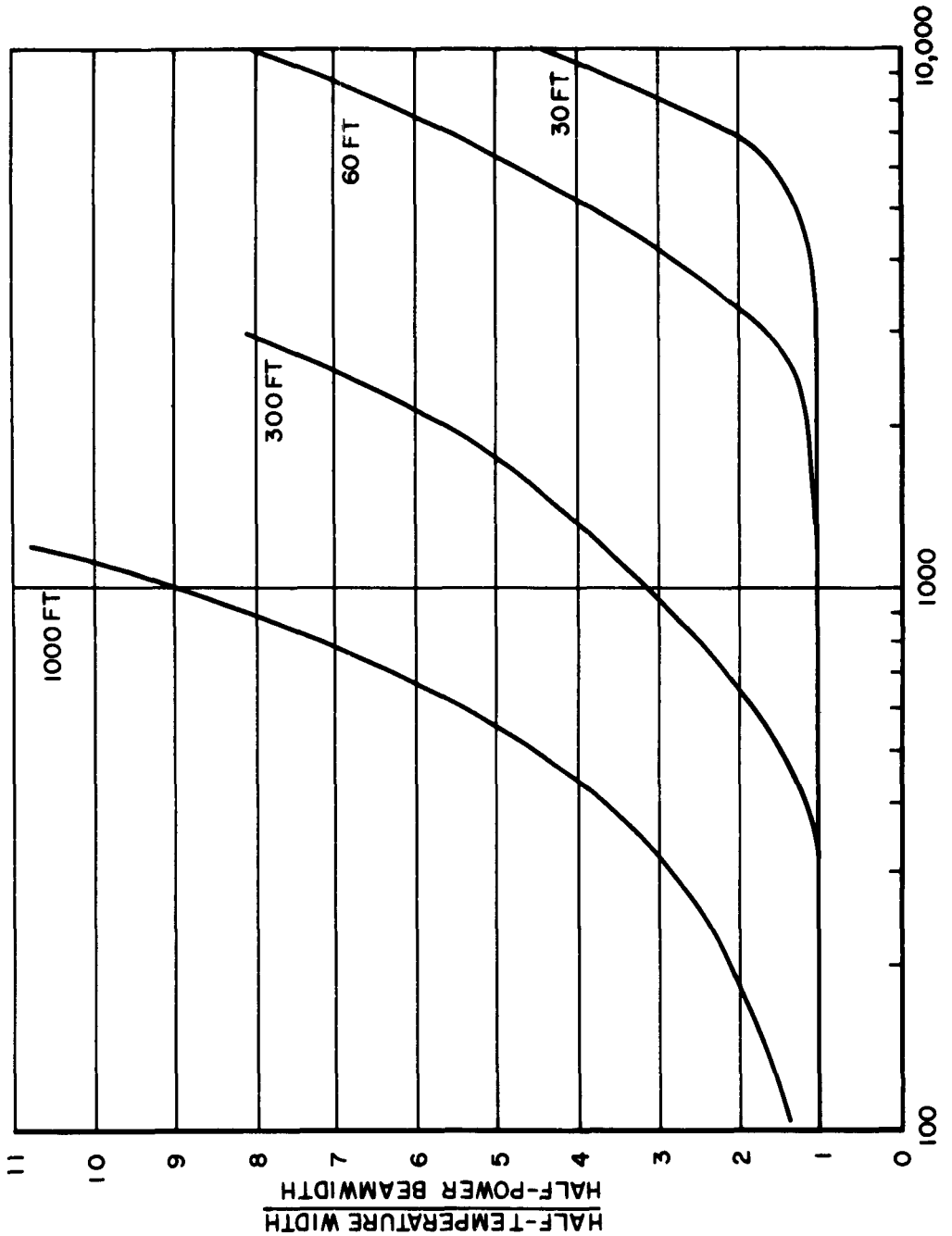

Figure 3-9 Relative Beam Broadening vs. Frequency

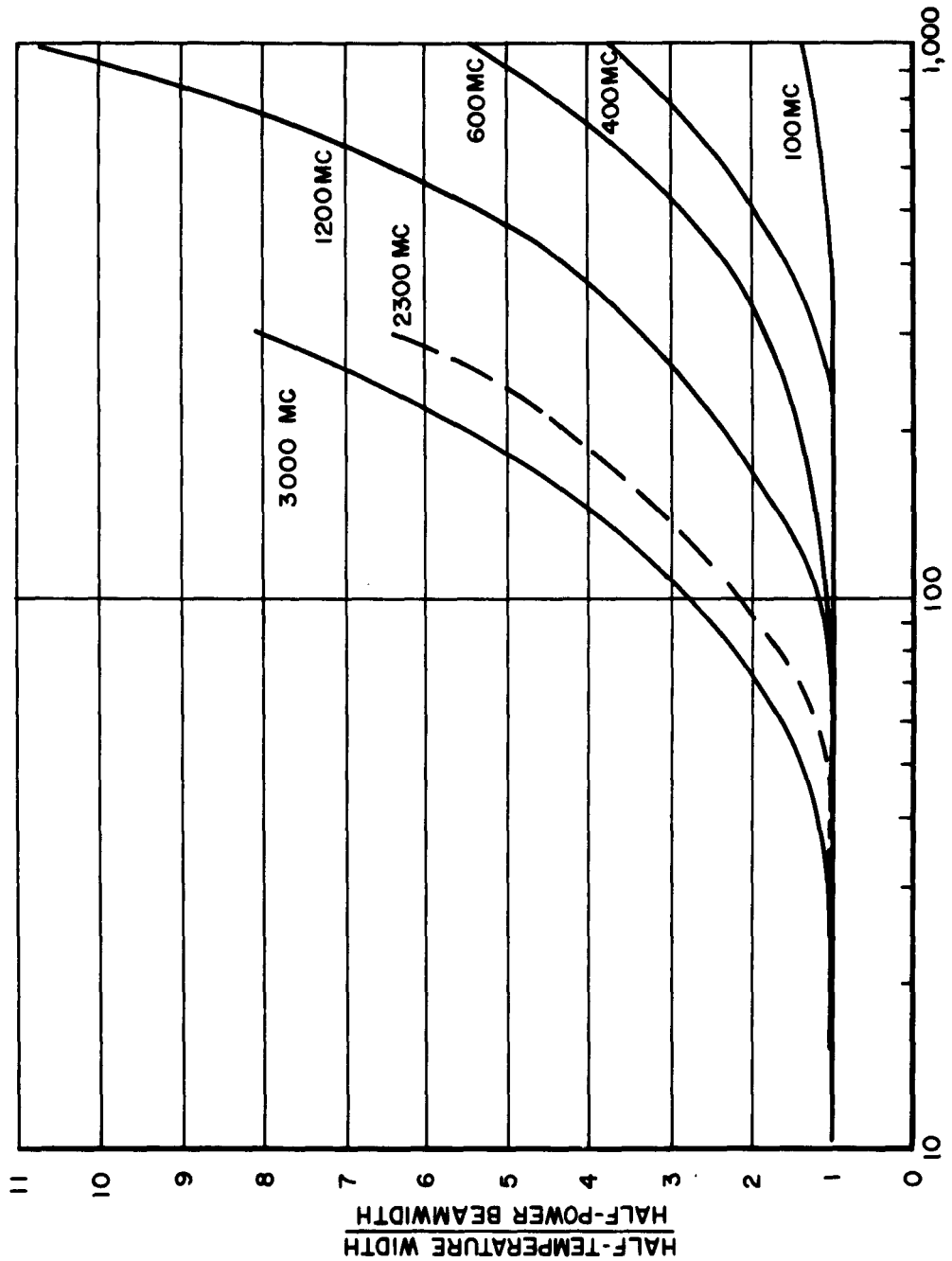

Figure 3-10 Relative Beam Broadening vs. Diameter

profile monotonically decreases and will lead to a beam broadening which is not the value expected when one scales down from the higher frequencies. For example, the 1000-foot/100-Mc beam broadening of 1.4 does not equal the 250-foot/400-Mc value of 1.05.

3.2.2.2 Locations of Nulls and Peaks. The locations of nulls and peaks on the curves of antenna temperature will depend on frequency, and therefore will be different even for the same diameter-frequency product. For example, the 60-foot/3000-Mc antenna temperature curve in Figure 3-6 and the 300-foot/600-Mc curve in Figure 3-7 do not exhibit maxima and minima at the same angles.

In general, at microwave frequencies where limb brightening is pronounced, the locations of nulls and peaks will not correspond to the nulls and peaks of the antenna pattern and may even be inverted. For example, the pattern of the 60-foot reflector at 2300 Mc in Figure 3-1 exhibits nulls and minor lobes at angles which produce respectively the maxima and minima of antenna temperature shown in Figure 3-2. In contrast, the 30-foot reflector at 1200 Mc produces the antenna temperature curve shown in Figure 3-5, whose minima and maxima occur at angles only 0.2° away from where the nulls and minor lobes of the 30-foot pattern occur. The smaller the diameter-frequency product, the smaller will be the deviation, because the product of the brightness temperature profile and the broad-beam pattern (whose integral determines the antenna temperature) will be less sensitive to variations of the temperature profile.

3.2.2.3 Antenna Temperature On-Axis. From Figures 3-4 to 3-8, on-axis antenna temperatures due to solar radiation are plotted vs. frequency on Figure 3-11. In general, as the frequency increases, the antenna temperature rises toward the average brightness temperature across the sun. The on-axis temperatures of the larger apertures peak up noticeably, and then decrease to converge ultimately to a value

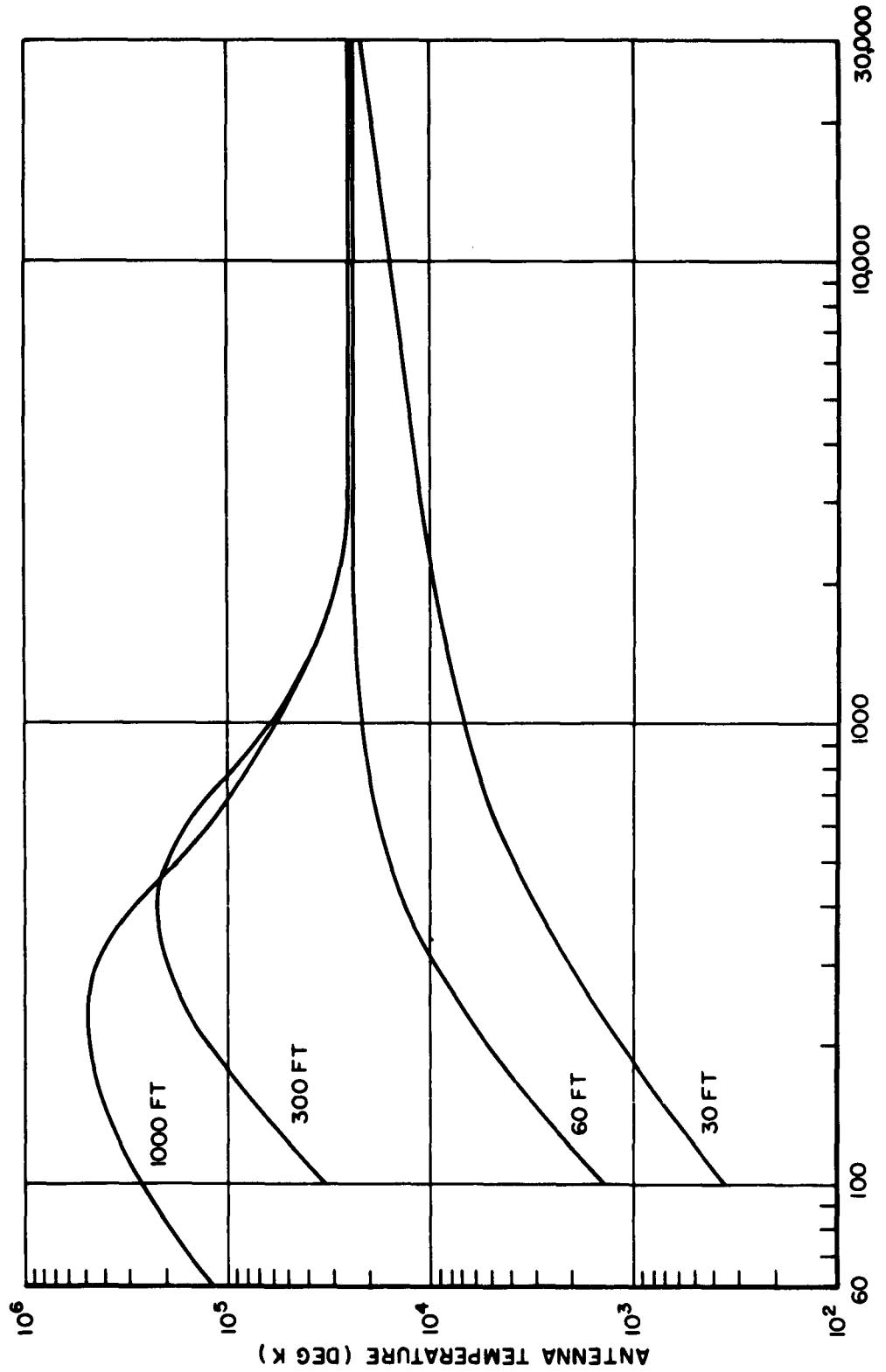

Figure 3-11 On-Axis Antenna Temperature vs. Frequency

which all reflector sizes will approach at extremely high frequencies. At these frequencies the significant portion of the patterns is essentially enveloped by the on-axis temperature region; the antenna temperatures are therefore equal to the average solar brightness temperature around the center of the sun (See Eq. 6-12 in Section 6.2 of the Appendix). The maxima occur usually at frequencies for which the antenna beamwidth is close to the half-temperature width of the radio sun.

In Figure 3-12 the on-axis temperature rises with an increase of reflector diameter and generally levels off after exhibiting a small maximum. The apparent exception is the curve for 100 Mc which shows nearly a square-law behavior. It too, however, will taper at diameters of several thousand feet. The behavior at 2300 Mc is indicated by a dashed curve to emphasize that it is based on a solar model different from the one for which the others were computed. Nevertheless, the curves are similar, as expected from a comparison of Swayze's 2300 Mc profile in Figure 3-4 with Smerd's 1200-Mc and 3000-Mc profiles in Figure 2-3.

3.2.2.4 Antenna Temperature Off-Axis. Corresponding graphs of antenna temperature vs. frequency and diameter for the sun at 1° off the main beam have been constructed. The variation of temperature with frequency in Figure 3-13 is irregular. The very large apertures indicate a decrease of temperature with increasing frequency. On the other hand, the medium-sized apertures show a peaking effect before displaying a corresponding decrease with frequency. A maximum will occur at all diameters. Figure 3-14 indicates a general decrease of antenna temperature with increasing reflector diameter. A maximum will occur at all frequencies. More points would help to define better the curves in both figures. For example, the 400-Mc curve in Figure 3-14 is in doubt between 60 feet and 300 feet, and may peak up between 85 feet and 100 feet.

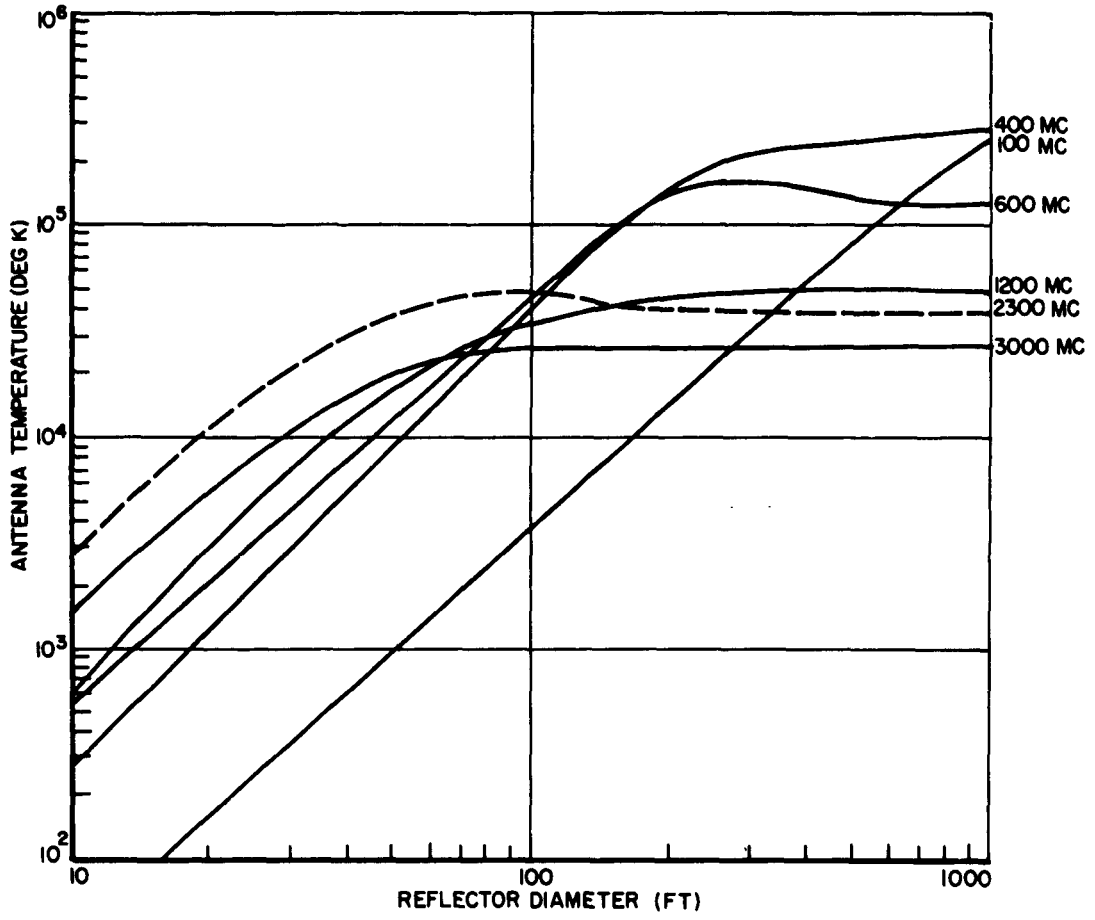

Figure 3-12 On-Axis Antenna Temperature vs. Diameter

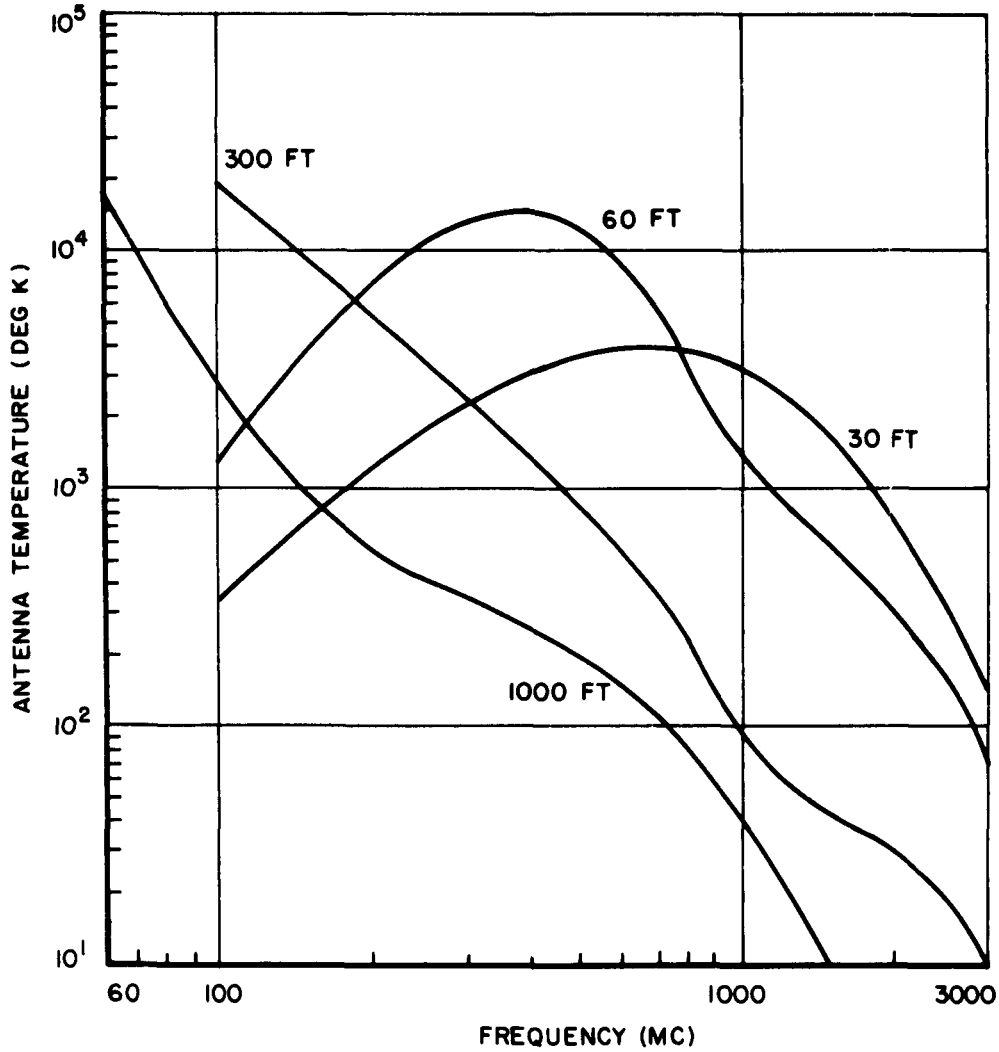

Figure 3-13 Antenna Temperature for Sun 1° off Main Beam vs. Frequency

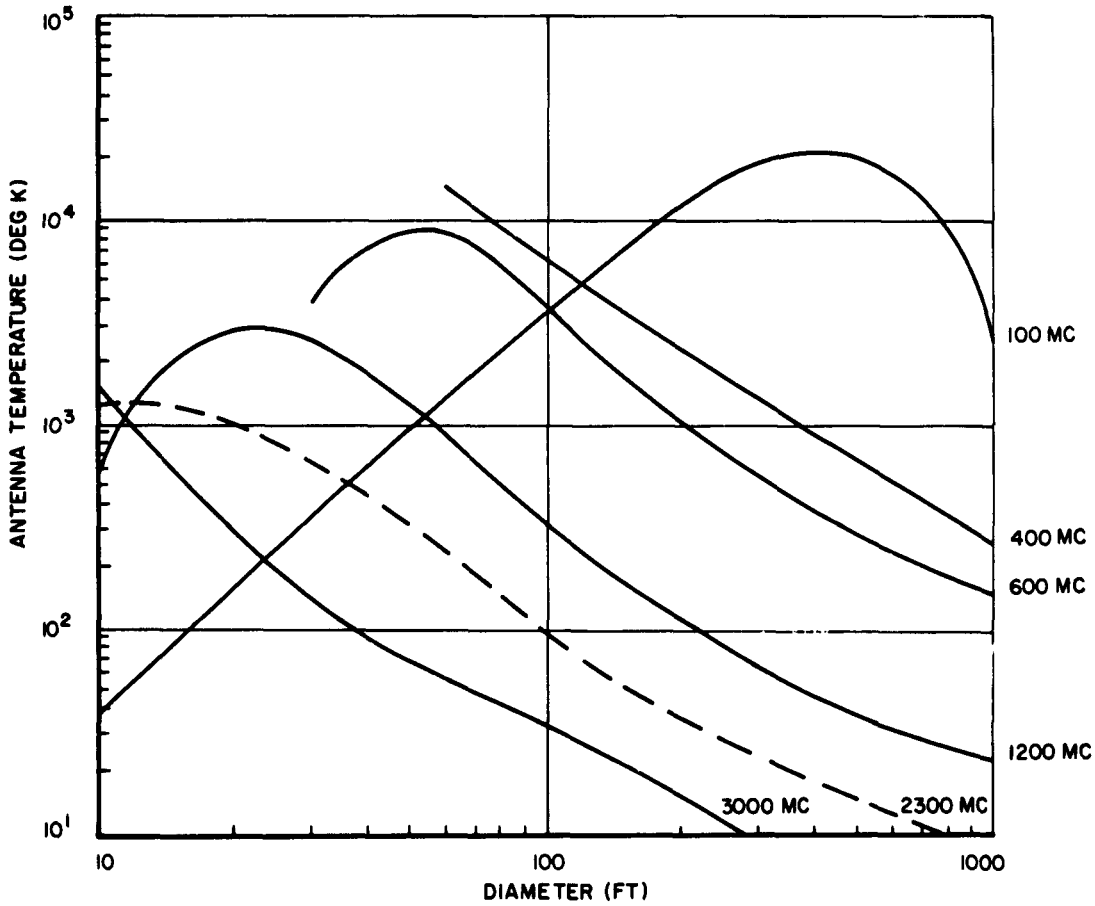

Figure 3-14 Antenna Temperature for Sun 1° off Main Beam vs. Diameter

3.3 EFFECTS OF OTHER EXTRATERRESTRIAL SOURCES

From prior work by the author on the influence of extraterrestrial sources upon antenna temperature (Ref. 6), one can now compare the contribution of the sun to antenna temperature with the contribution of other extraterrestrial sources. In Figure 3-15, the variation with frequency of the antenna temperature of a 60-foot reflector due to solar radiation on-axis (see Figure 3-11) is compared with antenna temperatures due to the following sources: (1) on-axis radiation from the radio stars Cassiopeia-A and Taurus-A, from the moon, and from the planets Venus, Mars and Jupiter; (2) maximum radiation from the galaxy for the reflector pointed at an equatorial synchronous satellite and for the reflector pointed at a space probe along the ecliptic; (3) mean radiation from the galaxy, labeled "galaxy-isotropic antenna." At frequencies above 100 Mc. the sun is the major source of noise. Below 100 Mc, the galactic background and radio stars will predominate.

Burst radiation from the sun (Figure 2-6) will raise the normal solar antenna temperature from one to three orders of magnitude, depending upon frequency and solar activity. For example, a burst flux density of 2×10^{-19} watts/meter^2/cps at 2300 Mc will raise the on-axis antenna temperature of a 60-foot reflector to nearly 2.5×10^6°K.

The predicted on-axis antenna temperature at 2300 Mc of 83°K due to Cassiopeia-A is matched closely by the value of 87°K measured with the Philco WDL 60-foot telemetry-and-data antenna (Ref. 7). The maximum antenna temperature due to galactic radiation is 3.5°K along the synchronous satellite path; whereas the mean antenna temperature is 0.27°K, which is about twice the minimum temperature expected along this path. The mean lunar antenna temperature for a

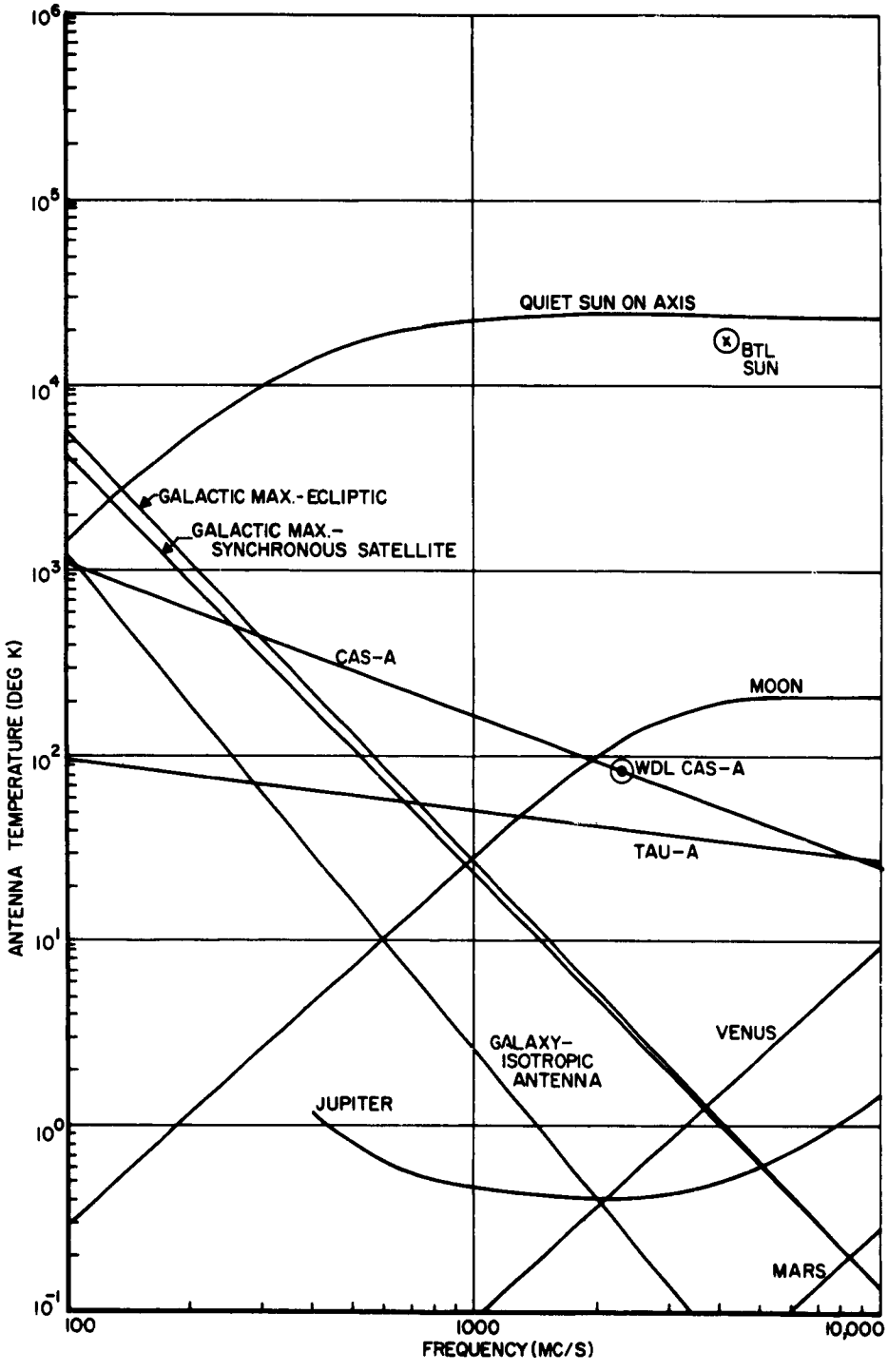

Figure 3-15 Comparative Antenna Temperatures of 60-Foot Reflector

disc size of 31' (9 mr) is 125°K. For Venus with a maximum disc size of 61.4" at inferior conjunction, the antenna temperature is 0.48°K; for Mars with a maximum disc size of 17.9" at opposition, the temperature is 0.015°K. At the same frequency of 2300 Mc, the Jovian antenna temperature will be 0.4°K from an apparent disc diameter of 46.5" in 1963.

A similar comparison of antenna temperatures is shown in Figure 3-16 for a 300-foot reflector and in Figure 3-17 for a 1000-foot reflector. The sun still predominates at UHF and microwave frequencies. The distant planets contribute very little, even for a 1000-foot reflector. For example, an average value for the noise temperature of a 1000-foot reflector due to Saturnal radiation at 2300 Mc should be less than 3°K. According to estimates by Coutrez (Ref. 8) of thermal radiation from the outer three planets, the antenna temperatures of a 1000-foot reflector at 2300 Mc should be at most 0.07°K for Uranus (3.62" disc size), 0.02°K for Neptune (2.12" disc size), and 0.001°K for Pluto (0.52" disc size).

3.4 EFFECTS OF THE ATMOSPHERE AND GROUND

If, while tracking a satellite or a probe, the antenna beam approaches the sun at an antenna elevation angle of about 10°, the effect of the atmosphere on signal and noise levels will be small at frequencies between 100 Mc and 10,000 Mc during normal weather and low geomagnetic activity. At lower angles, however, adjustments must be made.

The effect of a lossy atmosphere is to attenuate extraterrestrial radiation and to generate thermal noise consistent with the ambient temperature and loss. In order to adjust the antenna temperature along the main-beam axis to include atmospheric absorption at microwave frequencies, where the beamwidths are narrow for the large reflector sizes considered, it is sufficient to divide the antenna temperature by

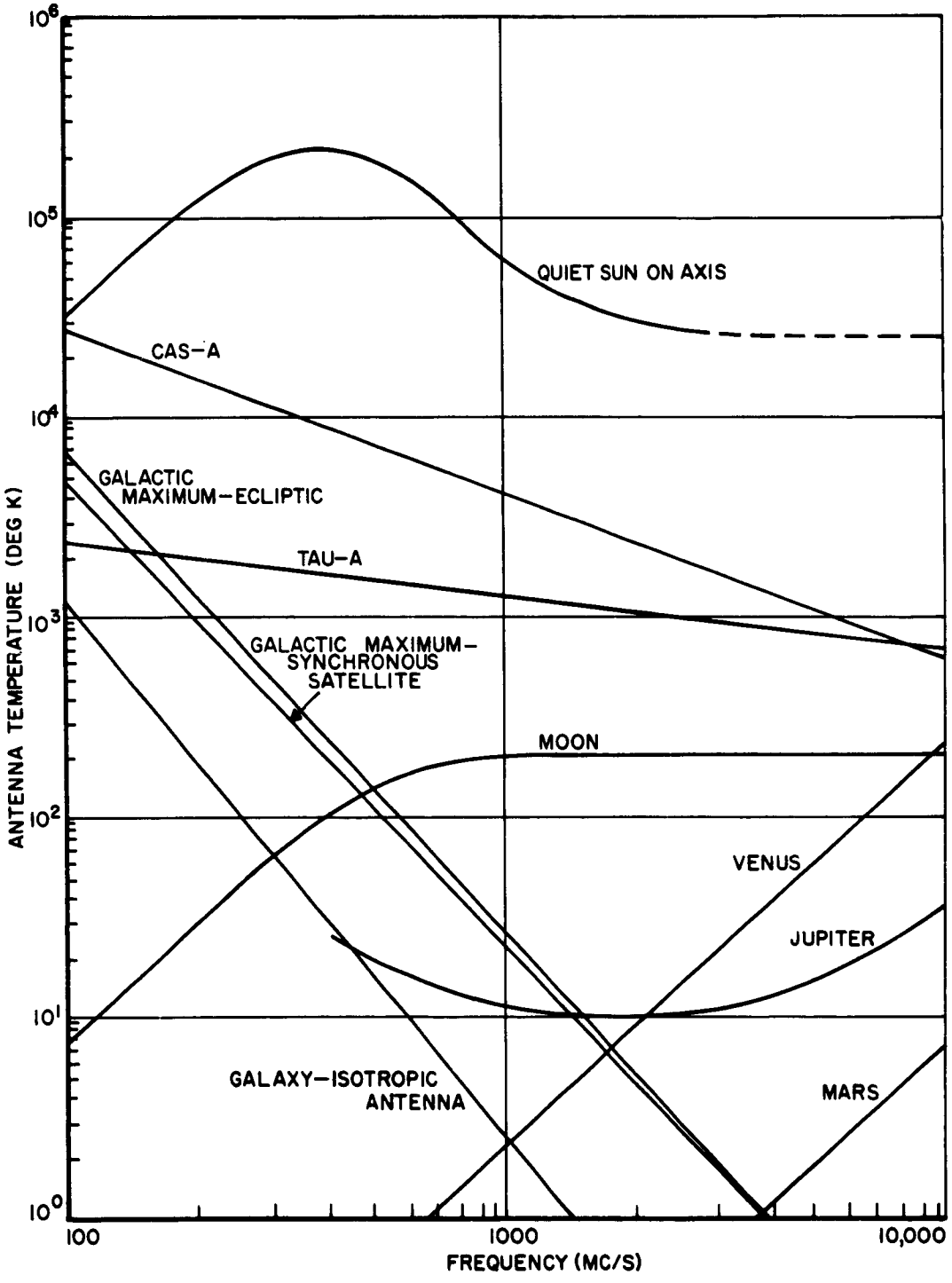

Figure 3-16 Comparative Antenna Temperatures of 300-Foot Reflector

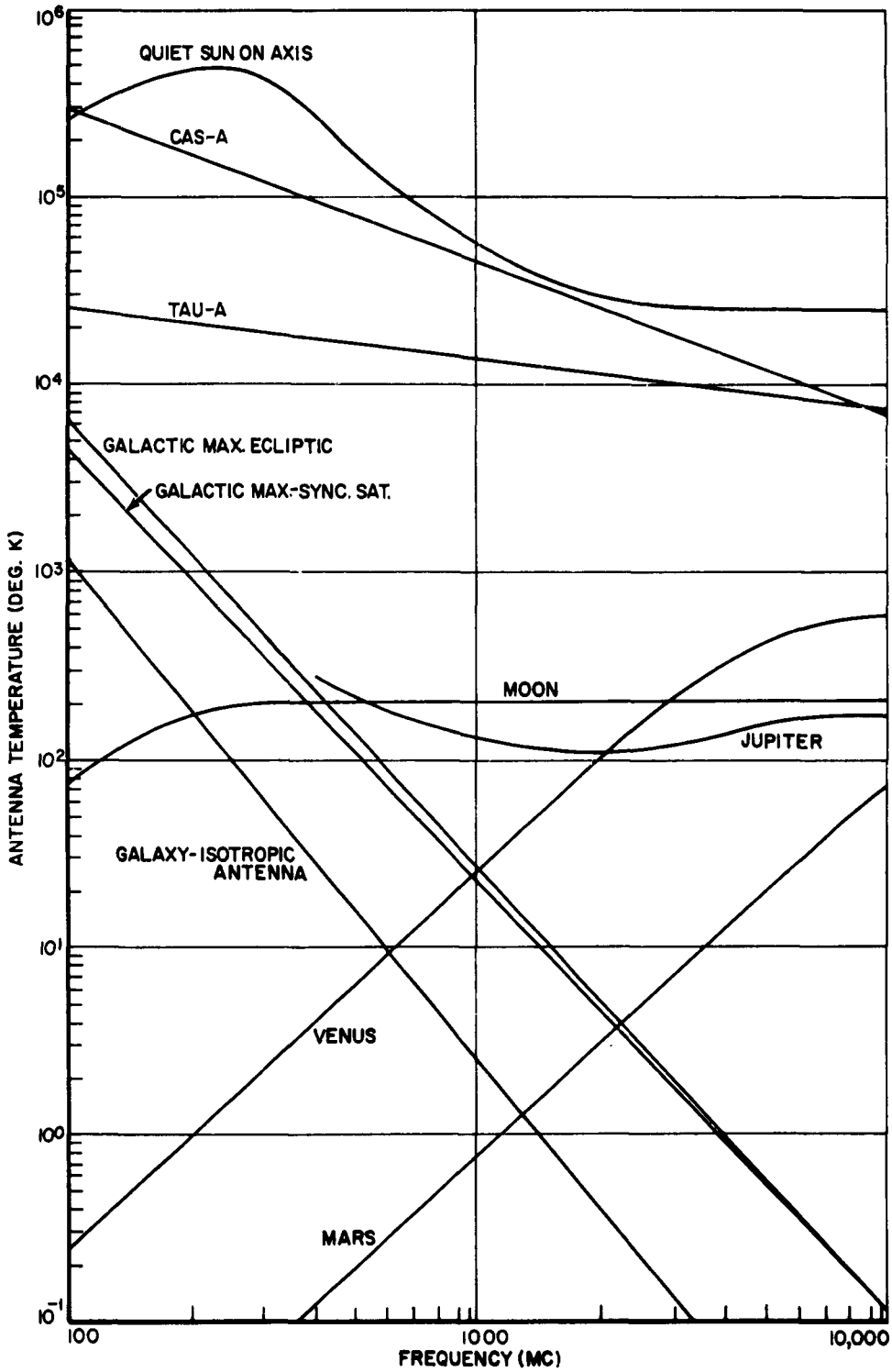

Figure 3-17 Comparative Antenna Temperatures of 1000-Foot Reflector

the loss through the atmosphere at the antenna pointing angle and to add a thermal noise term based on a mean atmospheric temperature. For extended sources such as the sun, the angular distribution of atmospheric loss and thermal noise is required.

When the earth's atmosphere significantly interposes itself between the antenna and extraterrestrial noise sources, a general expression for the apparent brightness temperature surrounding an antenna at a given frequency is the following:

$$T_b(\theta, \varphi) = \frac{T_s(\theta, \varphi)}{L_{atm}(\theta, \varphi)} + T_{atm}(\theta, \varphi) \qquad (3\text{-}3)$$

where T_s is the distribution of noise sources, L_{atm} is atmospheric absorption, and T_{atm} is the distribution of atmospheric absorption noise, often referred to as "sky noise temperature." Figure 3-18 shows one-way attenuation through the troposphere and ionosphere for normal daytime propagation and summer weather in the temperate zones (Ref. 9). Attenuation is plotted vs. frequency for several elevation angles. Figure 3-19 shows the corresponding brightness temperature of the atmosphere.

The ground also generates thermal noise. Figure 3-20 illustrates the geometry for antenna temperature calculations in which the main beam of an antenna, located at a height h above a spherical earth, is directed at some angle θ_o measured from the zenith. Ground thermal radiation arrives at the antenna from all angles roughly within the hemisphere below the antenna. Figure 3-21 shows the variation of apparent ground temperature with elevation angle at 2300 Mc for soil with the electrical properties of a coarse-grained, sandy-silt mixture.

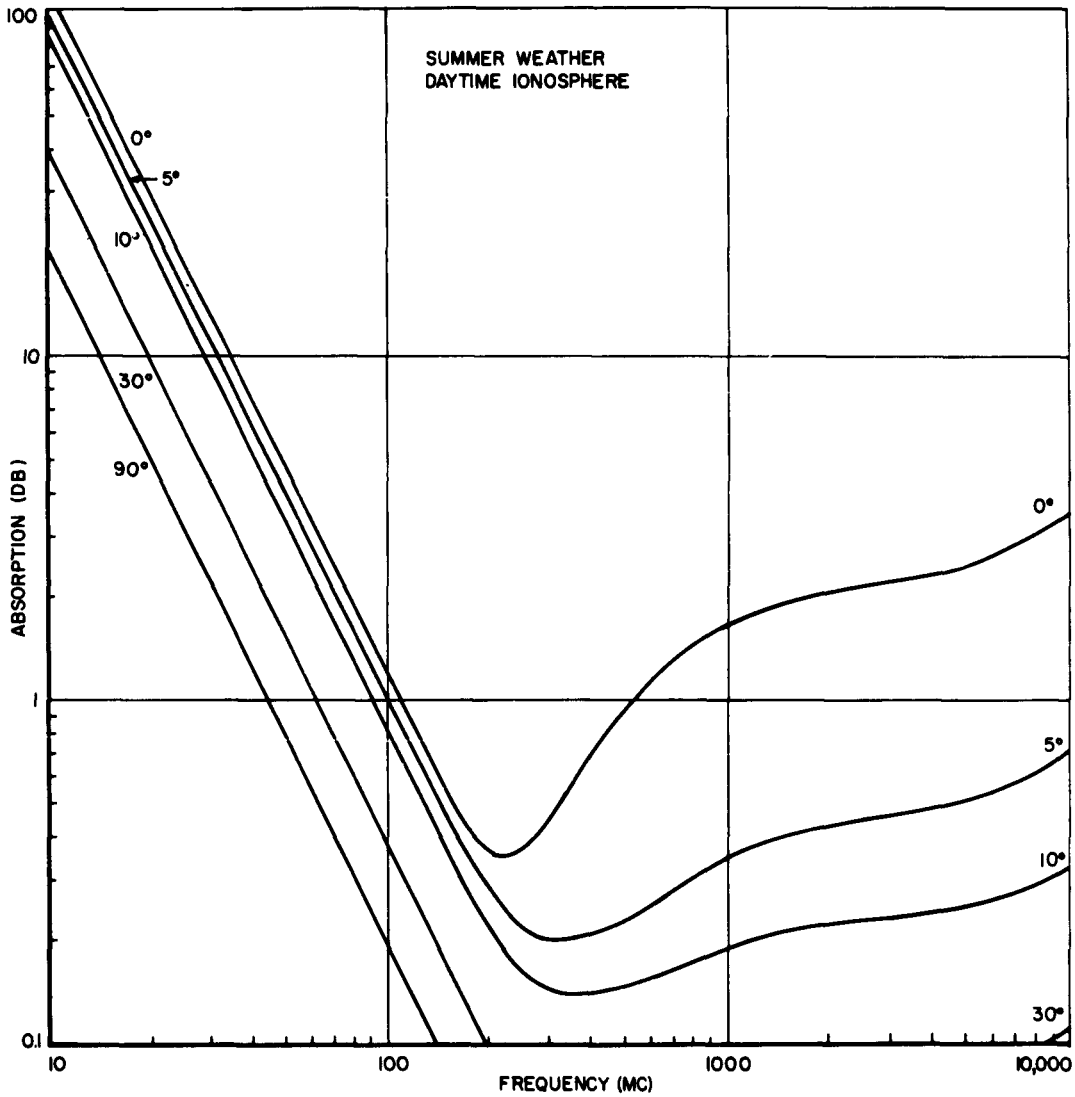

Figure 3-18 Absorption of Signal through the Total Atmosphere

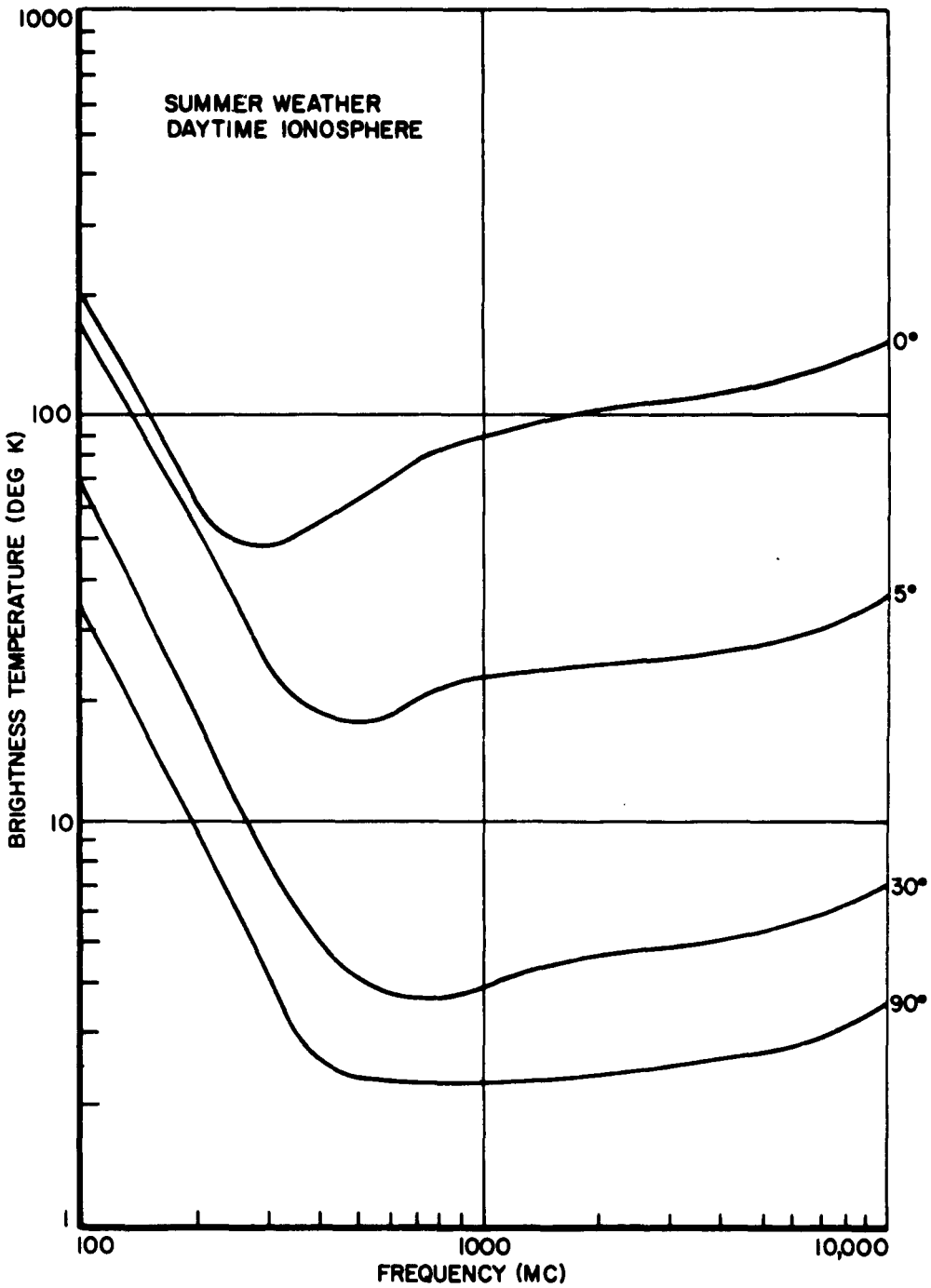

Figure 3-19 Brightness Temperature of the Atmosphere

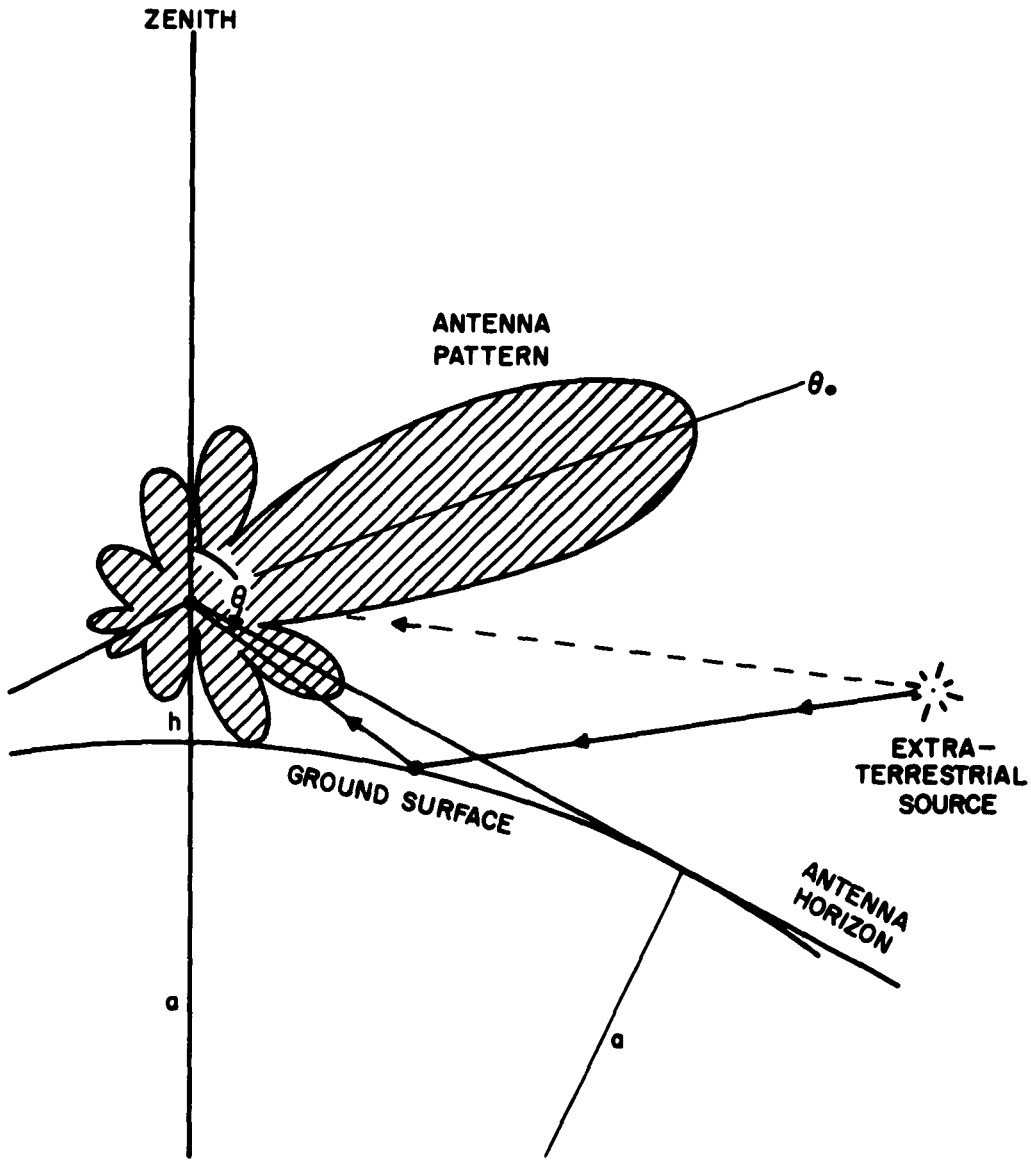

Figure 3-20 Geometry for Antenna Temperature

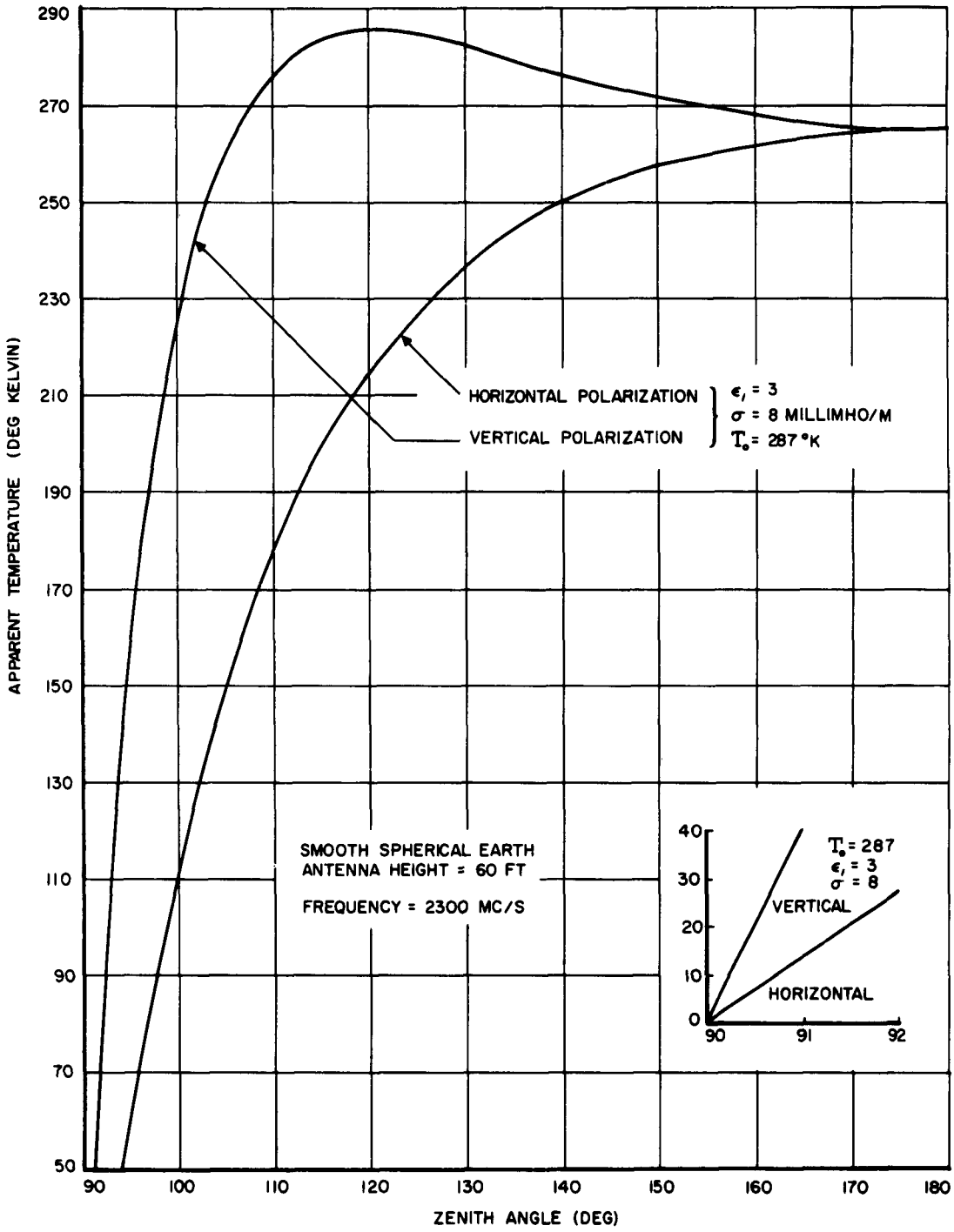

Figure 3-21 Apparent Temperature of the Ground

The combined effect of atmospheric and ground radiation upon antenna temperature is shown as a function of elevation angle in Figure 3-22 for a 60-foot reflector at 2300 Mc. The solid curve labeled "vertical polarization" and the short dashed curve below 2.5°, labeled "horizontal polarization," are the results of computation. The two dashed curves through the data points are the results of a measurement program carried out on a Philco WDL paraboloid with two different feeds (Ref. 7). The curve through the solid circles is the variation of antenna temperature with a 8.5-db feed taper; the curve through the open circles is for a 15-db taper. The agreement between the curves calculated for a smooth, homogeneous surface and the measurements for a rough surface is reasonable.

If the 60-foot reflector points toward the sun at an elevation angle of 5°, the solar antenna temperature values of the "min" curve in Figure 3-2 will be reduced by atmospheric absorption. Adding this reduced solar antenna temperature to the background antenna temperature of 42°K from Figure 3-22 gives the total antenna temperature curve shown in Figure 3-23. A similar curve has been constructed for the 300-foot reflector by using the same background temperature. The slight asymmetry in both curves is due to the atmospheric absorption gradient across the antenna pattern from horizon to zenith. During foggy or rainy weather at higher frequencies or during intense ionospheric absorption at much lower frequencies, the asymmetry would be more pronounced.

Similar curves can be developed for other antenna sizes at frequencies for which solar brightness temperature profiles have been derived.

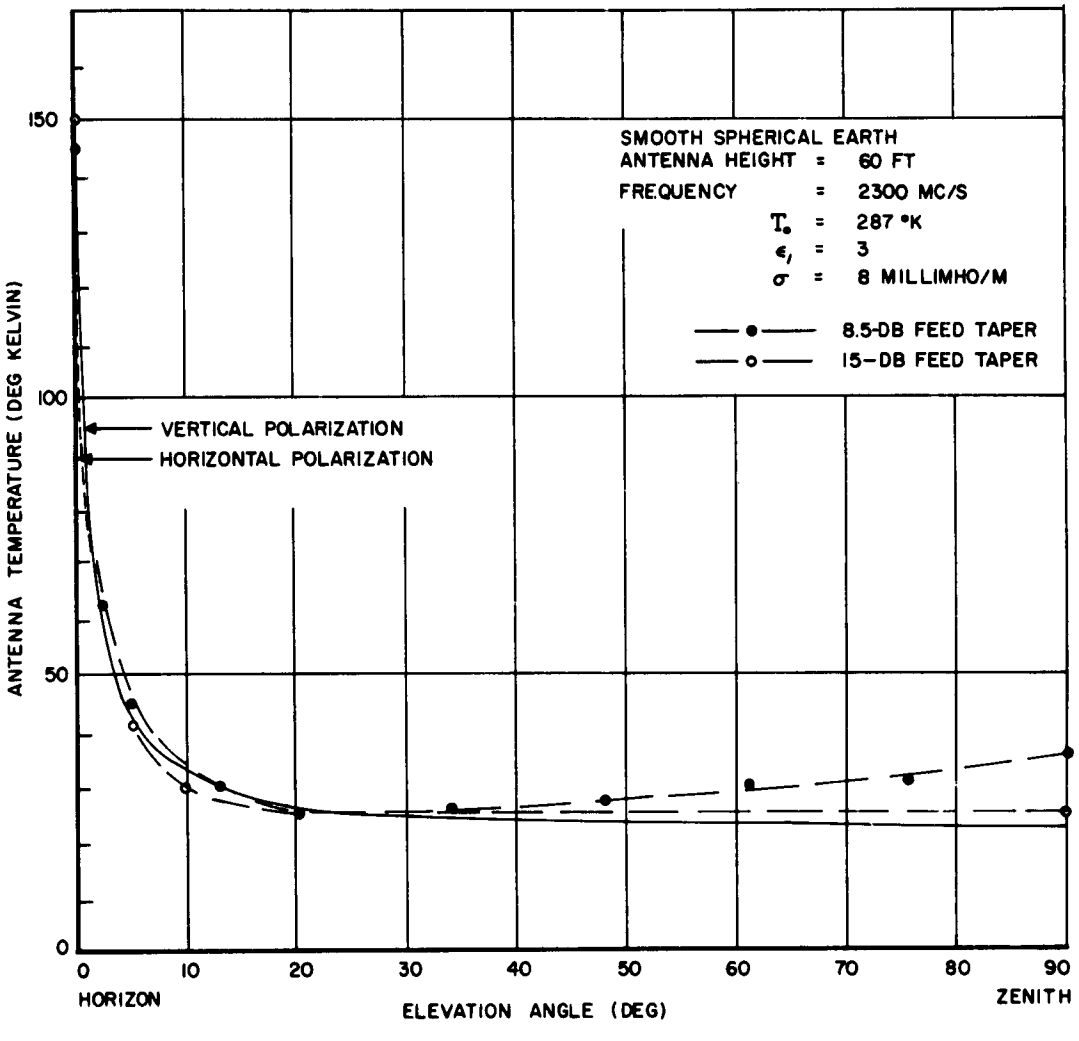

Figure 3-22 Background Antenna Temperature due to Atmosphere and Ground

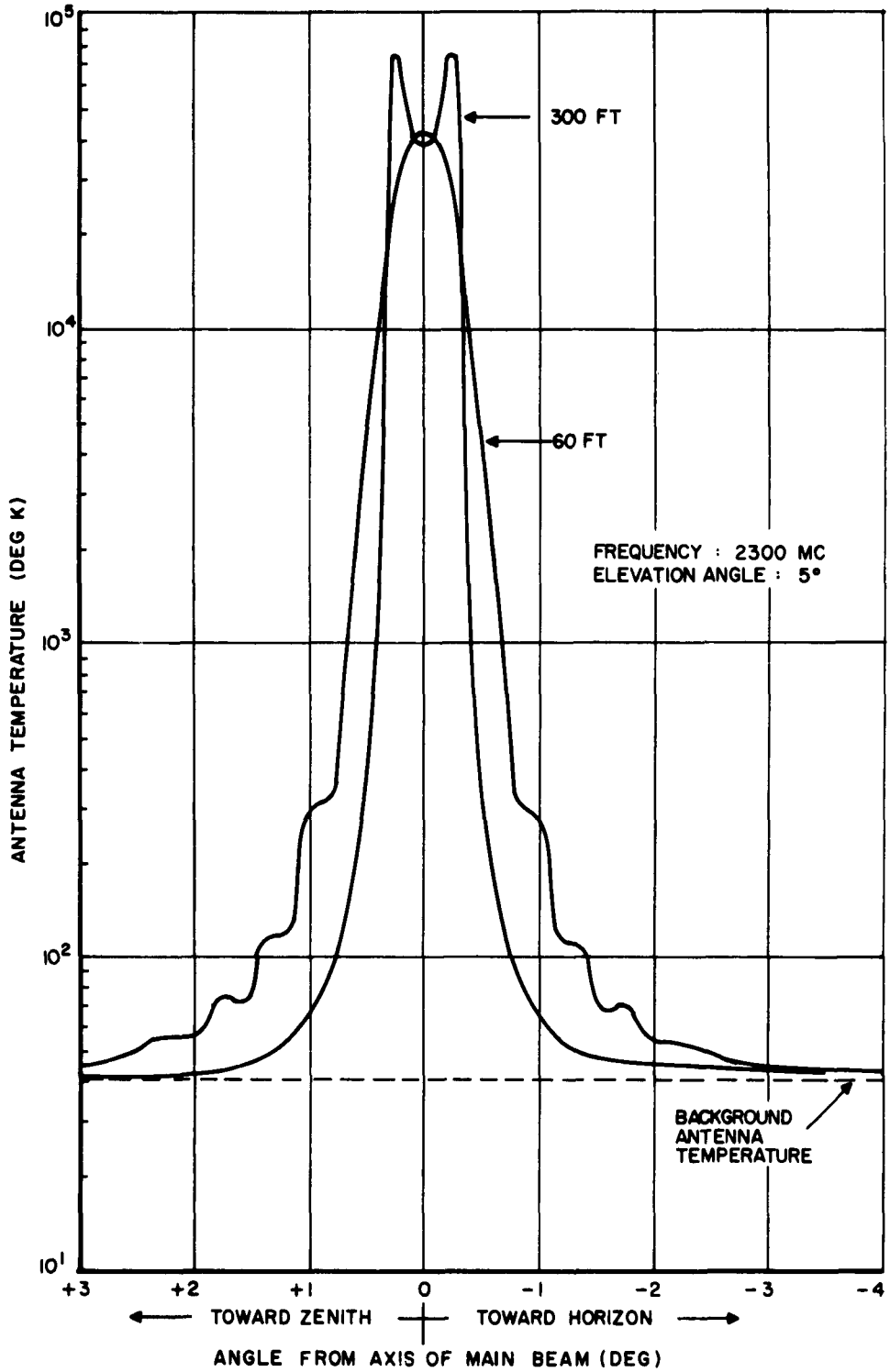

Figure 3-23 Total Antenna Temperature of 60-Foot and 300-Foot Reflectors at 2300 Mc

SECTION 4
CARRIER-TO-NOISE

4.1 INTRODUCTION

In this section, what has been developed in the previous section on antenna temperature will be used to determine the carrier-to-noise ratio of the following radio links: (1) a telemetry link between a 300-foot-diameter, ground-station antenna and a space probe one astronomical unit (1 A.U.) away; (2) a voice link between a 60-foot-diameter, ground-station antenna and a random-orbit satellite repeater orbiting the earth at an altitude of 6000 nautical miles. The carrier-to-noise ratios have been calculated according to the following relation:

$$\frac{C}{N} = \frac{P_T G_T G_R}{L_S L_A L_T \cdot k(T_A + T_B) B} \qquad (4\text{-}1)$$

where the symbols are defined in the table of parameters below, and

$$T_B = T_o (L_R - 1) + L_R T_R \qquad (4\text{-}2)$$

Table 1
SYSTEM PARAMETERS

Parameter	Probe Link	Satellite Link
Frequency	2300 Mc	2300 Mc
Transmitter Power (P_T)	25 w	4 w
Vehicle Antenna Size	4 ft	–
Gain (G_T)	26.5 db	0 db
RF Loss (L_T)	1 db	1 db
Range	10^8 n. mi.	8500 n. mi.
Space Loss (L_S)	263.5 db	182.1 db
Elevation Angle	5 deg.	5 deg.
Atmospheric Loss (L_A)	0.5 db	0.5 db
Ground Antenna Size	300 ft	60 ft
Gain (G_R)	62.5 db	45.5 db
RF Loss (L_R)	0.5 db	0.5 db
Total Antenna Temperature (T_A)	See Fig. 3-23	See Fig. 3-23
Receiver Temperature (T_R)	20° K	100° K
Bandwidth (B)	10 cps	10 kc

The ground antenna gains include 1.5 db tracking loss in a con-scan or a monopulse system due respectively to the cross-over level in con-scan or the decreased aperture efficiency in monopulse.

4.2 DEEP-SPACE LINK

Figure 4-1 shows the decrease in carrier/noise as the sun approaches the main beam of the 300-foot receiving antenna. For the link parameters assumed, transmission outage will not occur for a probe in transit across the sun. However, any substantial change in these parameters, such as

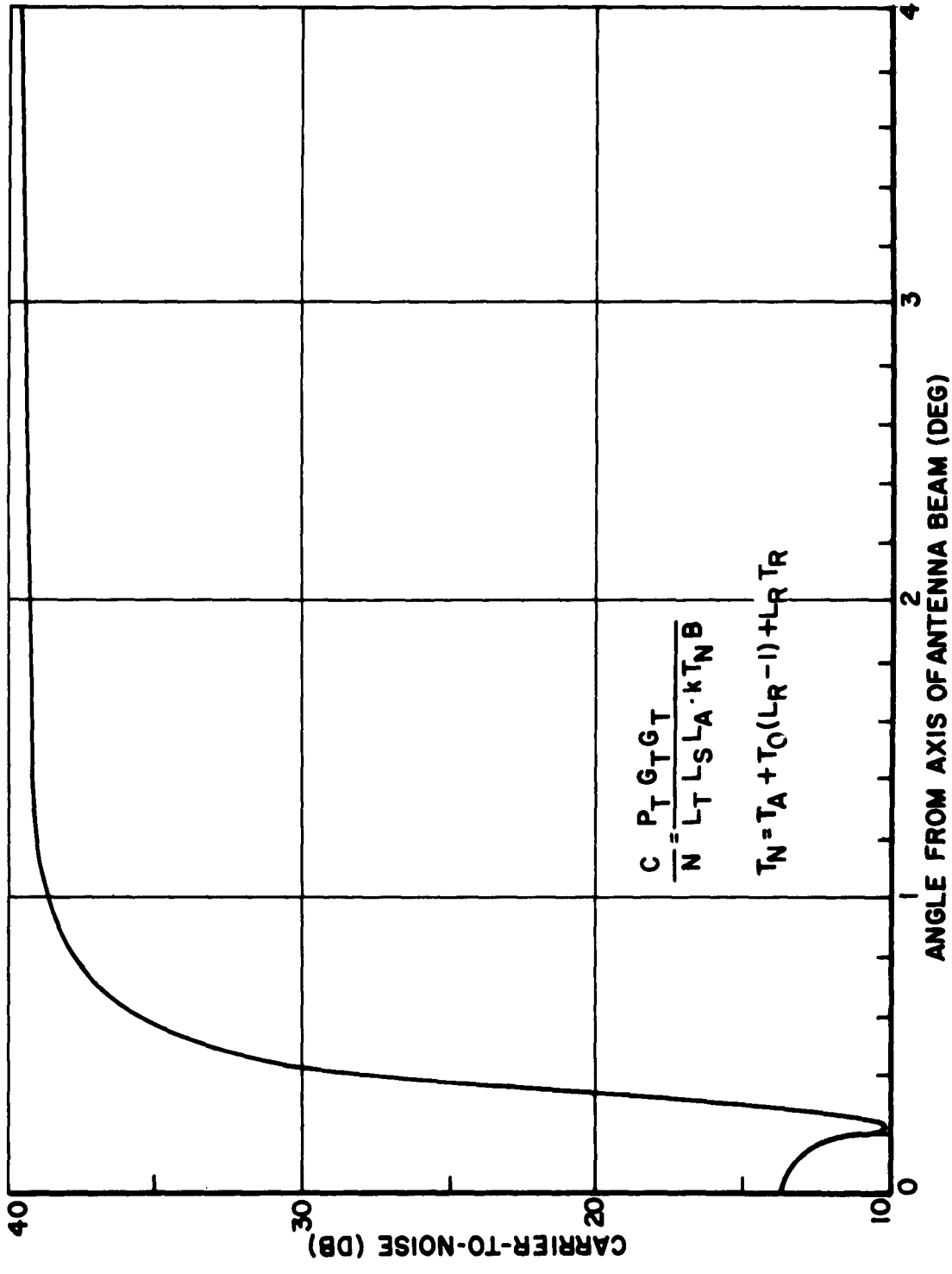

Figure 4-1 Carrier-to-Noise Ratio of Deep-Space Telemetry Link

doubling the range, or simultaneously reducing the transmitter power and increasing the bandwidth by factors of two, or imposing a 15-db to 20-db carrier-to-noise requirement would result in outage during transit. Even in such cases, it appears that a telemetry link can be maintained close to the limb of the sun's optical disc. For a solar probe (Refs. 1, 2) the conclusions are the same.

4.3 SATELLITE-TO-GROUND LINK

Figure 4-2 shows the decrease in carrier-to-noise ratio as the sun approaches the main beam of the 60-foot receiving antenna. For the link parameters assumed, outage as defined by a carrier-to-noise of less than 10 db occurs briefly for a satellite in transit across the sun. If a threshold of 15 db is established, outage occurs at angles of the main beam less than about 0.1 degree from the sun. Evidently a voice link can be maintained to within the limb of the sun's disc.

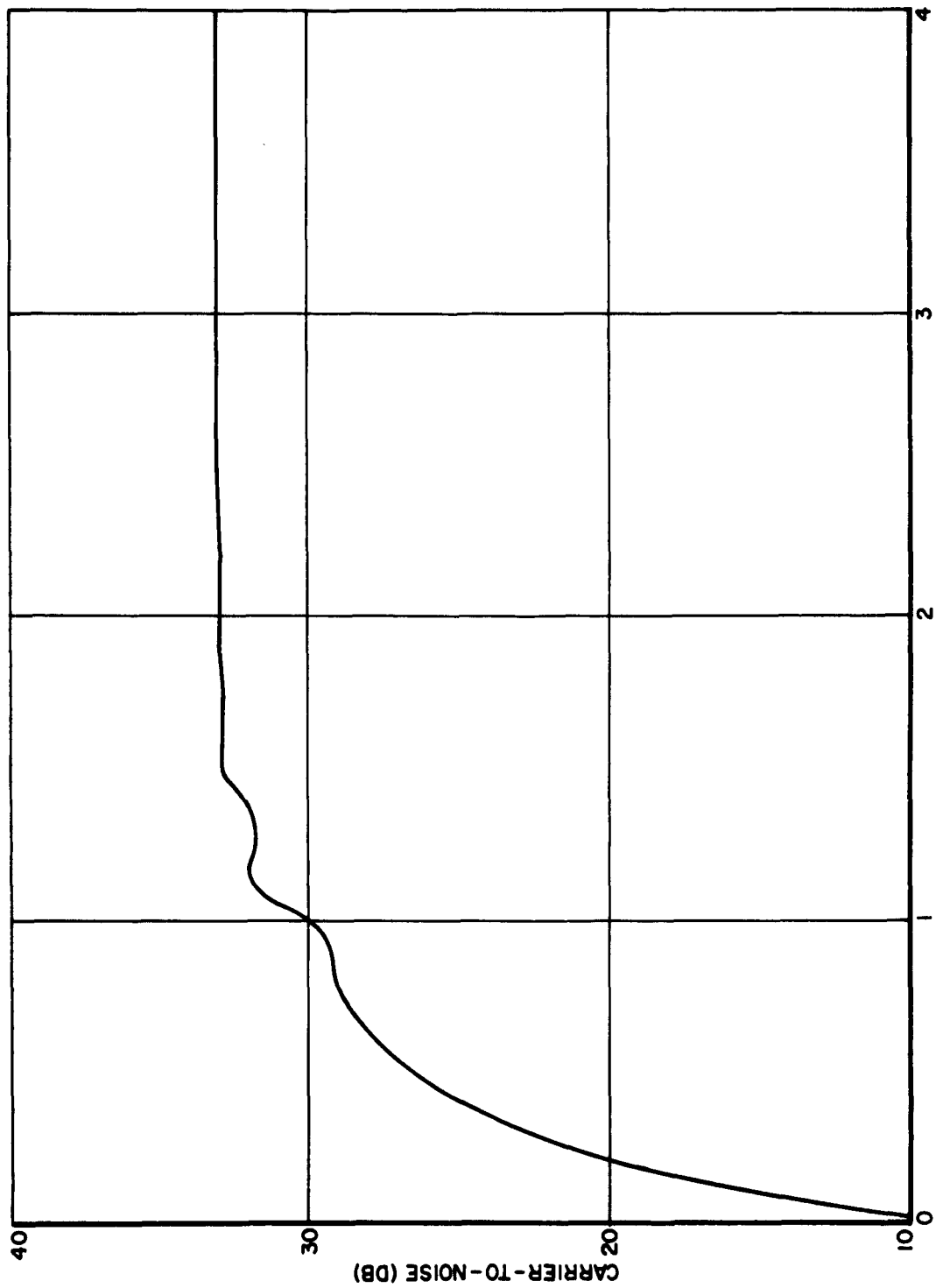

Figure 4-2 Carrier-to-Noise Ratio of Satellite-to-Ground Voice Link

SECTION 5
CONCLUSIONS

5.1 RESULTS

Of all the natural sources considered, the sun is the strongest source of interference at frequencies above 100 Mc. Below 100 Mc the galaxy and radio stars predominate.

For the system parameters assumed, a telemetry link can be supported between a low-noise, 300-foot-diameter, self-tracking, ground receiving system and a 4-foot spacecraft antenna transmitting 25 watts at 2300 Mc over a distance of 1 A. U. during the spacecraft's transit across the sun. A voice link can be supported between a low-noise, 60-foot-diameter, self-tracking, ground receiving system and an omnidirectional satellite antenna transmitting 4 watts at 2300 Mc over a distance of 8500 nautical miles during the satellite's approach to an angle of about 0.1 degree from the sun for a carrier-to-noise ratio of 15 db.

5.2 USEFULNESS OF STUDY

The imminent realization of global communication systems with their ground-to-satellite and satellite-to-satellite links raises the question of noise into spacecraft antennas from natural sources. From a knowledge of the spacecraft antenna pattern, the stabilization characteristics of the vehicle, and its flight path in relation to the sources of noise, one can readily compute antenna noise as a function of position in orbit. At this time, spacecraft antenna noise is small compared to the noise temperature of spacecraft receivers.

From a knowledge of antenna noise levels as a function of antenna size, pattern shape, frequency, polarization, and direction of the main beam, a systems engineer can determine the received carrier-to-noise during a mission, the resulting maximum range or maximum bandwidth, and the limitations to communication efficiency due to noise.

The computer programs that have been used during this study for computing antenna noise from mapped sources make it possible to specify any pencil-beam antenna pattern, any noise distribution, and any path across or in the vicinity of noise sources.

5.3 FURTHER STUDY

Brightness temperature profiles at frequencies between 3000 Mc and 30,000 Mc should be generated in view of present and planned uses of X-band frequencies for space communication links.

It would be instructive to compare the antenna temperatures in this report with those computed from selected radio maps of the sun representing its condition at 1420 Mc and 3000 Mc during a substantial portion of the sunspot cycle. The integration over a nonuniform sun, however, must be carried out with a modified version of the computer program developed for the nonuniform distribution of galactic radio noise (See WDL-TR1972), because the SUNRAD program is designed only for a spherically symmetrical source.

The SUNRAD program should be broadened to include several optional inputs. For example, one would prefer to let the conversion of solar radii to angular degrees from the center of the sun in the brightness temperature profiles (cf. Figures 2-3 and 2-4) vary according to the actual distance between the receiving antenna and the sun. This would permit computations of antenna temperature aboard spacecraft not necessarily at earth's distance from the sun, such as planetary orbiting satellites and fly-by probes. A corresponding change in N, the number

of integration steps (See Section 6.5.1) will have to be considered and should also be an explicit input.

SECTION 6
REFERENCES

All references are keyed to the sections in which they appear.

Section 1. Introduction

1. S. M. Taras, A. R. Giddis, J. D. Bowes, F. J. Zobel, and W. F. Williams, "Ground Terminal Noise Minimization Study, Final Report," Philco Tech. Rept. WDL-TR1972, Sect. 2; January 18, 1963.
2. A. R. Giddis, "The Influence of Natural Noise upon Antenna System Performance," paper to be published in the AIEE Proceedings of the Conference on Aerospace Support; August, 1963.

Section 2. Solar Radio Noise

1. R. N. Bracewell and G. Swarup, "The Stanford Microwave Spectroheliograph Antenna, A Microsteradian Pencil Beam Interferometer," IRE Trans. on Antennas and Propagation, vol. AP-9, pp. 22-30; January, 1961.
2. W. N. Christiansen, D. S. Mathewson, and J. L. Pawsey, "Radio Pictures of the Sun," Nature, vol. 180, pp. 944-946; November 9, 1957.
3. W. N. Christiansen and D. S. Mathewson, "The Origin of the Slowly Varying Component," Paris Symposium on Radio Astronomy, ed. R. N. Bracewell, Stanford University Press, Stanford, Calif., pp. 108-117; 1959.
4. G. Newkirk, Jr., "A Model of the Electron Corona with Reference to Radio Observations," ibid, pp. 149-158.

5. A. Hewish, "Radio Observations of the Solar Corona at Sunspot Minimum," I. A. U. Symposium on Radio Astronomy, ed. H. C. van de Hulst, Cambridge University Press, Cambridge, England, pp. 298-301; 1957.

6. Comptes Rendues, vol. 237, pp. 300-302; July 27, 1953.

7. W. N. Christiansen and J. A. Warburton, "The Distribution of Radio Brightness over the Solar Disk at a Wavelength of 21 Centimeters, Part III, The Quiet Sun, Two-Dimensional Observations," Aust. J. Phys., vol. 8, pp. 474-486; July, 1955.

8. A. E. Covington, W. J. Medd, G. A. Harvey, and W. W. Broten, "Radio Astronomy Brightness of the Sun at a Wavelength of 10.7 cm," J. Roy. Astron. Soc. of Canada, vol. 49, pp. 235-247; November, 1955.

9. G. Swarup, "Stanford Microwave Spectroheliograms for 1960 July," Stanford Radio Astronomy Inst. Pub. No. 12, pp. 1-32; March, 1962.

10. G. Swarup, "Studies of Solar Microwave Emission Using a Highly Directional Antenna," Stanford Elect. Lab. Scient. Rept. No. 13 under Contract AF18(603)-53, pp. 1-110; February 6, 1961. (Also ASTIA No. AD-252915.)

11. V. V. Vitkevich and L. I. Matreyenko, "Radio Picture of the Sun in the 3 cm Band," Radiofizika, vol. 3, No. 3, p. 541; 1960.

12. Annals of the International Geophysical Year, "I.G.Y. Solar Activity Maps (D-2)," ed. by M. A. Ellison, vol. XXII, Pergamon Press (Paris); 1961.

13. J. H. Piddington, "Model Solar Chromospheres," Ap. J., vol. 119, pp. 531-540; May, 1954.

14. N. R. Labrum, "The Radio Brightness of the Quiet Sun at 21 cm Wavelength Near Sunspot Minimum," Aust. J. Phys., vol. 13, pp. 700-711; December, 1960.

15. R. G. Conway and P. A. O'Brien, "The Distribution of Brightness at Metre Wavelengths Across the Sun's Disk," M. N., vol. 116, p. 386; 1956.

16. H. M. Stanier, "Distribution of Radiation from the Undisturbed Sun at a Wavelength of 69 cm," Nature, vol. 165, p. 354; 1950.

17. P. A. O'Brien, "The Distribution of Radiation Across the Solar Disk at Metre Wavelengths," M. N., vol. 113, p. 5; 1953.

18. K. Machin, " Distribution of Radiation Across the Solar Disk at a Frequency of 81.5 Mc/s," Nature, vol. 167, p. 889; 1951.

19. W. N. Christiansen and J. A. Warburton, "The Distribution of Radio Brightness over the Solar Disk at a Wavelength of 21 cm, I," Aust. J. Phys., vol. 6, pp. 190-202; June, 1953.

20. S. F. Smerd, "Radio-Frequency Radiation from the Quiet Sun," Aust. J. Scient. Res. A, vol. 3, pp. 34-59; March, 1950.

21. D. W. Swayze, "Influence of the Sun on Space Communication," Philco WDL Tech. Rept. in preparation.

22. J. Aarons, W. R. Barron, and J. P. Castelli, "Radio Astronomy Measurements at VHF and Microwaves," Proc. IRE, vol. 46, pp. 325-333; January, 1958.

23. A. E. Covington and N. W. Broten, "Brightness of the Solar Disk at a Wavelength of 10.3 cm," Ap. J., vol. 119, pp. 569-589; May, 1954.

24. A. Maxwell, W. E. Howard, III, and G. Garmire, "Solar Radio Interference at 125, 200, 425, 500 Mc/s, "Harvard Univ. Scient. Rept. No. 14; July, 1959. (Also ASTIA No. AD-230089.)

25. C. W. Tolbert, L. C. Krause, and W. W. Bahn, "Solar Emission and Atmospheric Attenuation of 2.15 mm Wavelength Radiation," Univ. of Texas Elect. Eng. Res. Lab. Rept. No. 5-45; July 15, 1960.

26. J. L. Pawsey and D. E. Yabsley, "Solar-Radio-Frequency Radiation of Thermal Origin," Aust. J. Scient. Res. A, vol. 2, pp. 198-214; 1949.

27. C. W. Tolbert and A. W. Straiton, "Solar Emission at Millimeter Wavelengths," Ap. J., vol. 134, pp. 91-95; July, 1961.

28. A. D. Fokker, Jr., "Studies of Enhanced Solar Radio Emission at Frequencies Near 200 MHz," Druco Drukkerij Bedrijven (Leiden); June, 1960.

29. H. W. Dodson, E. R. Hedeman, and L. Owren, "Solar Flares and Associated 200 Mc/sec Radiation," Ap. J., vol. 118, p. 169; September, 1953.

30. G. Reber, "Solar 480 Mc/sec Radiation," Nature, vol. 158, p. 945; 1946.

31. C. M. Hepperle, W. E. Giberson, H. J. Malandrinos, and R. M. Ringoen, "Interim Report on the Microwave Radiometry Project of the Collins Radio Company," Collins Res. Rept. CRR-102; August, 1949.

32. R. H. Dicke and R. Beringer, "Microwave Radiation from the Sun and Moon," Ap. J., vol. 103, pp. 375-376; May, 1946.

33. R. N. Whitehurst and F. H. Mitchell, "Solar Temperature and Atmospheric Attenuation in the 7-8 mm Wavelength Range," Proc. IRE, vol. 44, p. 1879; December, 1956.

34. A. W. Straiton, C. W. Tolbert, and C. O. Britt, "Apparent Temperatures of Some Terrestrial Materials and the Sun at 4.3-Millimeter Wavelength," J. Appl. Phys., vol. 29, pp. 776-782; May, 1958.

35. R. J. Coates, "Measurements of Solar Radiation and Atmospheric Attenuation at 4.3 Millimeters Wavelength," Proc. IRE, vol. 46, pp. 122-126; January, 1958.

36. J. A. Hagen, "Temperature Gradient in the Sun's Atmosphere Measured at Radio Frequencies," Ap. J., vol. 113, pp. 547-566, May, 1951.

37. C. W. Allen, "The Variation of Decimetre-Wave Radiation with Solar Activity," M. N., vol. 117, pp. 174-188; January, 1957.

38. R. Coutrez, "Radioastronomie," Edition du Patrimoine de l'Observatoire Royal de Belgique, Uccle, Belgium, pp. 214-215; 1956.

39. M. R. Kundu and F. T. Haddock, "Centimeter-Wave Solar Bursts and Associated Effects," IRE Trans.on Antennas and Propagation, vol. AP-9, pp. 82-88; January, 1961.

40. J. P. Wild, K. V. Sheridan, and G. H. Trent, "The Transverse Motions of the Sources of Solar Radio Bursts," Paris Symposium on Radio Astronomy, ed. R. N. Bracewell, Stanford University Press, Stanford, California, pp. 176-185; 1959.

41. A. E. Covington, "Solar Emission at 10 cm Wavelength," Paris Symposium on Radio Astronomy, ibid, pp. 159-165.

42. R. J. Coates, A. E. Covington, and S. Edelson, "The 4.3 mm and 10.7 cm Outbursts of June 9, 1959," A. J., vol. 64, p. 326; 1959.

43. T. Kakinuma and G. Swarup, "A Model for the Sources of the Slowly Varying Component of Microwave Solar Radiation," Stanford Radio Astronomy Inst. Pub. No. 17, pp. 1-31; March, 1962.

44. A. D. Fokker and J. Roosen, "Radio Characteristics of Solar Flare Families," B. A. N., vol. 16, pp. 83-97; November 24, 1961.

45. C. W. Young, C. L. Spencer, G. E. Moreton, and J. A. Roberts, "A Preliminary Study of the Dynamic Spectra of Solar Radio Bursts in the Frequency Range 500-950 Mc/s," Ap. J., vol. 133, pp. 243-254; January, 1961.

46. G. Newkirk, Jr., "The Solar Corona in Active Regions and the Thermal Origin of the Slowly Varying Component of Solar Radio Radiation," Ap. J., vol. 133, pp. 983-1013; May, 1961.

47. J. F. Denisse, "Les Sources d'Emissions Radioélectrique du Soleil," Paris Symposium on Radio Astronomy, pp. 86-87; 1959.

48. R. Coutrez, "Radioastronomie," Edition du Patrimoine de l'Observatoire Royal de Belgique, Uccle, Belgium, pp. 192-195; 1956.

49. J. D. Kraus, "Solar System Radio Radiation," Ohio State Univ. Scient. Rept. No. 1 under Contract AF 19(604)-1591 (ASTIA No. 211944), pp. 14-29; December, 1958.

50. C. de Jager, "Structure and Dynamics of the Solar Atmosphere," Handbuch der Physik, vol. 52, Astrophysics III: The Solar System, Springer-Verlag, Berlin, pp. 300-322; 1959.

51. M. R. Kundu, J. A. Roberts, C. L. Spencer, and J. W. Kuiper, "A Comparison of the Dynamic Spectra of Solar Radio Bursts in the Decimeter - and Meter-Wave-Length Ranges," Ap. J., vol. 133, pp. 255-257; January, 1961.

52. M. R. Kundu, "Some Studies on the Occurrence of Type IV Solar Bursts of Continuum Radiation," Ap. J., vol. 134, pp. 96-104; July, 1961.

53. S. J. Goldstein, Jr., "The Angular Size of Short-Lived Solar Radio Disturbances," A. J., vol. 64, p. 333; October, 1959.

54. M. H. Cohen, "Microwave Polarization and Coronal Magnetic Fields," Ap. J., vol. 133, pp. 978-982; May, 1961.

55. M. R. Kundu, "Association of Centimeter-Wave Bursts with Different Spectral Types of Meter-Wave Bursts of Solar Radio Emission," Journal of Geophysical Research, vol. 67, pp. 2695-2706; July, 1962.

56. J. M. Malville, "Characteristics of Type III Radio Bursts," Astrophysical Journal, vol. 136, pp. 266-275; July, 1962.

Section 3. Antenna Temperature

1. I. Richardson, "Notes Relative to the Antenna Noise Programs," Philco WDL Math. Anal. Dept. Rept. No. 15, pp. 1-13; September, 1962.

2. C. Dunbar, "Antenna Noise Programs," Documentation on file in Math. Anal. Dept., pp. 1-43; 1962.

3. A. R. Giddis, "Present and Future Development of Radio Telescopes," Philco Tech. Rept. WDL-TR-E313-1, June, 1962; Revised March, 1963.

4. A. R. Giddis, "Reflector Antennas for Radio and Radar Astronomy," Philco Tech. Rept. WDL-TR1500, pp. 1-85; August, 1961. (Also ASTIA No. AD-262336.)

5. "Preliminary Report - Telstar I," Bell Tel. Lab., pp. 1-117; July-September, 1962.

6. See Ref. 1, Sect. 2.

7. See Ref. 1, Sect. 3.

8. R. Coutrez, "Radioastronomie," Edition du Patrimoine de l'Observatoire Royal de Belgique, Uccle, Belgium, pp. 321-331; 1956.

9. D. C. Hogg and W. W. Mumford, "The Effective Noise Temperature of the Sky," Mic. J., vol. 3, pp. 80-84; March, 1960.

Section 4. Carrier-to-Noise

1. D. W. Dugan, "A Preliminary Study of a Solar-Probe Mission," NASA-Ames Tech. Note TN-D-783; April, 1961.

2. "Advanced Solar Probe Study," Philco WDL Int. Repts.; January-March, 1963.

APPENDIX

A.1 CHARACTERISTICS OF SOLAR RADIO EMISSION

Table A-1 summarizes essential data on solar noise components. The table is divided into three parts corresponding to meter-wave, decimeter-wave, and centimeter-wave radiation.

Table A-1 Data on Solar Noise Components
Meter - Wave Bursts

Component / Parameter	Quiet Sun	Noise-Storm Bursts (Type I)	Slow-Drift Bursts (Type II)	Fast-Drift Bursts (Type III)	Continuum (Type IV)	Continuum (Type V)
Frequency Range (Mc/s)	Full Radio Spectrum	20 to 500	20 to 500	20 to 500	20 to 250	20 to 250
Duration	Continuous (11-year cycle)	Tens of Seconds*	Minutes	Seconds	Minutes to Hours	Seconds to Minutes
Bandwidth (Mc/s)		4 to Tens	Tens	Tens to Hundreds	Hundreds	Tens
Source Diameter (min.)	>32 (depends on frequency)	<1 to about 10		up to about 10	≥ 10	
Flux Density ($w/m^2/cps$)	up to 10^{-18}	up to 10^{-19}	up to 10^{-18}	up to 10^{-18}	up to 10^{-20}	up to 10^{-18}
Apparent Temperature (Deg. K)	up to 10^6	10^{10} to 10^8	10^{13} to 10^{10}	up to $> 10^{11}$	10^7 to 10^{12}	up to 10^{11}
Polarization	Non-Polarized	Circular	Non-Polarized	Partially Circular	Circular	Partially Circular
Associated Optical Phenomena	Ionized Hydrogen in Corona	Area above Sunspot	Flares & Prominences	Flares & Prominences	Flares & Prominences	Flares & Primi-nences

*Storm lasts from hours to days

Table A-1 Data on Solar Noise Components (Cont'd)
Decimeter - Wave Bursts

Component / Parameter	Reverse-Drift Bursts	Major-Event Bursts	Fast-Drift Bursts (~ Type III)	"Continuum" Storm Bursts (~ Type IV)	U-Bursts	Slowly Varying Component
Frequency Range (Mc/s)	500–900	500–950	400–950	250–950	500–950	500 to 10,000
Duration	≤ 1 sec.	≤0.2 sec.	0.3-2 sec.	Minutes to Hours	Seconds	Days to Months (27-day cycle)
Bandwidth (Mc/s)	10		Tens to Hundreds	Hundreds		
Source Diameter(min.)				< 4		< 1 to 10
Flux Density ($w/m^2/cps$)			10^{-21} to 10^{-18}			Up to 10^{-19}
Apparent Temperature (Deg. K.)				10^9 to 10^6		10^6
Polarization				Circular		Partially Circular
Associated Optical			Flares & Prominences	Flares & Prominences	Flares	Loop Prominences

Table A-1 Data on Solar Noise Components (Cont'd)
Centimeter - Wave Bursts

Component / Parameter	Simple Burst (Type A)	Post-Burst (Type B)	Gradual Rise & Fall (Type C)	Microwave Outbursts (A + B)	Rare Short Outbursts (A or A + B)
Frequency Range (Mc/s)	3,000 to 10,000	3,000 to 10,000	3,000 to 10,000	3,000 to 10,000	3,000 to 10,000
Duration	Minutes	Minutes to Hours	Minutes to Hours	Minutes to Hours	Minutes
Source Diameter (min.)	< 2.5	> 3	0.5 to 1	2.5 to 1.5	2.5 to 5**
Flux Density ($w/m^2/cps$)	up to 10^{-18}		> 10^{-22}	up to > 10^{-18}	up to > 10^{-18}
Apparent Temperature (Deg. K)	10^9 to 10^6	10^7 to 10^5	< 10^7	10^9 to 10^8	> 10^7
Polarization	Non-polarized, or partially circular or linear	Non-polarized, or partially circular or linear	Non-polarized, or partially circular	Non-polarized or partially circular; trace of linear	
Associated Optical Phenomena	Area about Sunspots	Area above Sunspots	Loop Prominences	Flares	Flares

** up to 10^4 at 21 cm

A.2 DERIVATION OF ANTENNA NOISE TEMPERATURE

For an extended source of radio radiation with a given spatial intensity distribution, the spectral flux density in a spherical coordinate system is expressed by

$$F = \int_0^{2\pi} \int_0^{\pi} I(\theta, \phi) \sin\theta d\theta d\phi \qquad (A-1)$$

where the intensity I is defined as the energy passing through a unit area, in unit time, in a unit frequency interval, and within a unit solid angle. The intensity is expressed in watts/meter^2/cps/steradian and the spectral flux density in watts/meter^2/cps. From the Rayleigh-Jeans approximation to Planck's law for black-body radiation, the intensity of the source can be related to its equivalent brightness temperature T_b as follows:

$$I(\theta, \phi) = \frac{2k}{\lambda^2} T_b(\theta, \phi) (w/m^2/cps/sterad) \qquad (A-2)$$

where k is Boltzmann's constant and λ is the wavelength of radiated energy. Therefore, the spectral flux density is related to the brightness as

$$F = \frac{2k}{\lambda^2} \int_0^{2\pi} \int_0^{\pi} T_b(\theta, \phi) \sin\theta d\theta d\phi \ (w/m^2/cps) \qquad (A-3)$$

The noise power per unit bandwidth received by the antenna is a function of its collecting aperture area:

$$P = F A_e(\theta, \phi) \ (w/cps) \qquad (A-4)$$

Since most extra-terrestrial radiation under consideration from the sky, the planets, the moon, and the quiet sun is unpolarized ("randomly"

polarized), the effective aperture area is one-half of A_e. Equating the aperture area to the antenna gain,

$$A_e(\theta, \phi) = \frac{G(\theta, \phi)\, \lambda^2}{4\pi} \ (m^2) \qquad (A\text{-}5)$$

and substituting the effective aperture area into the expression for antenna noise power Eq. (A-4) gives

$$P = \frac{k}{4\pi} \int_0^{2\pi} \int_0^{\pi} G(\theta, \phi)\, T_b(\theta, \phi)\, \sin\theta\, d\theta\, d\phi \ (w/cps) \qquad (A\text{-}6)$$

Normalizing the gain function G to its maximum gain value G_o, the equivalent antenna noise temperature is

$$T_A = \frac{P}{k} = \frac{G_o}{4\pi} \int_0^{2\pi} \int_0^{\pi} \frac{G(\theta, \phi)}{G_o}\, T_b(\theta, \phi)\, \sin\theta\, d\theta\, d\phi \ (\text{deg. Kelvin}) \qquad (A\text{-}7)$$

It should be pointed out that the ratio $4\pi/G_o$ can be expressed by the following integral:

$$\int_0^{2\pi} \int_0^{\pi} \frac{G(\theta, \phi)}{G_o}\, \sin\theta\, d\theta\, d\phi \qquad (A\text{-}8)$$

Therefore, the antenna temperature in general normalized form may be written as

$$T_A = \frac{\int_0^{2\pi} \int_0^{\pi} G(\theta, \phi)\, T_b(\theta, \phi)\, \sin\theta\, d\theta\, d\phi}{\int_0^{2\pi} \int_0^{\pi} G(\theta, \phi)\, \sin\theta\, d\theta\, d\phi} \qquad (A\text{-}9)$$

If the source is uniformly intense across the solid angle Ω_s that it occupies, the flux density from Equation (A-1) is

$$F = I\Omega_s \ (w/m^2/cps) \tag{A-10}$$

The corresponding uniform brightness temperature from Equation (A-2) becomes

$$T_b = \frac{F}{\Omega_s} \cdot \frac{\lambda^2}{2k} \quad (deg.\ k) \tag{A-11}$$

If the brightness temperature T_b is constant over the solid angle subtended by the source and is zero elsewhere, Equation (6-7) reduces to

$$T_A = \frac{G_o}{4\pi} T_s \iint_{\Omega_s} \frac{G(\theta, \phi)}{G_o} \sin\theta \, d\theta \, d\phi \tag{A-12}$$

If, in addition, the source extends over the entire antenna pattern, where the antenna pattern is, in general, taken over 4π steradians, Equation (A-12) reduces further to

$$T_A = T_s \ (deg.\ K) \tag{A-13}$$

If the size of the source is very small compared to the antenna beamwidth and the temperature remains constant as above, then, to a good approximation, the normalized antenna pattern is unity, and the antenna temperature in Equation (A-12) is expressed as

$$T_A = \frac{G_o}{4\pi} T_s \Omega_s \ (deg.\ K) \tag{A-14}$$

Sometimes the quantity $G_o/4\pi$ is labeled the "beam area" and the expression is written as

$$T_A = T_s \frac{\Omega_s}{\Omega_A} \tag{A-15}$$

A. 3 SAMPLES OF INPUT AND OUTPUT DATA

In order to compute antenna temperature, it is necessary to provide the computer with the following input data: (a) brightness temperature profile, (b) antenna radiation pattern, and (c) distance of the sun from the antenna axis.

A. 3. 1 Brightness Temperature

A sample of a tabulated brightness temperature profile is given in Table A-2. The angle ξ is based on a mean earth-sun distance. The side lobes are enumerated by number (e. g. #1).

A. 3. 2 Antenna Pattern

A sample of a tabulated normalized antenna power pattern is given in Table A-3. The side lobes are enumerated by number (e. g. #1). The angle ξ is based on a mean earth-sun distance.

A. 3. 3 Angles from the Sun

A sample of tabulated distances of the sun from the antenna axis at which antenna temperatures are to be computed is given in Table A-4.

A. 3. 4 Input Data Format

A sample of the coded input to the sun radiation program ("SUNRAD") is illustrated in Table A-5. This table should be compared with the input data sheet (Table A-7) in Section A. 5 for an explanation of the location and designation of the inputs.

A. 3. 5 Computer Output

Table A-6 shows a sample of the resulting antenna temperature output from the Philco-2000 computer.

Table A-2

BRIGHTNESS TEMPERATURE PROFILE

f = 2300 Mc

Distance From Center a	Angle from Center* ξ (deg.)	Solar Temperature T_s (°K)
0	0	6.00×10^4
0.1	0.0266	6.10×10^4
0.2	0.0533	6.05×10^4
0.3	0.0800	6.10×10^4
0.35	0.0933	6.15×10^4
0.4	0.1067	6.20×10^4
0.45	0.1200	6.40×10^4
0.5	0.1333	6.70×10^4
0.6	0.1600	7.50×10^4
0.7	0.1866	8.80×10^4
0.8	0.2133	1.10×10^5
0.85	0.2266	1.30×10^5
0.9	0.2400	1.65×10^5
0.95	0.2533	2.30×10^5
0.96	0.2560	2.40×10^5
0.965	0.2573	2.55×10^5
0.97	0.2586	2.70×10^5
0.975	0.2600	3.20×10^5
0.98	0.2613	3.50×10^5
0.985	0.2626	5.00×10^5
0.99	0.2640	4.00×10^5
0.995	0.2653	2.00×10^5
1.00	0.2666	1.50×10^5
1.01	0.2693	5.00×10^4

* $\xi = \frac{a}{214.9}$ radian = 0.2666(a) degrees

Table A-2 (Cont'd)

Distance From Center a	Angle from Center* ξ (deg.)	Solar Temperature T_s (°K)
1.02	0.2720	2.70×10^4
1.03	0.2746	2.30×10^4
1.04	0.2773	2.00×10^4
1.05	0.2800	1.70×10^4
1.10	0.2933	8.5×10^3
1.15	0.3066	4.6×10^3
1.20	0.3200	2.8×10^3
⋮	⋮	⋮

* $\xi = \frac{a}{214.9}$ radian = 0.2666(a) degrees

Table A-3

ANTENNA POWER PATTERN

f = 2300 Mc

Angle from Axis θ (deg.)	Relative Power Response $G(\theta, \phi)/G_o$		Angle from Axis θ (deg.)	Relative Power Response $G(\theta, \phi)/G_o$	
0	1.00	Main Beam	1.425	1.00×10^{-4}	
0.1435	8.00×10^{-1}		1.45	8.00×10^{-4}	
0.180	6.31×10^{-1}		1.60	1.00×10^{-3}	#3
0.250	5.00×10^{-1}		1.62	8.00×10^{-4}	
0.325	2.50×10^{-1}		1.70	1.00×10^{-4}	
0.425	1.00×10^{-1}		1.75	0	
0.450	5.00×10^{-2}		1.825	1.00×10^{-4}	
0.500	2.50×10^{-2}		1.875	4.00×10^{-4}	
0.540	1.00×10^{-2}		2.00	5.00×10^{-4}	#4
0.575	3.16×10^{-3}		2.025	4.00×10^{-4}	
0.600	1.00×10^{-3}		2.10	1.00×10^{-4}	
0.640	1.00×10^{-4}		2.20	0	
0.650	0		2.30	1.00×10^{-4}	
0.660	1.00×10^{-4}		2.32	2.00×10^{-4}	
0.700	8.00×10^{-3}		2.40	2.50×10^{-4}	#5
0.775	1.00×10^{-2}	#1	2.45	2.00×10^{-4}	
0.825	8.00×10^{-3}		2.50	1.00×10^{-4}	
0.925	1.00×10^{-4}		2.60	0	
0.975	0		2.70	1.00×10^{-4}	
1.02	1.00×10^{-4}		2.80	1.43×10^{-4}	#6
1.05	2.50×10^{-3}		2.90	1.00×10^{-4}	
1.15	3.18×10^{-3}	#2	3.00	0	
1.18	2.50×10^{-3}		3.125	5.00×10^{-5}	
1.28	1.00×10^{-4}		3.25	7.95×10^{-5}	#7
1.35	0		3.30	5.00×10^{-5}	

Table A-3 (Cont'd)

Angle from Axis θ (deg.)	Relative Power Response $G(\theta, \phi)/G_o$		Angle from Axis θ (deg.)	Relative Power Response $G(\theta, \phi)/G_o$	
3.45	0		4.45	3.02×10^{-5}	#10
3.60	4.00×10^{-5}		4.525	2.50×10^{-5}	
3.65	5.62×10^{-5}	#8	4.70	0	
3.70	4.00×10^{-5}		4.90	2.24×10^{-5}	#11
3.85	0		5.25	0	
3.98	3.00×10^{-5}		5.40	2.00×10^{-5}	#12
4.05	3.98×10^{-5}	#9	5.75	0	
4.10	3.00×10^{-5}		6.00	1.00×10^{-5}	#13
4.25	0		7.00	0	
4.40	2.50×10^{-5}		⋮	⋮	

Table A-4

DISTANCES OF SUN FROM ANTENNA AXIS

f = 2300 Mc
D = 60 ft

Angle from Antenna Axis α (deg.)
0
0.250
0.425
0.600
0.650
0.775
0.875
0.975
1.15
1.25
1.35
1.50
1.60
1.75
1.875
1.90
2.00
2.20
2.35
2.50
2.60
2.70
2.80
3.00
3.25
3.45
3.65
3.85
⋮

Table A-5 Input Data Form

WDL TAC CODING FORM

PROGRAM: ______ JOB NUMBER: ______ PAGE ___ OF ___

PROGRAMMER: ______ CHECKED BY: ______ DATE: ______

IDENTITY	8	L 9	LOCATION 10	COMMAND 17	ADDRESS AND REMARKS 25	70–80
6	CASE 1			1BI5,1BI	5,1BI5,0BI5,30BI5,27BI5,	
6	2			100,210,		
6	8			0,1,1.5,	2,2.5,2.75,3,3.25,3.5,3.75,4,4.25,4.5,4.75	,5,5.25,5.5,
				5.75,6,6	.25,6.5,6.75,7,7.25,7.5,7.75,8,	
6	9			0,0,0,0,	0,0,0,0,0,0,0,0,0,0,0,0,0,0,0,0,0,0,0,0,0,	0,0,
6	10			0,0,0,0,	0,0,0,0,0,0,0,0,0,0,0,0,0,0,0,0,0,0,0,0,0,	0,0,
6	11			0,0,0,0,	0,0,0,0,0,0,0,0,0,0,0,0,0,0,0,0,0,0,0,0,0,	0,0,
6	12			-90,-90,	-90,-90,-90,-90,-90,-90,-90,-90,-90,-90,-9	0,-90,-90,-90,
				-90,-90,	-90,-90,-90,-90,-90,-90,-90,-90,-90,	
6	CASE 5			0BI5,1BI	5,1BI5,0BI5,30BI5,5BI5,	
6	2			100,300,		
6	8			4.6,5,5.	5,5.9,8.8,	

FREQUENCY .2295 .PC/S

ANTENNA DIAMETER .00 FEET

ALPHA	DELTA PT. FAL.	SUN ALPHA I	SUN DELTA I1	DEL STAR I2	I1/I	I2/I	Q0
.0000000	.0000000	.0000000	.0000000	.8999+2			
	.0000+5	.6899+5	.6899+5	.0000000	.9999+1	.0000000	.7661-4
.2499999	.0000000	.0000000	.0000000	.8999+2			
	.2134+6	.4219+5	.4219+5	.0000000	.9999+1	.0000000	.7661-4
.4999999	.0000000	.0000000	.0000000	.8999+2			
	.0000000	.1747+5	.1744+5	.2919+2	.9982+2	.1711-2	.7661-4
.5999999	.0000000	.0000000	.0000000	.8999+2			
	.0000000	.3925+4	.3961+4	.3632+3	.9074+2	.9255-1	.7661-4
.6499999	.0000000	.0000000	.0000000	.8999+2			
	.0000000	.2178+4	.1789+4	.3869+3	.8215+0	.1784+0	.7661-4
.7749999	.0000000	.0000000	.0000000	.8999+2			
	.0000000	.4860+3	.1440+3	.3420+3	.2962+3	.7037+0	.7661-4
.9749999	.0000000	.0000000	.0000000	.8999+2			
	.0000000	.3953+3	.0000000	.3953+3	.0000000	.9999+1	.7661-4
.1149+1	.0000000	.0000000	.0000000	.8999+2			
	.0000000	.1229+3	.0000000	.1229+3	.0000000	.9999+1	.7661-4
.1349+1	.0000000	.0000000	.0000000	.8999+2			
	.0000000	.1192+3	.0000000	.1192+3	.0000000	.9999+1	.7661-4
.1599+1	.0000000	.0000000	.0000000	.8999+2			
	.0000000	.4511+2	.0000000	.4511+2	.0000000	.9999+1	.7661-4
.1749+1	.0000000	.0000000	.0000000	.8999+2			
	.0000000	.5122+2	.0000000	.5122+2	.0000000	.9999+1	.7661-4
.1999+1	.0000000	.0000000	.0000000	.8999+2			
	.0000000	.2289+2	.0000000	.2289+2	.0000000	.9999+1	.7661-4
.2199+1	.0000000	.0000000	.0000000	.8999+2			
	.0000000	.2252+2	.0000000	.2252+2	.0000000	.9999+1	.7661-4
.2499+1	.0000000	.0000000	.0000000	.8999+2			
	.0000000	.1332+2	.0000000	.1332+2	.0000000	.9999+1	.7661-4

Location of antenna in right ascension	Location of antenna in declination	Brightness temperature at antenna pointing angle	Total antenna temperature	Location of sum in right ascension	Location of sum in declination	Antenna temperature in main beam	Lower limit of sum in declination	Antenna temperature outside main beam	Relative tempera-ture in main beam	Relative temperature outside main beam	Normalising factor related to antenna gain

Table A-6 Computer Results for Antenna Temperature

A. 4 ANALYTICAL NOTES ON SOLAR ANTENNA TEMPERATURE

In the course of programming antenna temperature, several problems arose of a geometric nature peculiar to the type of integration involved. The solutions to these problems are presented in this section.

A. 4. 1 Solar Noise Integration

With the earth as the origin, one wishes to integrate across the projected surface of the sun. The integral is:

$$\int_{\Omega} Tg\, dS \qquad \text{(A-16)}$$

where

T = sun's brightness temperature (a function of the angular distance, ξ, from the center of the sun)

$\equiv T_b(\theta, \phi)$ in Eq. (3-1) of Section 3 on Antenna Temperature.

g = antenna gain function (symmetric about the antenna's principal axis and depends upon the angular distance from the antenna's axis)

$\equiv G(\theta, \phi)/G_o$ is Eq. (3-1)

The geometry is depicted in Figure A-1. The integration is performed in (θ, ϕ) coordinates, where (θ_1, ϕ_1) represents the center of the sun. At an arbitrary point (θ, ϕ), the angle ξ is given by:

$$\begin{aligned} \cos\xi = {} & \sin\theta \sin\theta_1 \cos\phi \cos\phi_1 \\ & + \sin\theta \sin\theta_1 \sin\phi \sin\phi_1 \\ & + \cos\theta \cos\theta_1 \end{aligned} \qquad \text{(A-17)}$$

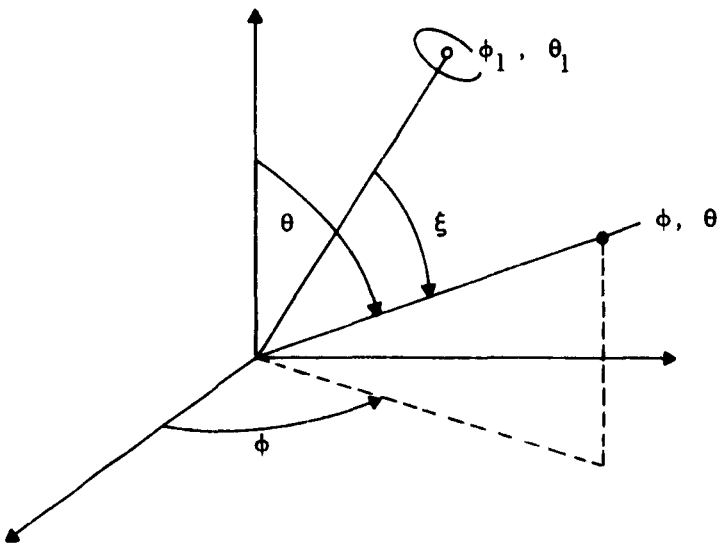

Figure A-1 Geometry for Integration of Solar Noise in Spherical Coordinates

Figure A-2 illustrates the sun and antenna in celestial coordinates.

A.4.1.1 Limits of Integration Across the Sun. If the sun's coordinates are (α_1, δ_1) and the antenna's coordinates are (α_0, δ_0), then the angle, β, between the two is given by:

$$\cos\beta = \cos\delta_0 \cos\alpha_0 \cos\delta_1 \cos\alpha_1 + \cos\delta_0 \sin\alpha_0 \cos\delta_1 \sin\alpha_1 + \sin\delta_0 \sin\delta_1 \qquad (A\text{-}18)$$

Therefore, the integration has the following limits in θ:

$$\beta - \gamma \leq \theta \leq \beta + \gamma \qquad (A\text{-}19)$$

where γ is the half-angular diameter of the radio sun.

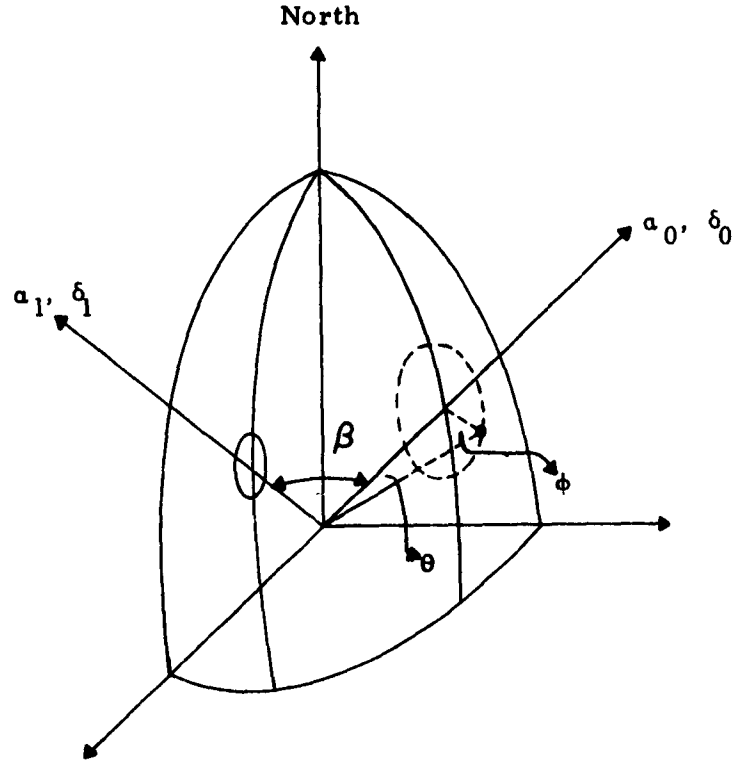

Figure A-2 Celestial Coordinate System

The limits of integration in ϕ are as follows. If $\beta < \gamma$, the antenna's axis lies within the solar disc, and the limits become:

$$0 \leq \phi \leq 2\pi \qquad \text{(A-20)}$$

If $\beta \geq \gamma$, then the ϕ limits of integration are determined from a consideration of Figure A-3.

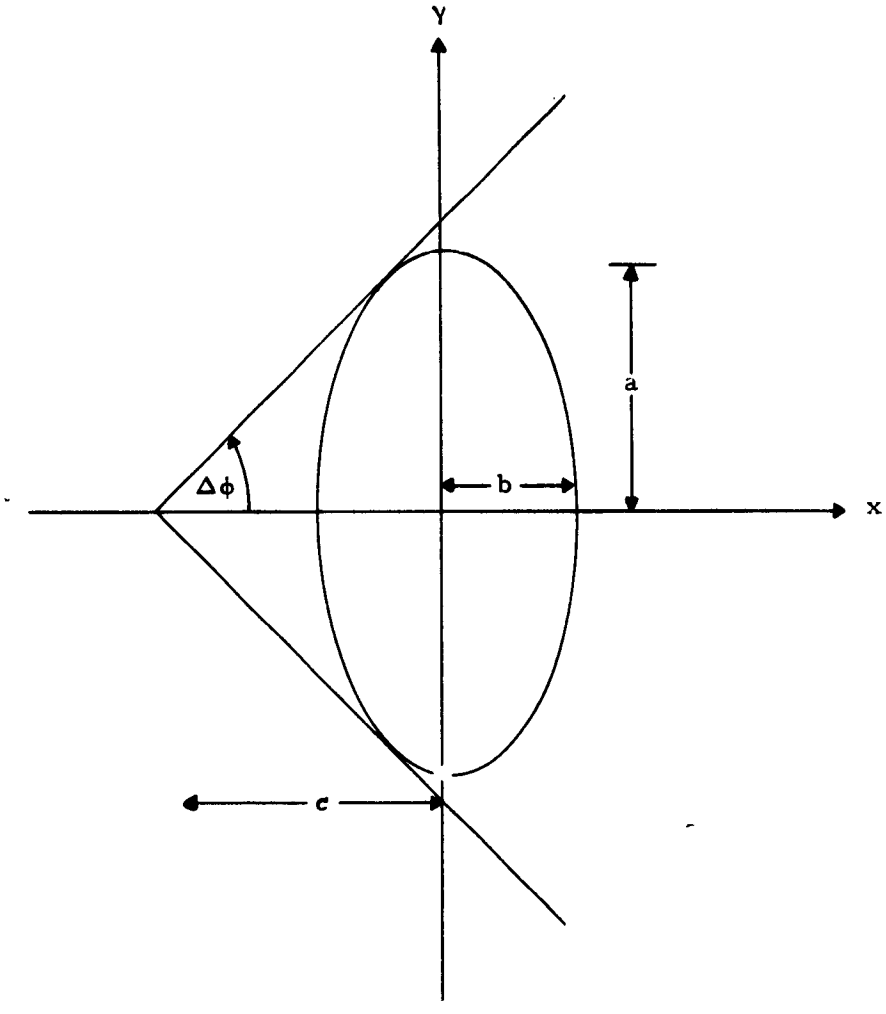

Figure A-3 Limits of Integration

This figure shows the projection of the solar disc upon the plane normal to the antenna axis; i. e., the antenna's pole is perpendicular to the (x, y) plane and passes through the point (-c, 0). The projection of the circular solar disc is an ellipse and the angle $\Delta\phi$ defines the limits of integration.

A point on the ellipse is described by the familiar equation,

$$\frac{y^2}{a^2} + \frac{x^2}{b^2} = 1 \qquad (A-21)$$

The equation for the tangent line through (-c, 0) is simply

$$y = m(x + c) \tag{A-22}$$

A determination of the slope m will determine $\Delta\phi$. Since m is a tangent,

$$m = \frac{dy}{dx} = \frac{a^2 x}{b^2 y} \tag{A-23}$$

Substituting in Eq. (A-22) yields

$$y^2 = -\frac{a^2}{b^2}(x^2 + xc) \tag{A-24}$$

Substituting Eq. (A-24) into Eq. (A-21) gives for the intersection of the ellipse and the tangent the following relation:

$$x = -\frac{b^2}{c} \tag{A-25}$$

Hence,

$$y = a\left(1 - \frac{b^2}{c^2}\right)^{1/2} \tag{A-26}$$

Substituting Eq. (A-25) and Eq. (A-26) into Eq. (A-23) defines the slope as follows:

$$m = \frac{a}{c}\left(1 - \frac{b^2}{c^2}\right)^{-1/2} \tag{A-27}$$

Therefore,

$$\Delta\phi = \tan^{-1} m \tag{A-28}$$

and the limits of integration are the following:

$$\phi_1 - \Delta\phi \leq \phi \leq \phi_1 + \Delta\phi \tag{A-29}$$

The constants a, b, and c are found by considering Figure A-4, which shows the solar disc in the antenna's coordinates.

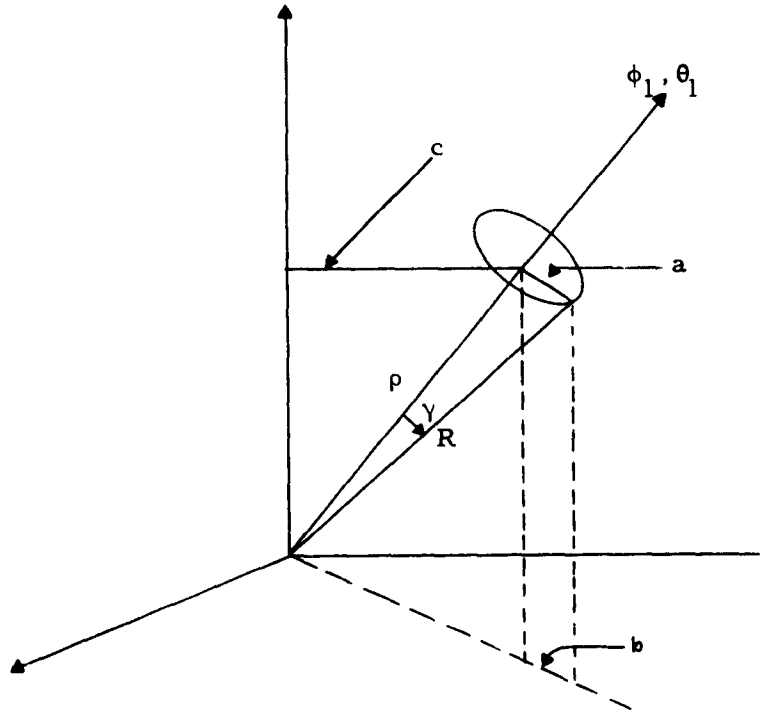

Figure A-4 Antenna Coordinate System

From this figure, it is apparent that:

$$a = R \sin \gamma$$
$$b = R \sin \gamma \cos \theta_1$$
$$c = \rho \sin \theta_1$$
$$\rho = R \cos \gamma \qquad \text{(A-30)}$$

However, the equation for $\Delta\phi$ is homogeneous in a, b, and c; so R can be made arbitrarily unity.

A.4.2 Test Case

To test the program, a test case with analytical solution is needed. In the following, the sun is located at ($\alpha_o = 0$, $\delta_o = \pi/2$) and the antenna is pointed at ($\alpha_1 = 0$, $\delta_1 = \pi/2$). The sun's half angle is γ. The integral of interest is the following:

$$I = \int_0^{2\pi} \int_0^{\gamma} g T_s R^2 \sin \theta \, d\theta \, d\phi \qquad \text{(A-31)}$$

where g is taken to be unity (an isotropic antenna), and the solar brightness temperature across the solar disc is given by

$$T_s = \gamma - \theta \qquad \text{(A-32)}$$

The geometry is shown in Figure A-5

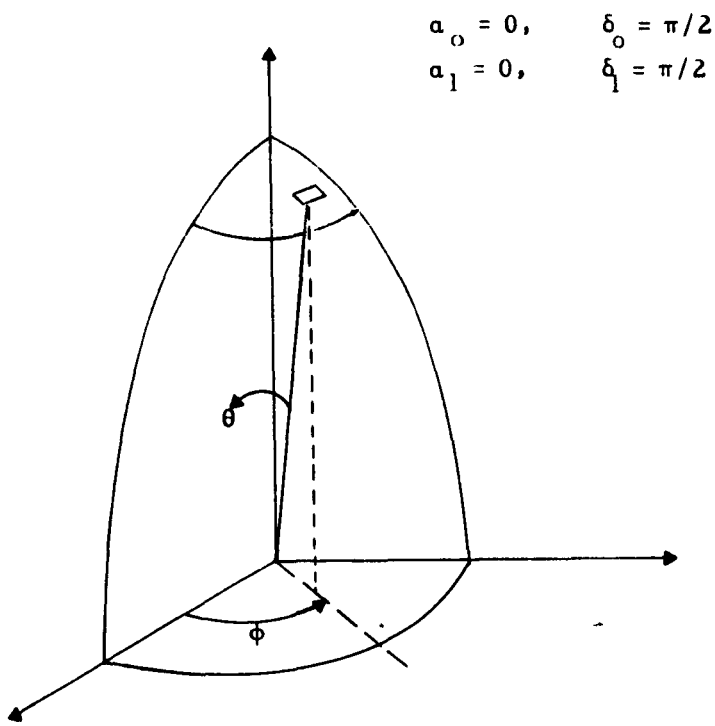

Figure A-5 Geometry for Test Case

Performing the integration and normalizing R to unity gives

$$I = 2\pi (\gamma - \sin \gamma). \qquad \text{(A-33)}$$

A. 5 DOCUMENTATION FOR THE COMPUTER PROGRAM

A. 5. 1 Input for SUNRAD

Cards 1 and 2 must be punched for each case.

Card 1: FIRST = 1B15 if this is the first or only case or the first case of a new frequency; otherwise = 0.

ASIZE = 1B15 if this case has a new antenna size; otherwise = 0.

NAPTS = 1B15 if there is a different set of antenna points for this case; otherwise = 0.

LAST = 1B15 if this is the last case of the total production run; otherwise = 0.

N = number of integration steps around the antenna-fixed point B15 (30 steps at present but in general would depend upon extent of radio sun).

NAPO = number of antenna points - fixed point B15.

Card 2: FREQ = frequency of input data in megacycles/second - floating point.

AS = diameter of antenna in feet - floating point.

Cards 3 - 7 to be punched for first case only or when FIRST = 1B15.

Card 3: GAMMA = half angle of the radio sun in degrees - floating point.

Card 4: XI = angles for brightness temperature table in degrees - floating point (100 points maximum).

Card 5: TXI = sun brightness temperature values in degrees Kelvin - floating point (100 points maximum).

Card 6: THETAO = angles for antenna function values in degrees, beginning with zero (80 points maximum).

Card 7: G = normalized antenna power pattern values, beginning with unity (80 points maximum) from the Reference Antenna Pattern Table (Table (A-5).

Cards 8 - 12 must be punched for the first case and for each case thereafter where NAPTS = 1B15.

Card 8: ALPHAO = antenna pointing coordinate in degrees right ascension (50 points maximum).

Card 9: DELTAO = antenna pointing coordinate in degrees declination (50 points maximum).

Note: In most cases, α_o is varied while δ_o, α_1, and δ_1, are set to zero. Also, $0 \leq \alpha_o < \theta_{o_{max}} \cdot K - \gamma$,

where

K = pattern factor

$$= \frac{2300}{f_{Mc}} \cdot \frac{60}{D_{ft}}$$

$\theta_{o_{max}}$ = 30° for present antenna pattern.

Card 10: ALPHA1 = sun position in degrees right ascension (50 points maximum).

Card 11: DELTA1 = sun position in degrees (declination) (50 points maximum).

Card 12: DELSTAR = lower limit of sun position (horizon) (50 points maximum) = -90° for entire sun.

The input data sheet in Table A-7 identifies the input data according to card number along the left-hand margin and according to code in adjacent spaces. This table should be compared with Table A-5 of Section A. 3 which represents a typical input format.

Table A-7

INPUT DATA SHEET – SUNRAD

1	17						
	FIRST	A SIZE	NAPTS	LAST	N	NAP ϕ	
G1	B15,	B15,	B15,	B15,	B15,	B15,	
	FREQ	AS					
G2	,	,					
	GAMMA						
G3	,						
	XI						
G4	100 values						
	TXI						
G5	100 values						
	THETA ϕ						
G6	80 values						
	G						
G7	80 values						
	ALPHA ϕ						
G8	max 50 points						

Table A-7 (Cont'd)

1	17
	DELTA ϕ
G9	max 50 points
	ALPHA 1
G10	max 50 points
	DELTA 1
G11	max 50 points
	DELSTAR
G12	max 50 points

A.5.2 Sun Noise Program

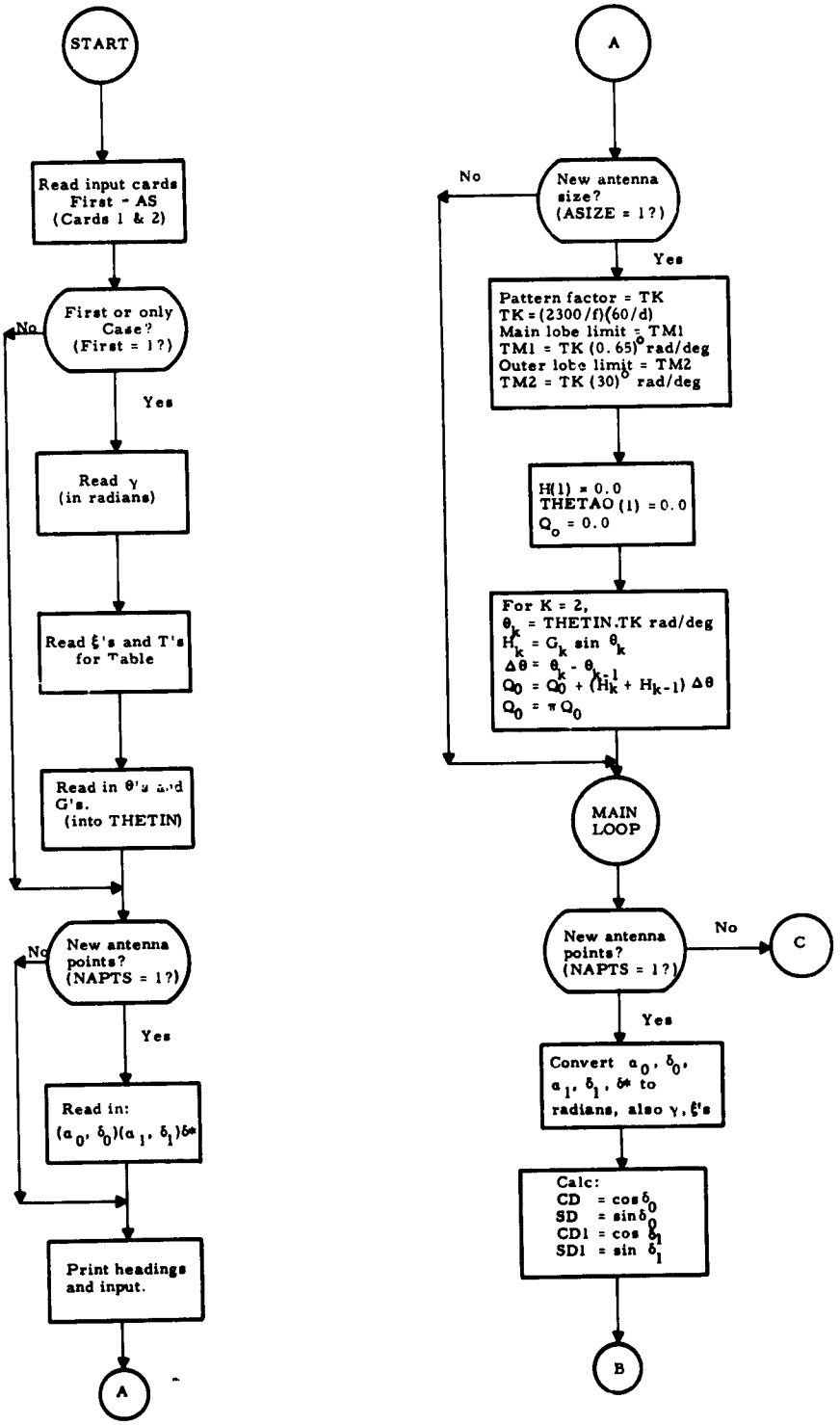

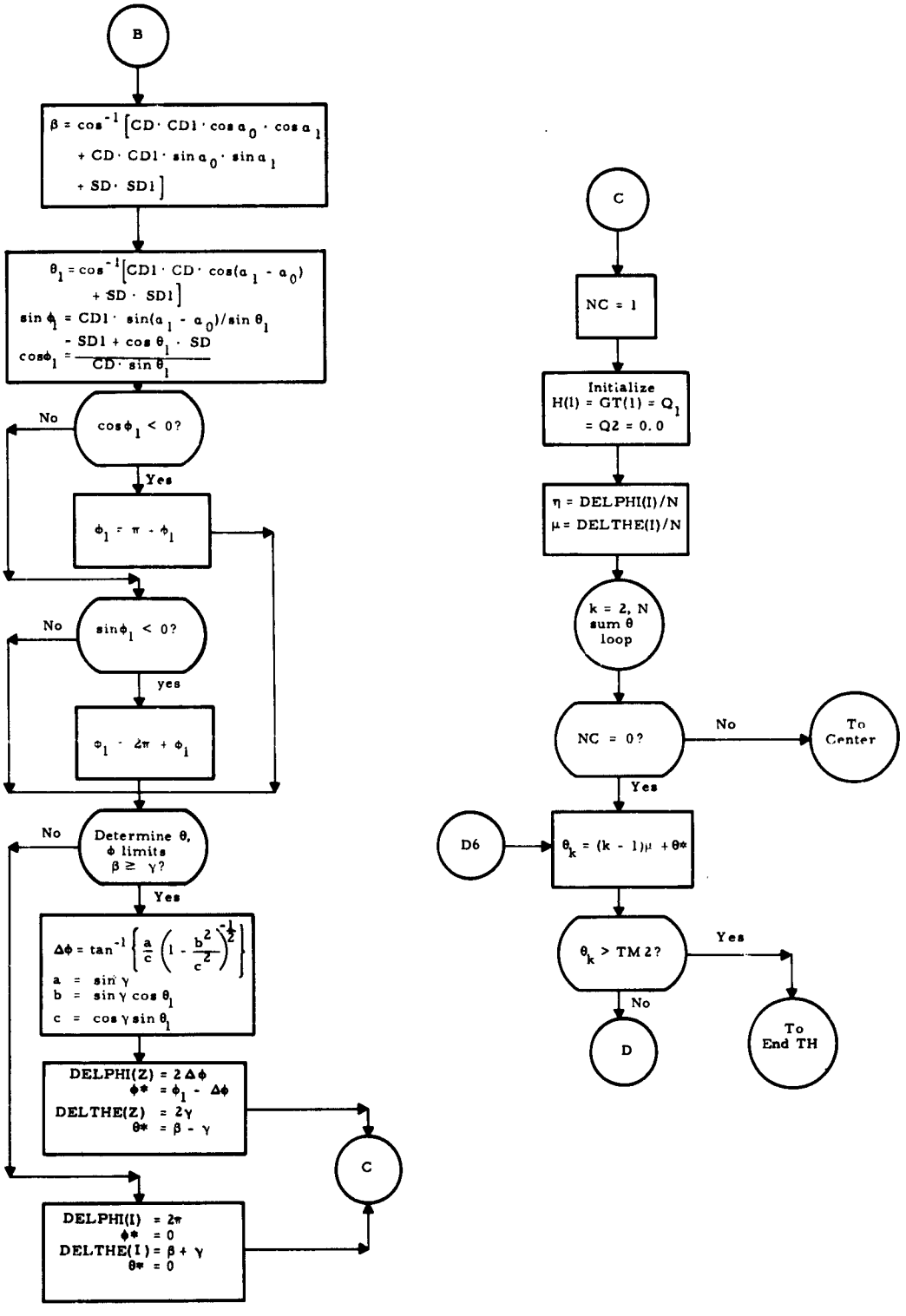
B
$\beta = \cos^{-1}[CD \cdot CD1 \cdot \cos\alpha_0 \cdot \cos\alpha_1 + CD \cdot CD1 \cdot \sin\alpha_0 \cdot \sin\alpha_1 + SD \cdot SD1]$
$\theta_1 = \cos^{-1}[CD1 \cdot CD \cdot \cos(\alpha_1 - \alpha_0) + SD \cdot SD1]$
$\sin\phi_1 = CD1 \cdot \sin(\alpha_1 - \alpha_0)/\sin\theta_1$
$\cos\phi_1 = \frac{-SD1 + \cos\theta_1 \cdot SD}{CD \cdot \sin\theta_1}$
$\cos\phi_1 < 0$?
No
Yes
$\phi_1 = \pi - \phi_1$
$\sin\phi_1 < 0$?
No
yes
$\phi_1 = 2\pi + \phi_1$
Determine θ, ϕ limits $\beta \geq \gamma$?
No
Yes
$\Delta\phi = \tan^{-1}\left\{\frac{a}{c}\left(1 - \frac{b^2}{c^2}\right)^{\frac{1}{2}}\right\}$
$a = \sin\gamma$
$b = \sin\gamma\cos\theta_1$
$c = \cos\gamma\sin\theta_1$
DELPHI(Z) = $2\Delta\phi$
$\phi^* = \phi_1 - \Delta\phi$
DELTHE(Z) = 2γ
$\theta^* = \beta - \gamma$
C
DELPHI(I) = 2π
$\phi^* = 0$
DELTHE(I) = $\beta + \gamma$
$\theta^* = 0$
C
NC = 1
Initialize H(I) = GT(1) = Q_1 = Q2 = 0.0
η = DELPHI(I)/N
μ = DELTHE(I)/N
k = 2, N sum θ loop
NC = 0?
No
To Center
Yes
D6
$\theta_k = (k-1)\mu + \theta^*$
$\theta_k >$ TM 2?
Yes
To End TH
No
D

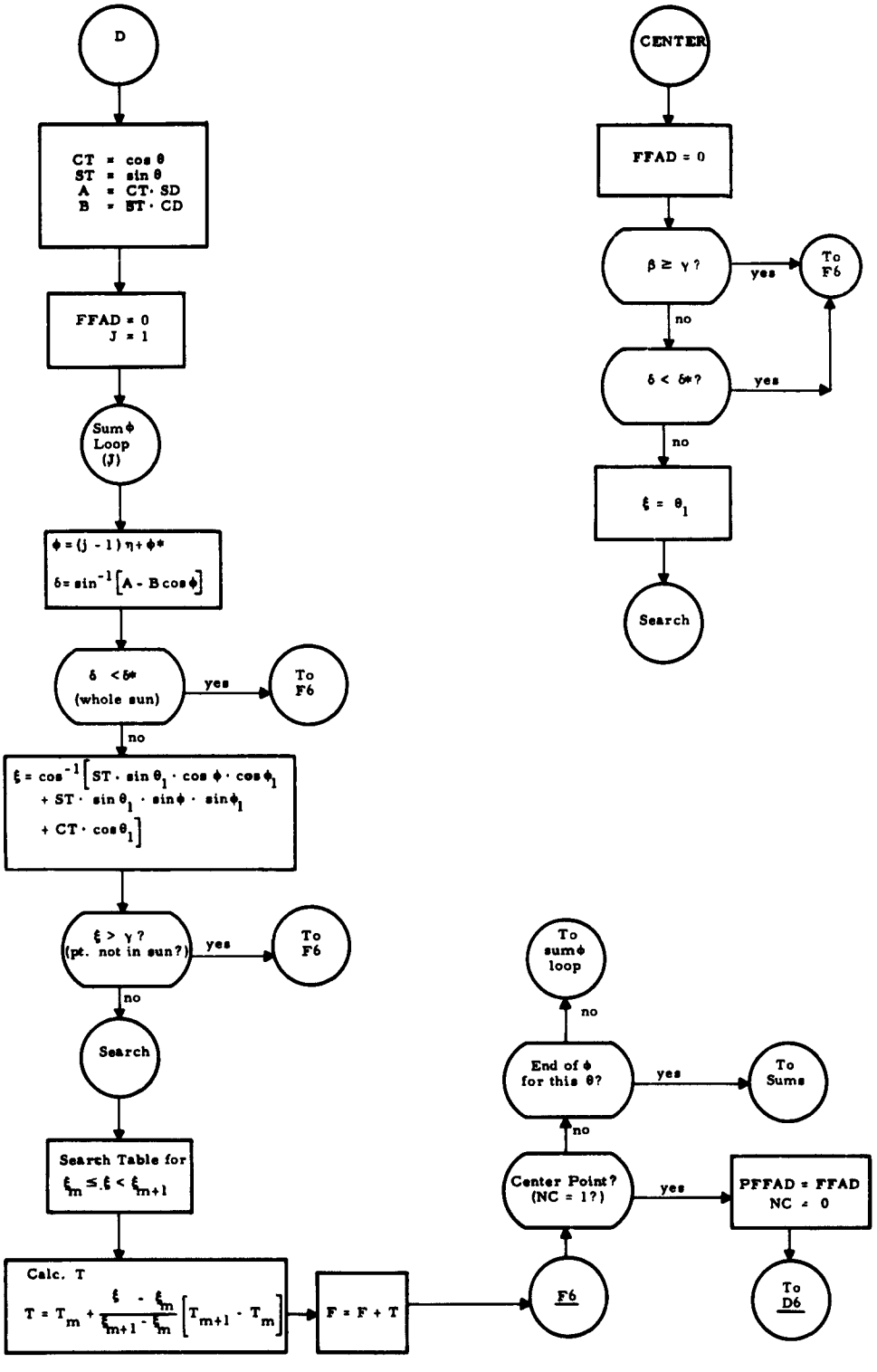
D
CT = cos θ
ST = sin θ
A = CT · SD
B = ST · CD
FFAD = 0
J = 1
Sum φ Loop (J)
φ = (j - 1) η + φ*
δ = sin⁻¹ [A - B cos φ]
δ < δ* (whole sun)
yes
To F6
no
ξ = cos⁻¹ [ST · sin θ1 · cos φ · cos φ1 + ST · sin θ1 · sin φ · sin φ1 + CT · cos θ1]
ξ > γ ? (pt. not in sun?)
yes
To F6
no
Search
Search Table for ξm ≤ ξ < ξm+1
Calc. T
T = Tm + (ξ - ξm) / (ξm+1 - ξm) [Tm+1 - Tm]
F = F + T
F6
Center Point? (NC = 1?)
yes
PFFAD = FFAD
NC = 0
To D6
no
End of φ for this θ?
yes
To Sums
no
To sum φ loop
CENTER
FFAD = 0
β ≥ γ ?
yes
To F6
no
δ < δ* ?
yes
no
ξ = θ1
Search

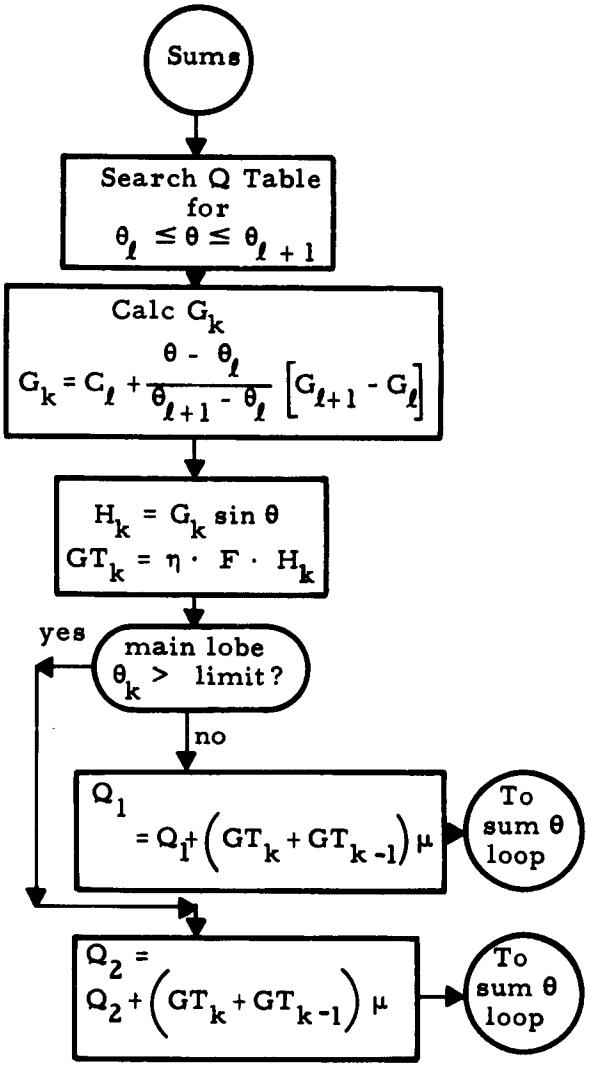
Sums
Search Q Table for $\theta_\ell \leq \theta \leq \theta_{\ell+1}$
Calc G_k
$G_k = G_\ell + \frac{\theta - \theta_\ell}{\theta_{\ell+1} - \theta_\ell} \left[G_{\ell+1} - G_\ell\right]$
$H_k = G_k \sin \theta$
$GT_k = \eta \cdot F \cdot H_k$
yes
main lobe $\theta_k >$ limit?
no
$Q_1 = Q_1 + \left(GT_k + GT_{k-1}\right) \mu$
To sum θ loop
$Q_2 = Q_2 + \left(GT_k + GT_{k-1}\right) \mu$
To sum θ loop

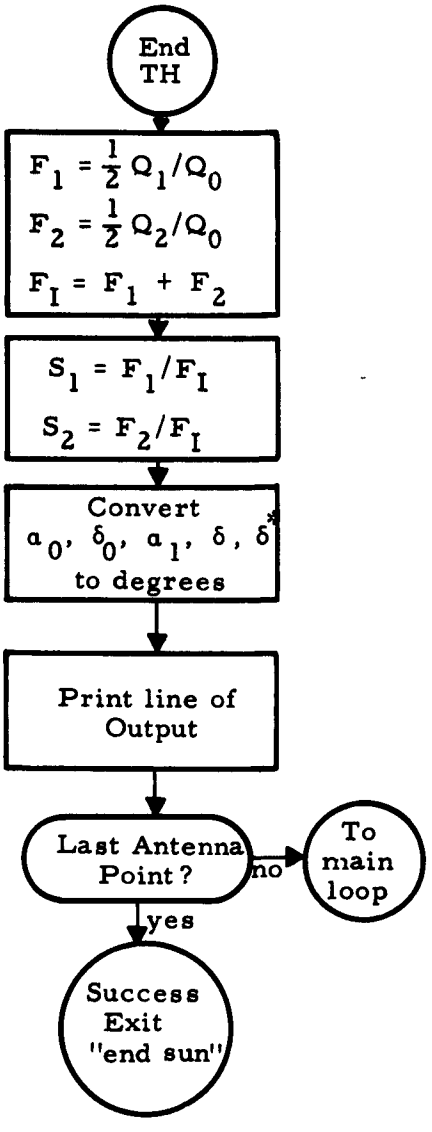
End TH
$F_1 = \frac{1}{2} Q_1/Q_0$
$F_2 = \frac{1}{2} Q_2/Q_0$
$F_I = F_1 + F_2$
$S_1 = F_1/F_I$
$S_2 = F_2/F_I$
Convert a_0, δ_0, a_1, δ, δ^* to degrees
Print line of Output
Last Antenna Point?
no
To main loop
yes
Success Exit "end sun"

WDL-TR-E320; Giddis, Albert R.; "EFFECT OF THE SUN UPON ANTENNA TEMPERATURE"; issued March 1963; Philco Corporation, WDL Division, Palo Alto, California, USA; vii plus 100 pp; unclassified report.

This report presents results of a study on computations by means of analytical models of the quiet sun and, from measurements of its flux density, the effect of solar radiation upon antenna noise temperature. The spatial and spectral properties of solar radio noise are described, and brightness temperature distributions over the sun at several frequencies are presented. The method by which antenna temperature is evaluated, using the Philco 2000 computer, is discussed. The computations are systematized, integrated, and compared with antenna temperatures contributed by other extraterrestrial sources. In addition, the effect of the earth's atmosphere and ground on the total noise temperature is determined. These results are used to calculate the variation of carrier-to-noise ratio as an antenna scans toward and across the sun while receiving signals from a deep-space probe and from a random-orbit satellite.

WDL-TR-E320; Giddis, Albert R.; "EFFECT OF THE SUN UPON ANTENNA TEMPERATURE"; issued March 1963; Philco Corporation, WDL Division, Palo Alto, California, USA; vii plus 100 pp; unclassified report.

This report presents results of a study on computations by means of analytical models of the quiet sun and, from measurements of its flux density, the effect of solar radiation upon antenna noise temperature. The spatial and spectral properties of solar radio noise are described, and brightness temperature distributions over the sun at several frequencies are presented. The method by which antenna temperature is evaluated, using the Philco 2000 computer, is discussed. The computations are systematized, integrated, and compared with antenna temperatures contributed by other extraterrestrial sources. In addition, the effect of the earth's atmosphere and ground on the total noise temperature is determined. These results are used to calculate the variation of carrier-to-noise ratio as an antenna scans toward the sun while receiving signals from a deep-space probe and from a random-orbit satellite.

WDL-TR-E320; Giddis, Albert R.; "EFFECT OF THE SUN UPON ANTENNA TEMPERATURE"; issued March 1963; Philco Corporation, WDL Division, Palo Alto, California, USA; vii plus 100 pp; unclassified report.

This report presents results of a study on computations by means of analytical models of the quiet sun and, from measurements of its flux density, the effect of solar radiation upon antenna noise temperature. The spatial and spectral properties of solar radio noise are described, and brightness temperature distributions over the sun at several frequencies are presented. The method by which antenna temperature is evaluated, using the Philco 2000 computer, is discussed. The computations are systematized, integrated, and compared with antenna temperatures contributed by other extraterrestrial sources. In addition, the effect of the earth's atmosphere and ground on the total noise temperature is determined. These results are used to calculate the variation of carrier-to-noise ratio as an antenna scans toward the sun while receiving signals from a deep-space probe and from a random-orbit satellite.

WDL-TR-E320; Giddis, Albert R.; "EFFECT OF THE SUN UPON ANTENNA TEMPERATURE"; issued March 1963; Philco Corporation, WDL Division, Palo Alto, California, USA; vii plus 100 pp; unclassified report.

This report presents results of a study on computations by means of analytical models of the quiet sun and, from measurements of its flux density, the effect of solar radiation upon antenna noise temperature. The spatial and spectral properties of solar radio noise are described, and brightness temperature distributions over the sun at several frequencies are presented. The method by which antenna temperature is evaluated, using the Philco 2000 computer, is discussed. The computations are systematized, integrated, and compared with antenna temperatures contributed by other extraterrestrial sources. In addition, the effect of the earth's atmosphere and ground on the total noise temperature is determined. These results are used to calculate the variation of carrier-to-noise ratio as an antenna scans toward the sun while receiving signals from a deep-space probe and from a random-orbit satellite.